TRANSPORTATION RESEARCH

RECORD

No. 1420

Highway and Facility Design

Hydrology, Hydraulics, and Water Quality

A peer-reviewed publication of the Transportation Research Board

TRANSPORTATION RESEARCH BOARD
NATIONAL RESEARCH COUNCIL

NATIONAL ACADEMY PRESS
WASHINGTON, D.C. 1993

Transportation Research Record 1420
ISSN 0361-1981
ISBN 0-309-05568-7
Price: $25.00

Subscriber Category
IIA highway and facility design

TRB Publications Staff
Director of Reports and Editorial Services: Nancy A. Ackerman
Associate Editor/Supervisor: Luanne Crayton
Associate Editors: Naomi Kassabian, Alison G. Tobias
Assistant Editors: Susan E. G. Brown, Norman Solomon
Office Manager: Phyllis D. Barber
Senior Production Assistant: Betty L. Hawkins

Printed in the United States of America

Transportation Research Record 1420

Contents

Foreword

The 11 papers in this volume were presented at the 1993 Annual Meeting of the Transportation Research Board during sessions sponsored or cosponsored by the TRB Committee on Hydrology, Hydraulics, and Water Quality. The first six papers focus on scour prevention, the next four on water contamination, and the final paper on rainfall frequency.

Sheppard discusses the complex and unique features affecting sediment scour near bridges over coastal waters due to tidal flows. Vincent et al. present a model to evaluate and assess bridge scour specifically at tidal inlets, and Maynord presents and discusses the U.S. Army Corps of Engineers riprap design guidance. Southard focuses on bridge scour data from 12 selected sites on streams in Arkansas, evaluates five local-scour equations, and derives a regression equation for scour prediction. Fotherby evaluates four methods as alternatives to riprap for preventing scour around bridge piers. Atayee used a physical model composed of a channel, a floodplain, spill-through abutments of various lengths, and riprap of various grain sizes to develop empirical design guidelines for riprap as scour protection for spill-through abutments.

Barbé et al. summarize the results of a series of research projects to develop a methodology for investigating non-stormwater entries into storm drainage systems. Church and Friesz discuss field test sites in Massachusetts with four specific highway drainage designs that have been monitored for several years in order to evaluate the effectiveness of each in preventing road-salt contamination of groundwater. Hinz et al. used batch and miscible displacement experiments, the two-region model, and the convective-dispersive equation to evaluate the transport behavior of 2,4-D. Finley and Young propose grassy swales along highways, roads, and local streets as an alternative to curb and gutter for improving the quality of runoff. In the last paper, Naghavi and Yu present a comparative study of five rainfall frequency distribution and three parameter estimation methods conducted on rainfall data from 92 stations in Louisiana.

Bridge Scour in Tidal Waters

D. MAX SHEPPARD

Sediment scour near bridges in tidal waters is discussed. A brief overview of the coastal processes that influence bridge scour is presented and followed by a discussion of the various types of scour. The complexity and unsteady nature of tidal flows complicate the scour processes and make them difficult to predict. Existing scour prediction methods and equations were developed for steady, homogeneous, unidirectional flows that are significantly different from those found in the coastal zone. Some of the unique features of bridge scour in the coastal zone are discussed, and areas in which research is needed are delineated.

This paper discusses sediment scour near bridges in waters that are strongly influenced by astronomical tides. In general, this refers to rivers and estuaries along the coast. Depending on the terrain, range of tide, and river discharge, astronomical tides can have a significant influence many miles inland. For the purposes of this paper, locations where spring tidal currents are at least half of the total current will be considered as tidal waters. Even though this region is defined by the tide, tidal currents are by no means the only coastal process that influences scour at bridges in this area. Such quantities and processes as mass density stratification, water salinity, longshore (sediment) transport, surface waves, and tidal inlet instability can all play a significant role in bridge scour. The closer the location of interest is to the open coast, the larger the influence of these quantities. A brief discussion of how bridge scour is affected by these quantities is presented in this paper.

Sediment scour at bridges spanning inland streams and waterways has been divided into three major categories: (a) local, (b) contraction, and (c) aggradation and degradation. These same classifications can be used for tidal waters even though the scour mechanisms are, for the most part, different.

The paper is organized such that a brief review of the salient coastal processes is followed by a discussion of how these processes affect both the scour and the manner in which it is predicted.

COASTAL PROCESSES

Coastal processes are defined as the hydrodynamic and sediment transport processes that take place on open coastlines and in the adjoining bays, estuaries, river mouths, and tidal inlets. These processes are primarily driven by wind, wind waves, and astronomical and meteorological tides, although mass density stratification can be a forcing function as well as a process-modifying agent.

Coastal and Oceanographic Engineering Department, 336 Weil Hall, University of Florida, Gainesville, Fla. 32611.

Tides

Astronomical tides are the result of gravitational and centrifugal forces between the ocean waters and the sun and planets in the universe, the most significant being the sun and the earth's moon. Components of this tide have many frequencies ranging from 0.857 to 2.90 cycles per day (cpd), but the frequencies of the dominant components are 1.932 (M_2), 2.000 (S_2), 1.076 (O_1), and 1.003 cpd (K_1). Even though they are generated by gravitational and centrifugal forces, these long waves, known as astronomical tides, are influenced by Coriolis accelerations (resulting from the earth's rotation about its axis), shoaling, refraction, diffraction, bottom friction, interaction between different frequencies, and resonance.

Meteorological tides are alterations of the water surface due to wind-generated mass transport in the ocean. These tides are most noticeable during long-duration winter storms and subtropical storms or hurricanes. An interesting aspect of the net wind-driven mass transport in deep water is that it is (according to Ekman's theory) at right angles to the wind direction as a result of Coriolis acceleration. As viewed from above, the net transport is to the right of the wind direction in the northern hemisphere and to the left in the southern hemisphere. These tides and the waves that usually accompany them are agents of mass destruction along the coasts and in the coastal zone.

In this discussion, wind-driven currents are treated separately from meteorological tides even though they are both generated by wind shear on the water surface. Meteorological tides (sometimes called storm surge) are the change in water elevation resulting from the net movement of water by the wind and changes in barometric pressure. Wind-generated currents are the actual water movements that create the changes in water elevation. Both are important in sediment scour processes. For bodies of water connected to the ocean at more than one location, such as bays separated from the ocean by barrier islands, the design conditions for scour could very well be created by wind-generated currents rather than meteorological tides.

Waves

Surface waves play a major role in coastal processes. One convenient way of classifying surface waves is according to their period (or frequency). Table 1 gives such a breakdown ranging in periods for small ripples to the long periods associated with tsunamis (i.e., seismically generated waves) and astronomical tides. As waves propagate through water, the water particles undergo an orbital motion that extends to a depth of approximately half the length of the wave. Therefore,

TABLE 1 Classification of Ocean Surface Waves by Period

Classification	Range of Periods
Ripples	0 sec < T < 1 sec
Chop	1 sec < T < 4 sec
Sea	5 sec < T < 12 sec
Swell	6 sec < T < 25 sec
Surf Beat	1 min < T < 3 min
Tsunamis	10 min < T < 20 min
Tides	6 hr < T < 24 hr

when waves approaching the beach from offshore reach a water depth of less than approximately half their length, they begin to exert an oscillating shear stress on the bottom. This, coupled with a current (generated by any one or more of a number of possible mechanisms), can cause sediment movement.

Perhaps more important, however, are the indirect effects of waves on erosion and deposition of sediment. When large-amplitude swells generated by distant storms (perhaps combined with locally generated sea) approach a sandy beach coastline at an angle, a strong longshore current is generated. This current is bounded by the shore on one side and the edge of the breaker zone on the other. The width of this current can range from tens of meters for a steep-sloped nearshore beach face to a few hundred meters for a flat-sloped beach face. Breaking waves place sediment in suspension and fluidize the bed, enabling the longshore current to transport vast quantities of sand along the coast. This process is known as longshore transport. Estimated net transport rates for the continental U.S. coastline are shown in Figure 1.

The significance here is not so much what is happening along the open coast, but rather what happens to this "river of sand" when it reaches a tidal inlet or a river delta where a bridge might be located. What does happen depends to some degree on the nature of the inlet and bay system and the existence of manmade or natural structures nearby. Consider the so-called unimproved inlet shown as Inlet 2 in Figure 2 (i.e., an inlet that does not have a jetty system or hardened shorelines). During flood tide (flow from the ocean to the bay), a large percentage of the sediment transported along the coast moves into the bay and forms bars and shoals known

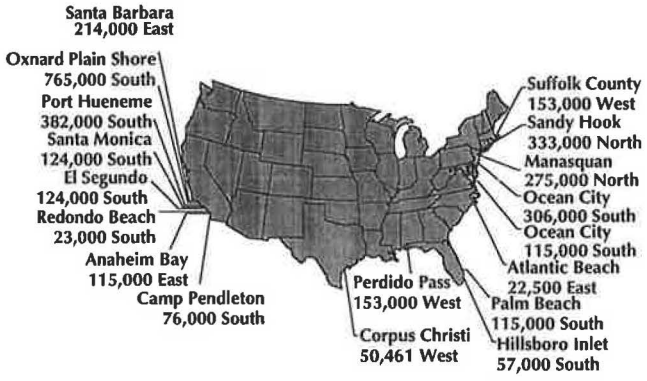

FIGURE 1 Approximate net longshore sediment transport rates along U.S. coastline (m^3/year).

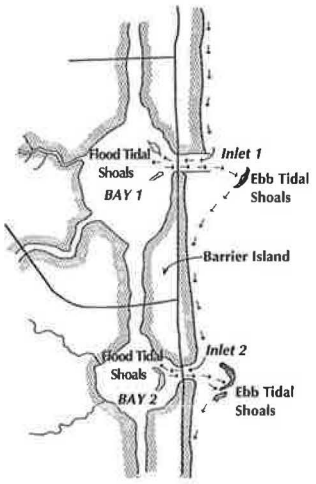

FIGURE 2 Schematic drawing of coastline with barrier islands and tidal inlets.

as flood shoals. Under ebb tide conditions (flow from the bay to the ocean), a portion of the sediment from the flood shoals is transported to offshore or ebb shoals (also shown in Figure 2). From there the sediment is transported to the downdrift shore and on down the coast. When jetties exist (see Inlet 1 in Figure 2) the sediment movement is similar to that for the unimproved inlet except a portion of the sand is trapped by the updrift jetty and there is generally less transport into and out of the inlet.

If on an annual basis there is a net transport in one direction along the coast (due to larger or more persistent waves approaching the coast from that direction), sand will accrete near the updrift jetty and erosion will occur downdrift of the inlet. The significance of these processes on the different types of bridge scour is discussed later in the paper.

Mass Density Stratification

Mass density stratification and salt wedges can have a dramatic effect on the flow in an inlet or coastal channel. This effect can alter both sediment scour and the manner in which scour depths are predicted. Salt wedges occur when the denser and more saline ocean water enters a river mouth or tidal inlet to a bay or estuary where there is significant freshwater runoff (see Figure 3). The interface between the fresh and salt water has a wedge shape, thus the name salt wedge. Typical velocity profiles in the water column through a wedge are shown in Figure 3. Note that with flow reversal in the water column, the depth average velocity can be very small even though the velocity near the bottom (and the bottom shear stress) is large. A local scour prediction based on average velocity for this case would be meaningless.

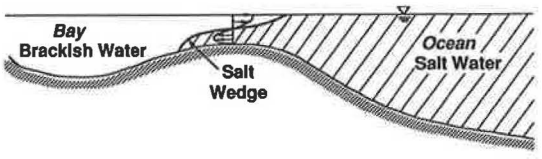

FIGURE 3 Profile of salt wedge.

Salinity

The direct effects of salinity on sediment transport processes can also be significant. This is particularly true when cohesive (fine) sediments are present. The deposition and consolidation of fine sediments is greatly influenced by the ions present in saline water. Thus the "erodible characteristics" of the sediment near bridge piers will be different in saline than in fresh-water systems.

General

Even though a wide range of geological conditions exists around the coast of the United States and each situation is somewhat unique, some general comments about shoreline and inlet stability can be made. Portions of the coast on the eastern continental United States and the Gulf of Mexico are lined with barrier islands. These islands are very dynamic in that they migrate normal to and along (perpendicular to and parallel with) the coast. The tidal inlets that connect the bays and estuaries behind these islands to the ocean or gulf are equally unstable. Despite the unstable nature of barrier islands and their vulnerability to severe storms, many have become heavily populated, thus creating the need for elaborate road systems and bridges in these areas.

Changes in these coastal features take place on time scales that range from hours to hundreds of thousands of years. Even though the long-term (geological time) changes taking place at a particular location are important to the overall understanding of the situation, the changes that will occur over the life of the bridge that are of most interest to the design engineer. This time span is on the order of 60 years.

Armed with an understanding of the geology of the area; local historic charts and maps; aerial photographs; information on planned modifications to the system to which the inlet of interest belongs (in the form of proposed dredging of existing or new channels, reclamation of land, construction of dams on rivers leading into the system, etc.); knowledge of the nature, frequency, and intensity of storms in that area; and output from the appropriate hydrodynamic models, the coastal engineer can estimate with some degree of certainty what the inlet will do over the life of the bridge. This estimate is based on the quantities listed earlier and is, of course, subject to the accuracies of these projections, forecasts, and computations.

All flows in nature are unsteady. Some, however, are more unsteady than others, in both the frequency with which changes occur and the magnitude of the variations. In general, tidal flows undergo much higher frequency changes than inland river flows. In most cases the changes are not only in magnitude but in direction as well. In locations where the maximum tidal currents are sufficiently large, the bottom roughness can undergo large changes during a tidal cycle, ranging from sand ripples to dunes to a flat bed, thus making flow and sediment transport computations much more difficult than for steady flow situations. Also, the duration of extreme events in tidal waters is different than those for inland waters. Figure 4 shows a storm hydrograph for an inland river situation and a computed hurricane storm surge (meteorological tide) for a location on the east coast of Florida. Note the dramatic differences in the rates of rise and fall of water elevation and the overall duration of the events.

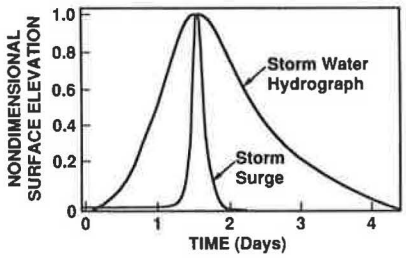

FIGURE 4 Schematic of typical storm water hydrograph and hurricane storm surge.

Another characteristic of tidal inlets that adds to the complexity of the scour processes is the strong tendency for the ebb channel to be different from the flood channel—that is, the dominant flow from the ocean to the bay is at a different location in the inlet channel than the dominant flow from the bay to the ocean. This can result in different phases of tidal flow occurring at the same time at a channel cross section. For example, slack water may exist over a portion of the channel while ebb or flood flow exists over the remainder of the channel. A one-dimensional hydrodynamic model, calibrated for this particular inlet, might give reasonable values for the discharge and the average velocity in the inlet, but using the computed average velocity for local scour prediction may not be appropriate.

LOCAL SCOUR

The processes governing local structure-induced sediment scour due to steady flows are reasonably well understood. Detailed descriptions of these processes can be found in any number of review articles on the subject (*1–9*); therefore, only a brief summary will be presented here.

The conditions under which sediment movement is initiated are not thoroughly understood, but it is generally accepted that movement occurs once the bottom shear stress exceeds a certain value. Bottom shear stress depends on both the mean flow and the level of turbulence near the bottom. Steady flow around a bluff structure that is embedded in the bottom results in several mechanisms that produce bottom shear stress. If the (open channel) flow is fully developed, the boundary layer will reach from the bottom to the water surface. When this flow, whose velocity increases with distance from the bottom, impinges on the structure, a vertical pressure gradient along the leading edge of the structure is formed. This produces a downward flow that results in a vortex that wraps around the structure and trails off downstream. When viewed from above this vortex looks like a horseshoe, thus the name horseshoe vortex.

The flow is also accelerated to higher velocities as it moves around the structure. Once the flow reaches a sharp corner or a region of increasing pressure (i.e., an adverse pressure gradient), flow separation occurs and a wake region forms. Flow in the wake region is more turbulent than the surrounding flow and contains strong vertical vortices that are attached or shed from the structure. All three of these flow mechanisms enhance the bottom shear stress in the neighborhood of the

structure. The complexity of this flow and the associated sediment transport processes have hampered progress in the analytical and numerical treatment of these problems.

These flows are inherently three-dimensional and turbulent and require full three-dimensional turbulent flow equations for their modeling. Even if turbulence (math) models were available for these flows, they would require substantial amounts of supercomputer time for their solution. Recent attempts by the author to explore the possibilities of estimating local scour by combining a three-dimensional laminar Navier-Stokes equation solver with a sediment transport model for the flow in the vicinity of a single vertical pile led to the conclusion that additional research is needed before this approach can be used to solve practical problems. For these reasons much of the success in predicting local scour depths (and volumes) has been with empirical equations.

Empirical equations have been invaluable to engineers over the years in providing tools for analyzing complex situations before analytical and computational models could be developed. They are, however, very dependent on the data used in their creation and as such not easily extended to situations different from those for which they were developed. Care must be exercised in using empirical local scour prediction equations—which are based primarily on steady, homogeneous flow laboratory data—for unsteady tidal flow situations.

The duration of hurricane storm surges is much shorter than river flood hydrographs (see Figure 4). The effect of this time difference on local and contraction bridge scour is not known since there are very few data on rates of scour (*1*,*5*,*10*). Because the duration of scour-producing events for most inland rivers is longer than the time to reach equilibrium, there has been little interest in scour rates in the past. Shen (*1*) plotted data from Chabert and Engeldinger (*11*) on coordinates of velocity squared (V^2) versus time to reach 75 percent of maximum scour depth. Even though there is considerable scatter in the data, the plot does show that the rate of scour increases with decreasing grain size. Baker found that the time required to reach equilibrium scour depth increased as the velocity was increased to the transition from clearwater to live bed conditions, then decreased as the velocity was increased further (*5*). Clearly, more data and analysis on the time dependency of scour, especially in reversing tidal flows, are needed.

Those responsible for specifying the local scour design equations wisely have made them conservative to account for uncertainties in the equations and the input data. As long as sufficient care is taken in arriving at the input quantities, these equations should be used in tidal waters until questions regarding their applicability to these conditions are resolved. It is likely, however, that these equations will prove to be too conservative for most coastal situations.

CONTRACTION SCOUR

Contraction scour occurs in erodible inland rivers and streams when there is a natural or manmade obstruction to the flow. When a bridge causes the obstruction, it usually means that under flood conditions the river is out of its banks upstream and perhaps downstream of the obstruction but is forced into the main channel at the bridge. Channel scour will occur at the bridge until the sediment transport entering the bridge cross section equals that leaving the section. The flow driving mechanism at the bridge is the water elevation difference (i.e., the head difference) across the bridge. The water elevation upstream of the bridge will simply rise until the velocity and cross section are such that the river discharge is accommodated.

Once the river overflows its banks, the width of the stream usually increases rapidly (i.e., the area adjacent to the main channel is usually relatively flat and in many cases vegetated). This means that velocities in the overbank flow region are smaller than in the main channel, resulting in little or no sediment transport in that part of the flow. With the increased flow velocities at the bridge and the sediment transport into that section coming primarily from the main channel upstream, scour at the bridge will occur until sediment transport equilibrium is reached—that is, when the sediment transported out of the bridge area equals that entering the region. Larsen's equation (*12*,Ch.4) appears to either directly or indirectly take most of these mechanisms into consideration for this flow situation.

In tidal waters, where the design storm event is usually produced by a hurricane storm surge, the situation is somewhat different. Unlike the design flood condition, the ocean water level at the inlet is essentially unaffected by the flow through the inlet (i.e., the ocean water level is only slightly modified by the presence of the inlet). Therefore, at least during the flood stage, the head difference across the bridge and average velocity are limited by the storm surge height, not by the obstruction. For the inland river situation the head difference and velocity will increase with increasing constriction until the hydrograph peaks or overtopping occurs.

The quantity of bedload and suspended sediment entering the inlet during the flood phase of a severe storm event can be substantial (due to large longshore transport). This can have a major impact on local as well as contraction scour by modifying the near-bottom flow and shear stress and, because of the high sediment concentrations, the ability of the flow to transport additional sediment.

AGGRADATION AND DEGRADATION SCOUR

Aggradation and degradation result from channel movement in the vicinity of the bridge. In general, the bridge plays only a minor role in this process. This is not to say that under certain circumstances the bridge will not retard or accelerate the migration, but for the most part it is a separate process driven by mechanisms unrelated to the bridge. In tidal waters aggradation and degradation occur when (a) the deeper channels in a bay or estuary migrate as a result of natural or manmade alterations to the system, and (b) tidal inlets become unstable.

The term "system" is used here to denote bodies of water along the coast connected by rivers, navigation channels, and such. These bodies are usually connected to a gulf or ocean by one or more tidal inlets. For a location to be part of the system associated with a particular point of interest, a physical alteration at the location must result in a measurable physical change at the point of interest. For example, the system associated with a bridge connecting the mainland to a barrier

island might include the bay spanned by the bridge, rivers, and streams running into the bay, a manmade navigation canal connecting this bay with the adjoining bay, and the two or more tidal inlets connecting these bays to the ocean. Modifications of the system that influence aggradation and degradation at the bridge in question include dredging of an inlet or canal, addition of a marina in one of the bays, dredging of finger canals for a housing development, reclamation of land to extend a runway for an airport, changes in land use that affect runoff in the bays and rivers, coastal construction in the bays and at the inlets (seawalls, revetments, bulkheads, jetties, groins, etc.), and construction of other bridges.

SEDIMENT SCOUR DESIGN CRITERIA

In some types of structural design not much emphasis is placed on environmental design conditions (i.e., on the prediction of the loading on the structure due to the environment). Sometimes this is completely justified, because other types of loading far exceed the anticipated environmental loads. In other situations this lack of emphasis appears to stem from a lack of appreciation for the possible magnitude of these loads. The return interval for design events—say, 50, 100, or even 500 years—makes it unlikely that the design engineer has personally experienced such conditions in his or her lifetime. Thus, the loading predicted for such an event may appear to be unreasonable when in fact it may be correct.

On the other hand, sufficient resources, time, and effort must be devoted to establishing accurate environmental design criteria to ensure that they neither under- nor overpredicts design load conditions. Overprediction can result in unnecessary construction costs that are orders of magnitude greater than the costs of studies needed to establish more accurate design criteria. Underprediction is more rare but can be costly as well in terms of risk to lives and property.

The offshore industry (consisting primarily of the major oil companies) spends large sums of money each year for environmental data collection and analysis, sophisticated analytical and computer model development and execution, elaborate wind, wave, and current hindcast and laboratory testing, all for the purpose of establishing environmental design criteria for near- and offshore locations around the world. Sediment scour near bottom-mounted structures in bays and in the more shallow waters on continental shelves is one of the design parameters examined. Sediment scour in tidal waters is a difficult quantity to predict for the reasons just given. The methods used for predicting bridge scour for inland rivers and waterways may not be sufficient for tidal waters because of the complexity of the flows, the effects of waves, density stratification, longshore transport, wind-generated currents, and so forth.

A general methodology should be developed that applies to the wide range of conditions found in the coastal zone around the United States. The weighting and details of the various procedures would vary with the local geology, sediment types, tidal range, nature of extreme storm events, and so on, but the basic approach would be the same. This approach could benefit from techniques developed by the offshore industry over the past 20 years. The resulting product could be a procedures manual that outlines the processes that must be considered. The procedures might start with a determination of whether sediment scour is possible. If an erodible substrate is present and scour is deemed possible, then the procedures manual would guide the user through the necessary steps to obtain design scour depth predictions. In most if not all cases, the prediction of local and contraction scour would include the application of the appropriate computer flow models. The particular model needed will change depending on the local conditions, but for particular situations the guidelines can address the procedures that the model should include. If the location and conditions are such that surface waves are important, then they must be predicted as well. Local scour prediction, at least for now, needs to use the appropriate empirical scour relationships that have been and are being developed from laboratory experiments. The prediction of inlet instability and channel migration (aggradation and degradation scour) requires a rather complex analysis based on information and data produced by a variety of computer programs, historical charts and photographs, projected construction and activities in the area, and the like.

SUMMARY AND CONCLUSIONS

In summary, the environmental conditions in tidally influenced waters can be significantly different from those in inland streams and waterways. The effects of reversing flows, density stratification, longshore sediment transport, waves, inlet instability, short duration, and rapidly changing storm hydrographs, among other characteristics, on bridge scour in this zone can be great. Present scour prediction schemes and formulas were not developed for these conditions and as such may not be applicable. These equations are, however, designed to give conservative estimates of scour depths and therefore should be used in the coastal zone until questions about their appropriateness for these conditions have been resolved. As pointed out, it is more likely that further research will prove them to be too conservative in their predictions for most situations found in the coastal zone.

A field measurement program that is well-conceived and -executed is needed to obtain the data required to test existing scour prediction techniques and equations and develop new approaches and equations where needed. The payoff for the greater emphasis on the development of environmental design criteria will be better, safer, and more efficiently designed bridges that require less maintenance.

ACKNOWLEDGMENTS

The author would like to thank Shawn McLemore and Kenneth Weldon with the Florida Department of Transportation for funding a portion of the research covered in this paper.

REFERENCES

1. Shen, H. W., V. R. Schneider, and S. S. Karaki. *Mechanics of Local Scour*. Report CER 66 HWS-VRS-22. Structures and Applied Mechanics Division, Office of Research and Development, Bureau of Public Roads, U.S. Department of Commerce (Contract CPR11-8022); Colorado State University, Fort Collins, 1966.

2. Shen, H. W., V. R. Schneider, and S. S. Karaki. Local Scour Around Bridge Piers. *Journal of the Hydraulics Division*, ASCE, Paper 6891, Vol. 95, HY6, 1969, pp. 1919–1940.
3. Carstens, M. R. Similarity Laws for Localized Scour. *Journal of the Hydraulics Division*, ASCE, Paper 4818, Vol. 92, HY2, 1966, pp. 13–36.
4. Breusers, H. N. C., G. Nicollet, and H. W. Shen. Local Scour Around Cylindrical Piers. *Journal of Hydraulic Research*, Vol. 15, No. 3, 1977, pp. 211–252.
5. Baker, C. J. *Vortex Flow Around the Bases of Obstacles*. Ph.D. dissertation. University of Cambridge, 1978.
6. Arkhipov, G. A. Consideration of Sediment Transport When Calculating Local Scour. *Gidrotekhnicheskoe Stroitel'Stvo* (*Hydrotechnical Construction*), Vol. 18, No. 4, 1984, pp. 149–153.
7. Jones, J. S. Comparison of Prediction Equations for Bridge Pier and Abutment Scour. In *Transportation Research Record 950*, TRB, National Research Council, Washington, D.C., 1984.
8. Raudkivi, A. J. Functional Trends of Scour at Bridge Piers. *Journal of Hydraulic Engineering*, Vol. 112, No. 1, 1986, pp. 1–13.
9. Sheppard, D. M., A. W. Niedoroda, and A. Karunamuni. Structure-Induced Seafloor Scour. *Proc., Offshore Technology Conference*, Paper 6366, 1990, pp. 213–222.
10. Kothyari, U. C., R. C. J. Garde, and K. G. Raju. Temporal Variation of Scour Around Circular Bridge Piers. *Journal of Hydraulic Engineering*, ASCE, Vol. 118, No. 8, 1992, pp. 1091–1106.
11. Chabert, J., and P. Engeldinger. Etude des affouillements autour des piles de ponts (in French). *Lab. Nat. d'Hydr. Chatou,* 1956.
12. Richardson, E. V., L. J. Harrison, and S. R. Davis. *Evaluating Scour at Bridges*. FHWA-IP-90–017. FHWA, U.S. Department of Transportation, 1991.

Tidal Inlet Bridge Scour Assessment Model

MARK S. VINCENT, MARK A. ROSS, AND BERNARD E. ROSS

The undermining of bridge facilities constructed in tidal inlets is a common problem. Scour mechanisms in tidal inlets are often combinations of local contraction and regional tidal inlet dynamics. A numerical model for quantitatively evaluating and assessing the scour and deposition magnitudes associated with contraction and inlet geomorphological changes has been developed. The model uses a two-dimensional, dynamic numerical hydraulic model coupled to movable bed sediment scour and deposition subroutines developed specifically for this need. The model provides for subgrid features such as pier piles, as well as limited inhomogeneity in sediment grain size. A simplistic representation for armoring associated with sediment sorting is also provided. Initial application to Johns Pass in west-central Florida indicates reasonable comparisons between model predictions and observations of scour and deposition in the pass, warranting additional testing of this approach.

Tidal inlet stabilities are influenced by extremely complex hydrodynamics and sediment dynamics. These processes may act on nearfield or farfield spatial scales, as well as on event or continuous time frames. Of paramount concern to bridge hydraulic engineers is the resulting scour and deposition processes near proposed or existing bridge pilings. In severe cases, local, contraction, and geomorphological driven scour may undermine bridge pilings, thereby resulting in structural failure.

The University of South Florida Center for Modeling Hydrologic and Aquatic Systems (USF/CMHAS) is involved in research to develop and refine a numerical model that will help engineers make decisions about situating and designing new bridges and maintaining and replacing existing structures.

METHODOLOGY

The foundation of this method was a two-dimensional, finite difference, explicit hydraulic model (referred to here as "hydraulic model") previously developed for coastal studies at USF/CMHAS (*1*). After an extensive review of applicable sediment transport theories and hydrodynamic needs, appropriate subroutines for determining wave-current interactions, sediment scour, transport, and deposition were developed and coupled to the model. This permutation of the original hydraulic model, which integrates both the hydrodynamics and sediment dynamics of tidal inlets, will be called the USF/CMHAS scour model.

Department of Civil Engineering and Mechanics, University of South Florida, 4202 East Fowler Avenue, ENG 118, Tampa, Fla. 33620.

The basic hydraulic equations of the USF/CMHAS scour model are developed from the Navier-Stokes equations for incompressible viscous flow, extended to turbulent flow using first-order closure techniques. Applying assumptions for shallow, well-mixed water bodies, the differential equations developed for this model are the vertically integrated equations of motion and continuity, which can be stated as follows:

- Vertically integrated equations of motion:

$$\frac{\partial U}{\partial t} + \frac{\partial\left(\frac{U^2}{d}\right)}{\partial x} + \frac{\partial\left(\frac{UV}{d}\right)}{\partial y} - \Omega V = -\frac{1}{\rho_w} d \frac{\partial P}{\partial x} - gd\frac{\partial H}{\partial x} + X - \rho_w \frac{f|Q|U}{d^2} \quad (1)$$

$$\frac{\partial V}{\partial t} + \frac{\partial\left(\frac{V^2}{d}\right)}{\partial y} + \frac{\partial\left(\frac{UV}{d}\right)}{\partial x} + \Omega U = -\frac{1}{\rho_w} d \frac{\partial P}{\partial x} - gd\frac{\partial H}{\partial y} + Y - \rho_w \frac{f|Q|V}{d^2} \quad (2)$$

- Vertically integrated continuity equation:

$$\frac{\partial H}{\partial t} = -\frac{\partial U}{\partial x} - \frac{\partial V}{\partial y} + R \quad (3)$$

where

U = vertically integrated flow per unit width in x-direction,
t = time variable,
d = depth of water,
x = southward coordinate direction,
V = vertically integrated flow per unit width in y-direction,
ρ_w = density of water,
P = atmospheric pressure,
y = eastward coordinate direction,
Ω = Coriolis factor,
g = acceleration due to gravity,
H = height of tide above mean low water used in equations of motion,
X = x-component of wind stress per unit mass of water,
f = friction factor,
Q = fluid transport per unit width,

Y = y-component of wind stress per unit mass of water, and
R = sources and sinks of water.

Employing a grid-based finite difference approach and applicable boundary conditions, the three equations can be discretized to algebraic expressions that can be explicitly solved to describe the water surface elevation and U and V transports (discharges per unit width) as functions of time and spatial position. As with other models of this type, proper model calibration must occur with each application.

One advantage of the USF/CMHAS scour model is the provision for subgrid features required for evaluating bridge pier management alternatives (*1*). The model allows for the incorporation of features considerably smaller than the grid dimension, such as bridge piers, bascules, and small channels.

The contribution of waves to the tidal inlet system is incorporated into the model through subroutines employing the equations from the popular linear or airy wave theory. Discussions of the equations and logic by which the scour model solves for wave heights, lengths, orbital dimensions, and velocities can be found in work by Vincent and Ross (*2*) and Vincent (*3*).

In addition to fluid velocities, sediment transport equations are also a function of the shear stress at the bed, which in turn is a function of the combined friction factor at the bed. The scour model determines the friction due to currents and the friction due to waves following the approaches of Manning-Strickler (*4*) and Swart (*5*). From these two terms the combined friction factor can then be found using the method of Jonsson (*6*). These equations are

$$f_c = 0.122\left(\frac{k_s}{d}\right)^{1/3} \tag{4}$$

$$f_w = .00251 \exp^{\left[5.21\left(\frac{\zeta}{k_y}\right)-0.19\right]} \tag{5}$$

$$f_{cw} = \frac{u_c f_c + u_b f_w}{u_c + u_b} \tag{6}$$

where

f_c = current friction factor;
k_s = Nikuradse roughness number;
f_w = wave friction factor;
ζ = wave excursion number;
f_{cw} = combined friction factor due to currents and waves;
u_c = depth-integrated velocity, unidirectional current magnitudes at bed; and
u_b = wave orbital velocity at bed.

Once the combined friction factor due to waves and currents has been determined, the combined shear stress at the bed is calculated by the quadratic stress law as

$$\tau_{cw} = \frac{\rho f_{cw} u_{cw}^2}{2} \tag{7}$$

where τ_{cw} is the shear stress due to currents and waves and u_{cw} is the resultant velocity due to currents and waves.

A comprehensive screening and literature review of applicable sediment transport equations was conducted to ensure the selection of a competent and tested method for the scour model. Consistently ranked as among the most accurate in investigations was the Engelund and Hansen equation (*7*). This approach was selected because of its consistent performance in laboratory and field tests, as well as success in tidal inlet modeling endeavors by Ross (*8*) and Zarillo and Park (*9*). The total sediment load can be expressed by the Engelund and Hansen equation as

$$q_t = 0.05\, u_c^2 \left[\frac{D_{50}}{g(S_s - 1}\right]^{1/2} \left[\frac{\tau_{cw}}{(\rho_s - \rho_w)gD_{50}}\right]^{3/2} \tag{8}$$

where

q = fluid transport per unit area,
D_{50} = sediment grain diameter such that 50 percent of bed material is finer,
S_s = density of sediment relative to water, and
ρ_s = density of sediment.

The scour model uses a series of tests to determine the condition of transport or deposition within each grid. One of the principal methods applied by the code is the Hjulstrom curve, which provides a graphical relationship of the velocities needed for erosion, transport, and deposition, as a function of grain size (*10*).

A second test for potential scour is conducted by the equilibrium depth promoted by Bruun (*11*). This test, which is also used in the Corps of Engineers HEC 6 model, can be expressed as

$$d_{EQ} = \left[\frac{q}{10.21 D_{50}^{1/3}}\right]^{6/7} \tag{9}$$

where d_{EQ} is the maximum depth at which scour can occur for given grain size and flow condition.

The model also allows for the natural armoring of the inlet bed due to nonhomogeneous sediments following the method of Borah (*12*) as

$$T_{AL} = \frac{D_{AR}}{(1 - \varepsilon)F_{AR}} \tag{10}$$

where

T_{AL} = thickness of active layer of sediment bed,
D_{AR} = grain size of bed armoring material,
ε = porosity of bed sediment, and
F_{AR} = fraction of armor material.

In this approach, T_{AL} is defined as the active layer, which is the allowable depth of scour expressed as a function of the porosity, size, and fraction of armor size sediment.

At specified time increments, a continuity equation relates the volumetric rate of transport to the change in bed depth over time following

$$\frac{\partial q_{sx}}{\partial x} + \frac{\partial q_{sy}}{\partial y} = -(1 - \varepsilon)\frac{\partial z}{\partial t} \tag{11}$$

where

q_{s_x} = sediment transport flux in x-direction,
q_{s_y} = sediment transport flux in y-direction, and
z = vertical coordinate direction.

Boundary conditions and input data used by the scour model include initial bathymetry, tidal driving function at the open water boundaries, wind speeds and directions, offshore wave conditions, sediment characteristics, and specification of subgrid features. Model output includes arrays of all pertinent data (i.e., bathymetry or scour depths, velocities, etc.) at user-specified time increments.

A flow chart depicting the order of analysis used in the scour model is provided in Figure 1.

APPLICATION

To date, the USF/CMHAS scour model has been employed in several tidal inlet engineering investigations, including a bridge and channel design study for Clearwater Pass (*8*) and a bridge maintenance and replacement study for Johns Pass (*2*). Both of these inlets are located along littoral drift shorelines of the west-central coast of Florida. The application to Johns Pass will be discussed briefly in this paper.

In 1971 the new Johns Pass Bridge connecting Treasure Island and Madeira Beach was completed. As early as 1976, Florida Department of Transportation (FDOT) officials noted severe scour in the vicinity of the bridge. By 1984 the tips of three of the pilings, which had been driven 6.1 m (20 ft) below the original bed, had become exposed; others were within 1 m (1 to 2 ft) of exposure. In attempts to stabilize the bridge pilings and the surrounding bed, FDOT installed additional crutch pilings, fenders, and riprap rubble. Subsequent monitoring has indicated that these improvements may have further aggravated the scour conditions at the bridge. As of 1987 the bed beneath the bridge was eroding at an annual rate of 0.5 m (1.5 ft).

The objective of the Johns Pass investigation was to explore the cause of existing scour problems, the intensity and maximum extent of the present scour condition, and possible remediation alternatives. No attempt was made to explore the behavior of the inlet associated with a particular design magnitude return storm, but this would be an additional and useful application of the model.

For the Johns Pass Bridge scour investigation, 14 existing and hypothetical conditions were modeled.These were composed of combinations of two distinct seasonal scenarios, average winter-spring and summer-fall conditions, coupled with seven different structural alternatives described as follows:

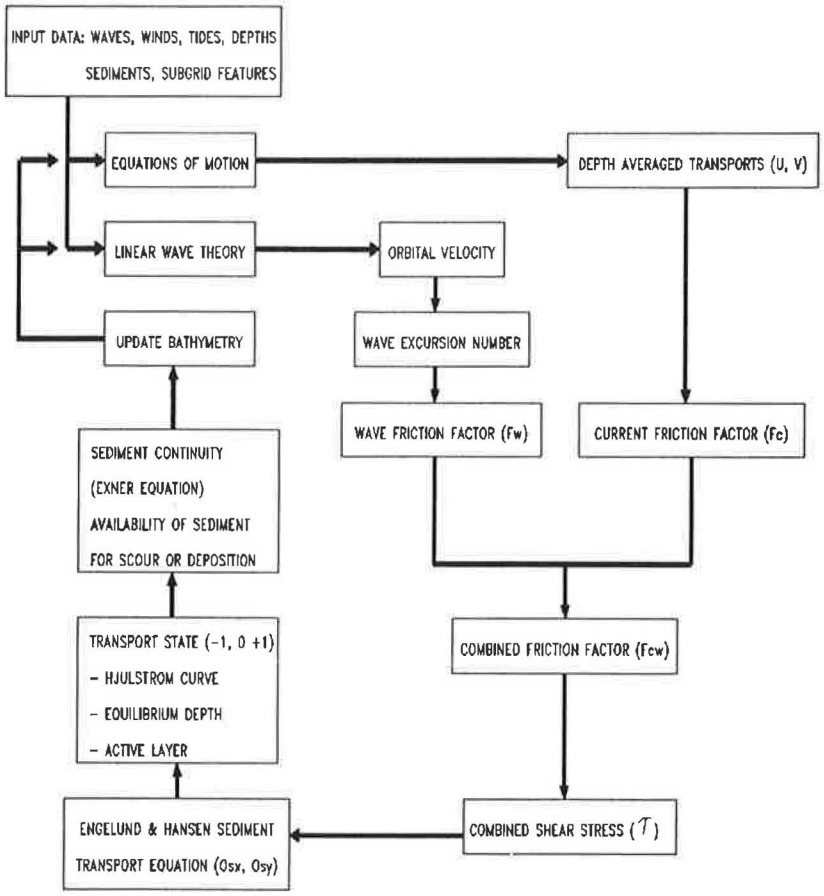

FIGURE 1 Flow chart of scour logic and equations.

1. No build: this model test was designed to obtain a baseline magnitude of existing scour rates if no improvements were implemented.
2. Future scour (future depths): existing depths were increased in accordance with the observed trends to determine if the scour rate significantly diminishes as the cross section deepens.
3. Addition of southern bent: this configuration evaluates the effectiveness of continuing the present course of remedial action of installing crutch bents when pile structural integrity is threatened.
4. Removal of all pilings: an unreasonable remedial alternative that is only of academic interest in evaluating the overall contribution of the bridge profile on the inlet geomorphology.
5. Removal of southern pilings: also a largely academic alternative, nevertheless one that is of interest because of the proximity and persistence of the south scour hole.
6. Half armor: there has been a casual discussion of armoring the inlet throat near the persistent scour hole along the southern half of the bridge. This alternative is easy to evaluate in the model but would require many other considerations.
7. Full armor: this condition is similar to the half-armor run condition but would continue completely across the inlet. It is also highly unlikely to implement successfully and very unpopular with other agencies.

A 10 × 15 array of grids 30.5 m² (100 ft²) was developed to simulate Johns Pass. This configuration covers the entire inlet from the Gulf of Mexico to Boca Ciega Bay. The grid size was selected as the optimum to provide both the necessary detailed resolution of critical areas as well as to allow reasonable computation time. By the Courant-Fiedrich-Levy stability criteria, a time step of 1.5 sec was selected. The inlet bathymetry and subgrid features (bridge bascules, pilings, and crutchbents) are depicted in Figures 2 and 3, respectively.

RESULTS

One of the key sets of output data from the scour model is the DELZB arrays, which contain the net bottom elevation change from scour or deposition within each individual grid of the model during the course of a run. From this information, sediment dynamic trends along various portions of the bridge structure can be identified.

To aid in the interpretation of this information, data from the DELZB arrays were converted into inlet cross sections along the bridge centerline. These centerline stations were selected to coincide with approximate centers of model grids beneath the bridge. Beginning at the southern revetment, the stations proceed northeast at locations of 0, 15, 52, 91, 128, 159, 195, and 213 m (0, 50, 170, 300, 420, 520, 640, and 700 ft). Of particular interest to this study were the data from

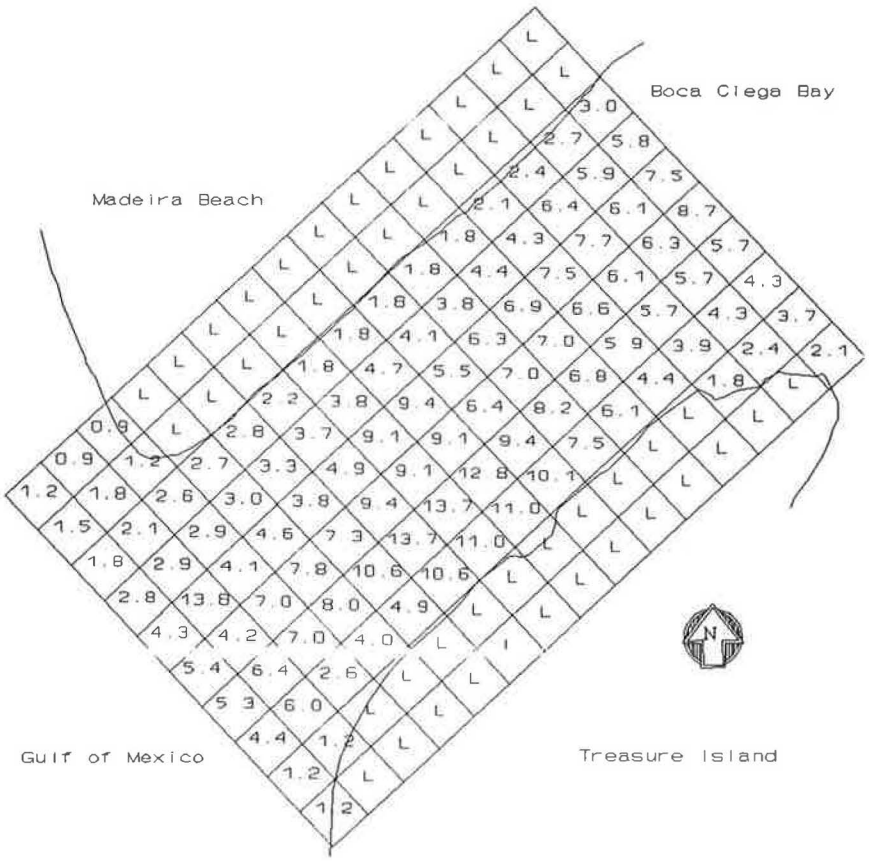

FIGURE 2 Johns Pass grid depths (m).

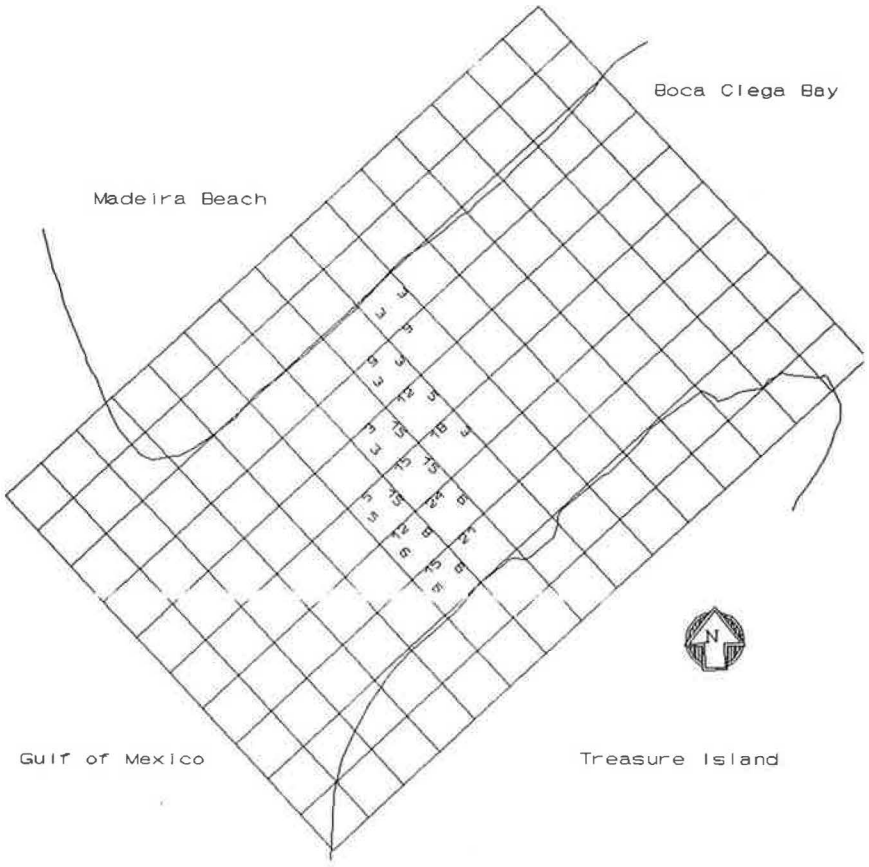

FIGURE 3 Johns Pass subgrid features (m).

Station 52, which is the deepest area beneath the bridge, with depths of 13.7 m (45 ft), and a location of persistent scour presence.

Given the constraints of even the most prominent sediment transport equations (7), the model results should be interpreted as scour-deposition trends (versus absolute rates), perhaps only within an order of magnitude in absolute accuracy. Furthermore, extrapolation of such rates should be done with caution, inasmuch as during extended time periods, bottom areas may become structurally or hydraulically stable (e.g., via deposits of natural shell lag, erosion down to strongly cohesive sediment or hardened bedrock, or reduced shear stress from deepening).

Figure 4 illustrates extrapolated results from two combined run scenarios: winter-spring and summer-fall conditions with the no-build option, as an example of model utility. Figure 5 summarizes the annual scour and deposition rates from all seven structural configurations.

DISCUSSION OF RESULTS

The bridge over Johns Pass has been seen to experience seasonal and annual variability in scour magnitude, with definite long-term trends toward increasing depths next to the southern bascules and nearby pier foundations. Application of the model using seasonal average conditions of summer quiescent periods followed by winter storms indicates that the order of magnitude of the scour rates and location are in general agreement with observed conditions. Scour depths of several feet per year under normal conditions have been observed and are predicted by the numerical model. As pointed out previously, many support piles at the Johns Pass Bridge have been undermined and a problem persists in the south span. The problem appears to be largely a result of contraction scour associated with the placement of the bridge and especially with the relatively large (10-m diameter) bascule support structures.

Preliminary runs with the model using estimated, extrapolated bathymetry—including up to 1.5 m (5 ft) of deepening—suggests that the present scour rates will continue at approximately the same rate. Bottom armoring scenarios indicated that the location of scour would merely shift immediately adjacent to the armor mats, and the scour rate could intensify, thereby potentially undermining the armor. In this regard the armoring of the inlet beneath the bridge does not appear to be a prudent alternative.

SUMMARY AND RECOMMENDATIONS

The potential utility of this model for tidal inlet scour assessment was demonstrated through application to the Johns Pass Bridge in Pinellas County, Florida. Simulations of 14 distinct seasonal and structural scenarios were conducted to evaluate the present and future scour deposition trends in areas of severe erosion along the bridge pilings. The simulated

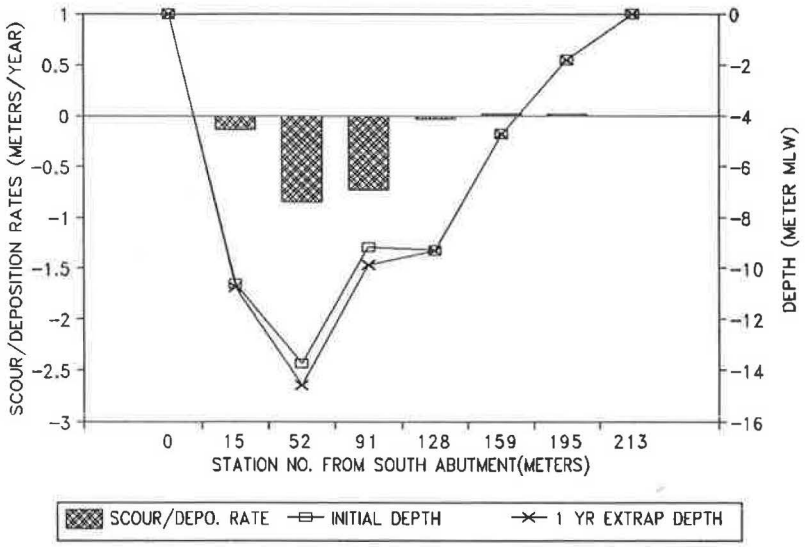

FIGURE 4 Annual no-build scenario.

hydrodynamics and sediment dynamic trends for existing conditions were in general agreement with documented observations, supporting further testing of this approach.

To date, the USF/CMHAS scour model has shown promise as a beneficial design and management tool for engineering evaluation of bridge scour and deposition in tidal inlets. However, the extreme complexity of sediment transport in coastal systems warrants continued aggressive research in both the laboratory and the field.

Unfortunately, many of the model components, although acceptable approaches for specific applications, were predicated on experiments using small flumes with conditions of uniform sediment grains, plain beds, and uniform steady flow. Moreover, most friction and shear stress equations as yet do not consider the compounding effects of sediment in motion.

An urgent need is seen here for model improvements to incorporate the transport of graded sediments, as well as spatial and temporal variability in sediment mixtures, bed forms, and bed armoring. Another potentially important feature that would complement the contraction scour processes that the model now handles would be the incorporation of equations for predicting subgrid local scour due to separation.

Although considerable theoretical and modeling improvements are needed, the USF/CMHAS scour model shows merit as a tool to be used in management and design studies as well as a vehicle for understanding basic processes and responses of tidal inlets.

The Fortran 77–based program runs on high-speed minicomputers as well as the desktop personal computers used in most engineering consulting and research facilities.

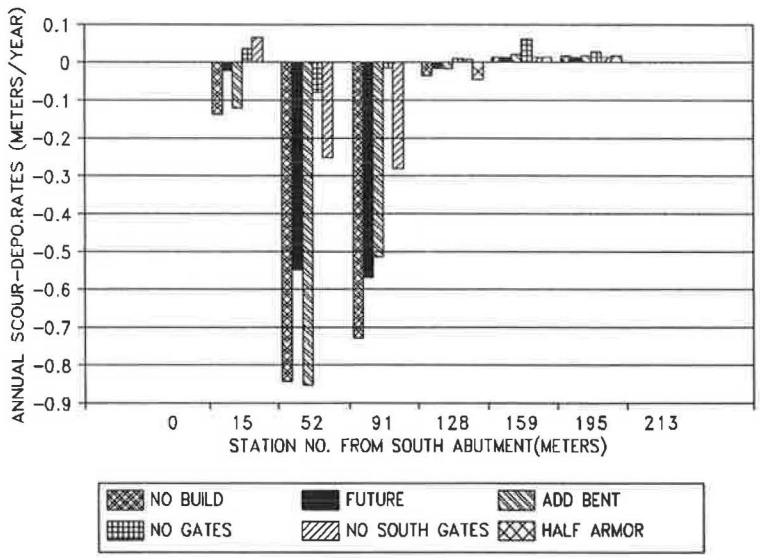

FIGURE 5 Comparison of annual scour rates.

ACKNOWLEDGMENTS

The authors gratefully acknowledge FDOT for funding this research and especially coauthor Bernard E. Ross for his leading role in the development of the USF/CMHAS hydraulic and scour models.

REFERENCES

1. Ross, B. E., and M. A. Ross. An Engineering Analysis of Sedimentation in Tidal Inlets. In *HydraulicEngineering 1991*, ASCE, Nashville, Tenn., 1991, pp. 1114–1119.
2. Vincent, M. S., and M. A. Ross. *Johns Pass Bridge Scour Assessment Model*. Center for Modeling Hydrologic and Aquatic Systems, University of South Florida, Tampa, 1992.
3. Vincent, M. S. *A Numerical Scour Deposition Model for Tidal Inlets*. Master's thesis. University of South Florida, Tampa, 1992.
4. Henderson, F. *Open Channel Flow*. Macmillan Company, New York, 1966.
5. Swart, D. H. Predictive Equations Regarding Coastal Transports. *Proc., 15th Coastal Engineering Conference*, ASCE, Honolulu, Hawaii, 1976.
6. Jonsson, I. G. Wave Boundary Layers and Friction Factors. *Proc., 10th Conference on Coastal Engineering*, ASCE, Tokyo, Japan, 1966, pp. 127–148.
7. Sleath, J. F. A. *Sea Bed Mechanics*. John Wiley & Sons, New York, 1984.
8. Ross, B. E., and M. A. Ross. *Clearwater Pass Study*. Hydrosystems Associates, Tampa, Fla., 1990.
9. Zarillo, G. A., and M. J. Park. Sediment Transport Prediction in a Tidal Inlet Using a Numerical Model: Application to Stony Brook Harbor, Long Island, New York, USA. *Journal of Coastal Research*, Vol. 3, No. 4, 1987, pp. 429–444.
10. Herbich, J. B., R. E. Schiller, R. K. Watanabe, and W. A. Dunlap. *Seafloor Scour: Design Guidelines for Ocean-Founded Structures*. Marcel Dekker, Inc., New York, 1984.
11. Bruun, P. *Stability of Tidal Inlets, Theory and Engineering*. Elsevier Scientific Publishing Company, Amsterdam, The Netherlands, 1978.
12. Borah, D. K. Scour Depth Prediction Under Armoring Conditions. *Journal of the Hydraulic Division*, ASCE, Vol. 115, No. 10, New York, 1989, pp. 1421–1425.

U.S. Army Corps of Engineers Riprap Design for Flood Channels

STEPHEN T. MAYNORD

The U.S. Army Corps of Engineers riprap design guidance for flood channels is presented, and the limitations and basis of several empirical coefficients are discussed. The method is based on depth-averaged velocity rather than shear stress, which was the basis of the previous guidance. The effects of bends, blanket thickness, side-slope angle, particle shape, and gradation on riprap stability are addressed in the design guidance.

The U.S. Army Corps of Engineers guidance for design of riprap in flood control channels is found in Engineer Manual (EM) 1110-2-1601 (*1*). This guidance is a departure from the traditional guidance based on shear stress or tractive force and uses a procedure based on local depth-averaged velocity. Although the new method can be derived from a modification of the shear stress equations, it does not use shear stress explicitly. Local depth-averaged velocity was adopted primarily because local shear stress is difficult to visualize, compute, and measure. Various methods, discussed in this paper, are available for estimating depth-averaged velocity. The objective of this paper is to provide assistance in application of the new procedure. Limitations of the method and several example problems will also be presented.

BASIC EQUATION

The basis and derivation of the basic equation used to determine stone size can be found in works by Maynord (*2*,*3*) and Maynord et al. (*4*). From EM 1110-2-1601 (*1*) the equation for determining stone size is

$$D_{30} = S_f C_S C_v C_T d \left[\left(\frac{\gamma_w}{\gamma_s - \gamma_w} \right)^{1/2} \frac{V}{\sqrt{K_1 g d}} \right]^{2.5} \quad (1)$$

where

D_{30} = riprap size of which 30 percent is finer by weight (for some gradations, use D_r);
D_r = $D_{85}(\text{min})[D_{15}(\text{min})^2]$;
S_f = safety factor (minimum = 1.1);
C_S = stability coefficient for incipient failure, thickness = $1D_{100}$(max) or $1.5D_{50}$(max), whichever is greater (D_{85}/D_{15} = 1.7 to 5.2),
= 0.30 for angular rock, and
= 0.375 for rounded rock [note: EM (*1*) is incorrect, giving 0.36];
D_{85}/D_{15} = gradation uniformity coefficient;
C_V = vertical velocity distribution coefficient,
= 1.0 for straight channels inside of bends,
= 1.283 − 0.2 log (R/W) for outside of bends (1 for $R/W > 26$),
= 1.25 downstream of concrete channels, and
= 1.25 at end of dikes;
R = centerline radius of curvature of bend;
W = water-surface width at upstream end of bend;
C_T = blanket thickness coefficient (see Figure 1);
d = local depth of flow;
γ_w = unit weight of water;
γ_s = unit weight of stone;
V = local depth-averaged velocity;
K_1 = side-slope correction factor; and
g = gravitational constant.

The power of 2.5 in this equation was based on laboratory data from straight, tilting flumes. The extreme values of the power in Equation 1 are from 2 to 3. A power of 2 results in the Isbash equation (no dependence on depth) and is generally used when there is no boundary layer development. A power of 3 results from application of existing shear stress and the Manning-Strickler equations and represents the condition of completely developed boundary layer and a relative roughness (roughness size/depth) that is low enough to yield a constant Shields coefficient. Because most bank and channel riprap protection problems fall somewhere between these two extremes, the 2.5 power was adopted for all bank and channel riprap protection problems, not just the straight, tilting flumes from which it was derived.

INPUT/OUTPUT DESCRIPTION AND LIMITATIONS

General

The method described herein is limited to what is normally referred to as "low turbulent flow": the method is applicable to sizing riprap in rivers and channels except those immediately downstream of hydraulic structures that create highly turbulent flow. Data used in the development of this method were limited to slopes less than or equal to 2 percent. Data are also limited to $D_{30}/d \geq 0.02$, which means that the method has not been verified for relatively deep flows.

U.S. Army Engineer Waterways Experiment Station, 3909 Halls Ferry Road, Vicksburg, Miss. 39180-6199.

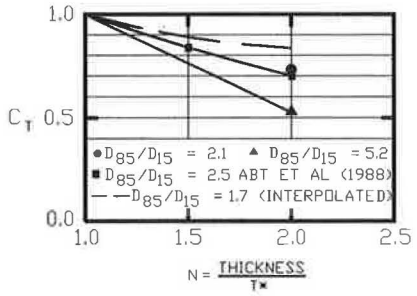

WHERE C_T = CORRECTION FOR THICKNESS

$= \frac{D_{30} \text{ FOR THICKNESS OF NT*}}{D_{30} \text{ FOR THICKNESS OF T*}}$

$T^* = 1D_{100}$ OR $1.5D_{50}$, WHICHEVER IS GREATER

FIGURE 1 Correction for riprap blanket thickness.

Design Conditions

Riprap should be designed for the combination of velocity and depth that gives the largest rock size. This combination is not always the design discharge. In many cases bank-full discharge produces the combination of velocity and depth that results in the largest rock size. Rock size in bendways is normally based on the maximum velocity-depth combination found along the bend. Bendways having stable upstream conditions could be designed with a variable rock size along the bend. This is generally not done because specifying multiple gradations has been found in some cases to increase construction costs.

Velocity Estimation

As stated earlier, the primary reason for adopting a design procedure based on depth-averaged velocity is that several techniques exist for estimating this velocity. Velocity is also easier to visualize and measure than is shear stress. Any riprap design problem has two parts: the first part is to estimate the imposed force, and the second is to use the imposed force and determine riprap size. The most difficult and most uncertain part of riprap design lies in estimating the imposed force, whether it be local depth-averaged velocity or shear stress. When riprap is designed for a channel bottom, local depth-averaged velocity is a straightforward concept even if it is difficult to determine. When side-slope riprap is designed, local depth-averaged velocity varies greatly from the toe of slope to the waterline, and near-bank velocity is meaningless unless the position is specified. The EM 1110-2-1601 method (*1*) uses depth-averaged velocity at a point 20 percent upslope from the toe V_{ss} for side-slope riprap design. The 20 percent point was selected because straight channel side-slope stability tests resulted in the same stability coefficient C_s as straight channel bottom stability tests with this position on the side slope and the appropriate adjustment for side-slope angle. This point is consistent with the location of maximum side-slope shear stress from straight channel studies.

Various tools exist to estimate depth-averaged velocity for use in riprap design and include the following with some of their limitations:

1. Two-dimensional (2D) depth-averaged *numerical models* have been shown to be unconservative in prismatic bends. Bernard (*5*) has developed a correction method for 2D depth-averaged models, and a version is available that can be used with 386 personal computers (PCs). This model has compared well with data from trapezoidal channels and is being tested against data from natural channels.
2. *Physical models* are rarely available for bank protection projects because of cost. If available, near bank velocity distributions should be measured to obtain V_{ss}.
3. *Empirical methods* must be applied only to cases similar to the data from which they were derived.
4. *Analytical methods*, which are based on conveyance [such as the ALPHA method given in EM 1110-2-1601 (*1*)], should be limited to straight channels because secondary currents cause ALPHA to be unconservative. Thorne and Abt (unpublished data) discuss additional analytical methods that incorporate the effects of secondary currents.
5. *Prototype data* normally require extrapolation to design conditions but are usually not available.

This paper focuses on the application of the empirical method given in EM 1110-2-1601 (*1*), presented in Figure 2. Figure 2 is applicable only for estimating characteristic side-slope velocity (V_{ss}) in straight or curved channels at 20 percent of slope length up from the toe. Figure 2 was derived from velocity data taken in physical models and prototypes. The amount of scatter in this type of data is large, and the curves were drawn on the conservative side of the data. In the case of bendways, Figure 2 is based on bends having fully devel-

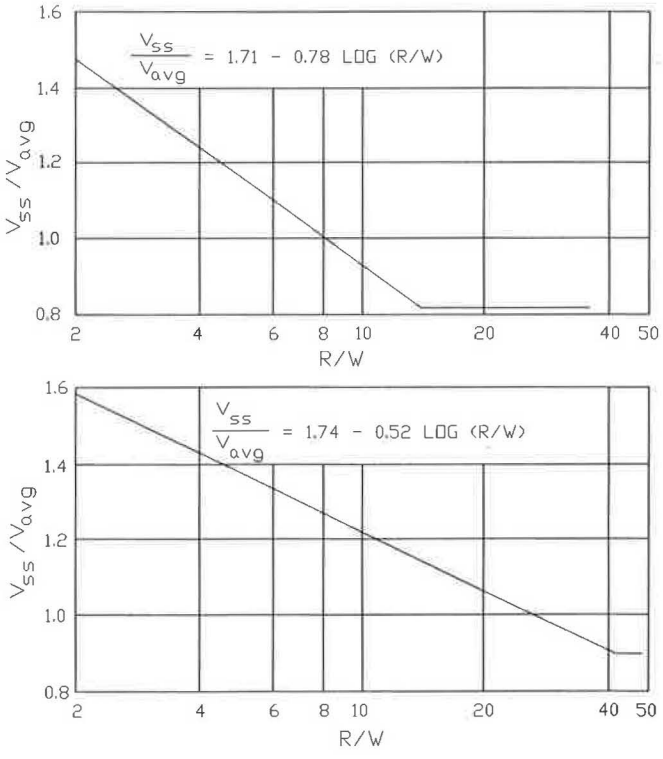

FIGURE 2 Velocity estimation based on EM 1110-2-1601 (*1*): *top*, trapezoidal channel; *bottom*, natural channel.

oped bend flow, which means that the bend angle is sufficiently large to develop close to the maximum velocity for that value of R/W. To use the minimum V_{ss}/V_{avg} in Figure 2 for straight channels requires that the channel be far enough downstream of bends, constrictions, or other devices that might create an imbalance of flow across the channel. Consequently one should be very cautious about specifying a straight channel—some investigators will not use $V_{ss}/V_{avg} < 1$. Figure 2 estimates V_{ss} from only average channel velocity V_{avg}, R, W, and channel type (natural or trapezoidal). The effects of other factors such as bend angle, bank angle, and bed/bank roughness have not been determined. It is important to note that V_{ss}/V_{avg} has rarely been found to exceed 1.6 in any alluvial or man-made fixed bed channel and is a minimum of 0.82 in straight trapezoidal channels and 0.9 in straight natural channels. Thus the designer is simply defining where in the range of V_{ss}/V_{avg} = 0.82 to 1.6 to design the protection. Figure 2 assists in that determination and generally provides a conservative estimate. Since Figure 2 is valid only for estimating side-slope velocity, velocity estimation for all problems other than bank protection (such as channel bottom protection) must use some other technique to determine local depth-averaged velocity, such as the numerical model described previously.

Average channel velocity is used only in the EM method (*1*) in conjunction with the empirical velocity estimation technique and is determined from discharge/channel area (Q/A). Area and discharge should be restricted to the main channel and should not include overbank areas.

Bend Radius and Water-Surface Width

The centerline radius of curvature of the bend and the water-surface width at the upstream end of the bend are used to characterize the bendway in both the EM rock sizing techniques (*1*) and the scour depth estimation techniques. The centerline radius and the width should be based on flow in the main channel and should not include overbank areas.

Natural Versus Trapezoidal Channel

In the empirical velocity estimation technique shown in Figure 2, two channel types, natural and trapezoidal, are used. Trapezoidal channels are often man-made with a smooth alignment; sediment transport is not sufficient to build point bars, which can concentrate flow against the outer bank. The data used in developing the trapezoidal channel curve were from clearwater channel models having riprap bottom and banks and aspect ratios (top width/average depth) ranging from 11 to 22. Though many trapezoidal channels have aspect ratios greater than 22, secondary currents in the channels with lower aspect ratios will provide more velocity concentration along the outer bank than those with higher aspect ratios.

In contrast, the natural channel curve in Figure 2 is applicable to channels having irregular alignment with sediment transport leading to point bars and toe scour that concentrate the flow along the outer bank.

Characteristic Particle Size for Gradation

One of the most controversial changes from the old to the new guidance has been the adoption of a characteristic particle size of D_{30}. A gradation plot in Figure 3 illustrates concepts such as the lower and upper gradation limits (also referred to as minimum and maximum) as well as D_{100}(max), D_{30}(min), and so forth. Stability tests conducted at a thickness of $1D_{100}$, which is the most commonly used thickness for bank protection, showed that gradations ranging from uniform to highly nonuniform exhibited the same stability if they had the same D_{30}. Maynord provides details of the comparison of D_{50} and D_{30} and documents other investigators who found a characteristic size less than the commonly used D_{50} (*2*). It is likely that if the tests had been conducted at another thickness, such as $1.5D_{100}$, the resulting characteristic size would have been different, probably larger. The use of D_{30} instead of D_{50} requires that the designer determine which of the available gradations has a D_{30}(min) greater than or equal to the computed D_{30} rather than to D_{50}. One of the results of this finding is that uniform gradations use the least volume of rock to achieve the same stability because the thickness is equal to the maximum stone size. One of the troubling aspects of these results is that an investigator of riprap subjected to channel flow has not yet been found who has been able to confirm the commonly held notion that a range of sizes gives increased stability due to better interlock.

If the designer prefers to work in terms of D_{50}, the approximate relation of D_{30} is

$$D_{50} = D_{30}(D_{85}/D_{15})^{0.32} \tag{2}$$

The use of a single particle size to characterize a gradation, whether D_{30}(min) or D_{50}(min), does not reflect all characteristics of that gradation. The following equation can be used to determine if D_{30}(min) is representative or if D_r(min) should be used as the characteristic particle size:

$$D_r(\text{min}) = \sqrt[3]{D_{85}(\text{min})[D_{15}(\text{min})^2]} \tag{3}$$

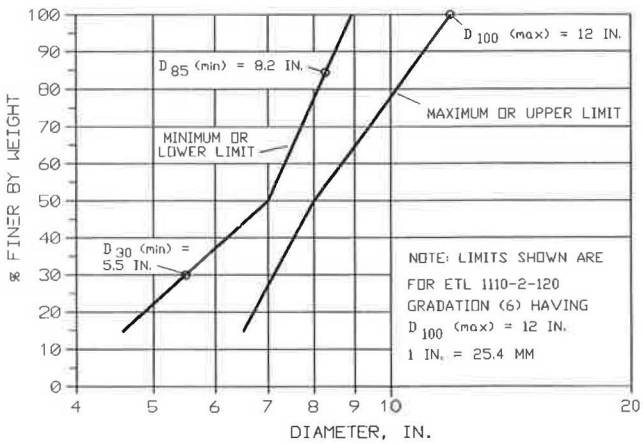

FIGURE 3 Explanation of gradation terminology.

If D_r(min) is significantly different from D_{30}(min), use D_r(min). The significance of Equation 3 is explained elsewhere (*3*).

One factor that should be considered is the impact of gradation on filter requirements. If a granular filter is used, the lower sizes of the riprap gradation must properly interface with the upper sizes of the filter. Consequently it is difficult to use a large uniform riprap and economically interface it with a granular filter. With geotextiles, this is not a problem, but a bedding layer is sometimes used on top of the geotextile to prevent damage from placing the riprap.

Unit Stone Weight

Unit stone weight is generally within the range of 2402 to 2803 kg/m³ (150 to 175 lb/ft³). Rock weighing less than 2402 kg/m³ (150 lb/ft³) can be used, but this is not very close to the unit weights that have been used in stability tests. When rock sizes required for different unit weights are compared, it is not correct simply to use equal rock weights and the relationship between size and weight of a sphere or cube. These comparisons must be made using the stone-sizing Equation 1 because this addresses the increased drag that would occur on a less dense but larger piece of riprap.

Riprap Blanket Thickness

Blanket thickness is generally measured in terms of the maximum stone size D_{100}. The minimum allowable blanket thickness is $1D_{100}$, and many streambank protection projects use this thickness. Only for very uniform gradations ($D_{85}/D_{15} \leq 2$) must the thickness also be at least $1.5D_{50}$. Stability tests show that uniform gradations must meet this requirement of $1.5D_{50}$(max) for equivalent stability. Stability tests have shown that a thickness greater than T^*, where T^* is the greater of $1.5D_{50}$ or $1.0D_{100}$, results in increased stability. Figure 1 shows guidance given in EM 1110-2-1601 (*1*) for thickness effects. The interpolated curve having $D_{85}/D_{15} = 1.7$ is applicable to the gradations in Table 1 (*6*). (This curve was interpolated between the curve for $D_{85}/D_{15} = 2.5$ and $D_{85}/D_{15} = 1$, which was conservatively assumed to have no increase in stability for increased thickness.) Gradations having $D_{85}/D_{15} \geq 5.2$ should use the curve for 5.2. When greater blanket thickness is used to increase stability, it must be realized that some rock movement will occur before the revetment becomes stable.

Local Flow Depth

The procedure presented in EM 1110-2-1601 is based on local depth-averaged velocity and local depth of flow. For channel bottoms, the local depth of flow is simply the depth at the point of interest. For side slopes the characteristic velocity and local depth are located 20 percent up the slope from the toe. At this point the local depth is 80 percent of the depth over the toe.

Side-Slope Angle

Stability studies have shown that the decrease in stability that occurs from placing a revetment on a side slope is not as significant as suggested in some of the previous guidance. This is probably because the angle of repose of a revetment is greater than the angle of repose of a rock dike. The relation of K_1 versus side-slope angle from EM 1110-2-1601 is shown in Figure 4. The solid line should be used for revetments. The least volume of riprap per foot of bank line is used when revetments are placed on slopes between 1V:1.5H and 1V:2H. For slopes flatter than 1V:4H, rock stability is not affected by the slope angle for revetments subject to channel flow. Slopes steeper than 1V:1.5H are not recommended.

Velocity Profile Correction

An evaluation of the velocity profile over bottom riprap in straight channels resulted in the following equation:

TABLE 1 Gradations for Specific Stone Weight of 165 lb/ft3, from ETL 1110-2-120 (*6*)

D_{100} (max) (in.)	Limits of Stone Weight for Percentage Lighter by Weight (lb)						D_{30} (min) (ft)	D_{90} (min) (ft)
	100		50		15			
	Max	Min	Max	Min	Max	Min		
12	86	35	26	17	13	5	0.48	0.70
15	169	67	50	34	25	11	0.61	0.88
18	292	117	86	58	43	18	0.73	1.06
21	463	185	137	93	69	29	0.85	1.23
24	691	276	205	138	102	43	0.97	1.40
27	984	394	292	197	146	62	1.10	1.59
30	1,350	540	400	270	200	84	1.22	1.77
33	1,797	719	532	359	266	112	1.34	1.96
36	2,331	933	691	467	346	146	1.46	2.11
42	3,704	1,482	1,098	741	549	232	1.70	2.47
48	5,529	2,212	1,638	1,106	819	346	1.95	2.82
54	7,873	3,149	2,335	1,575	1,168	492	2.19	3.17

NOTE: 1 lb/ft³ = 16.018 kg/m³; stone weight limit data from ETL 1110-2-120 (*6*). Relationship between diameter and weight is based on the shape of a sphere.

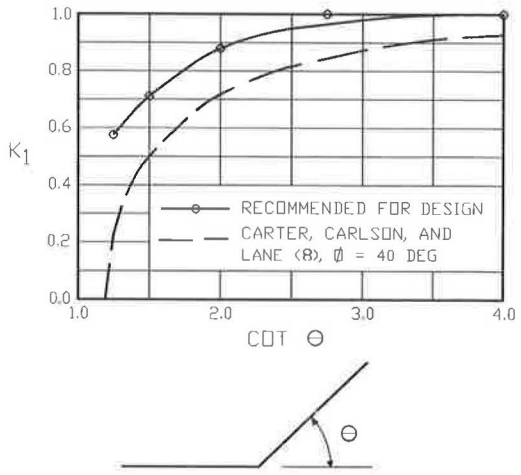

FIGURE 4 Side-slope correction coefficient.

$$\frac{V(y)}{V} = (1 + N)\left(\frac{y}{d}\right)^N \quad (4)$$

where

$V(y)$ = velocity at y,
N = 0.25 for d/D_{90} from 3 to 20, and
y = distance from top of riprap.

The velocity profile given by Equation 4 is the profile for which the stability coefficient for angular rock was found to be 0.30. In both bendways and just downstream of concrete channels, the profile is more nearly vertical with velocity in the upper zone (near the surface) less than Equation 4 and velocity in the lower zone (near the bottom) greater than Equation 4. For the same depth-averaged velocity, the vertical velocity profile in bends and just downstream of concrete channels tends to have a greater capacity to move the riprap because the velocities near the riprap and the shear stress are larger. For riprap just downstream of concrete channels, the velocity profile has not adjusted from the smooth concrete surface to the rough riprap. For bendways, secondary currents are suspected of causing the change in velocity profile.

In either case, an increased stone size is required. Two choices are available for making this increase. The first of these would involve returning to the basic shear stress equations, developing a velocity profile relationship for the bend or the area downstream of the concrete channel, and determining a new relationship between the shear stress, relative roughness, Shield's coefficient, and applicable velocity profile. Because this is a formidable task and would have made the design procedure difficult to use, the second choice—a completely empirical approach to velocity profile effects—was selected. For riprap just downstream of concrete channels, an empirical velocity profile correction C_V of 1.25 should be used in Equation 1. This increased size need be carried downstream only until the velocity profile has adjusted to the rougher riprap; 5 to 10 flow depths should be adequate. For riprap in channel bends, the velocity profile correction is dependent on the strength of the secondary currents, which is generally related to the parameter R/W. From stability tests in the Riprap Test Facility (RTF), U.S. Army Engineer Waterways Experiment Station, the empirical velocity profile correction to be multiplied by the computed rock size was found to be 1.2 for $R/W = 2.5$. The relationship used for the velocity profile correction given in EM 1110-2-1601 is

$$C_V = 1.283 - 0.2 \log (R/W) \quad (5)$$

where C_V is equal to 1 for $R/W \geq 26$.

A third area where the velocity profile departs significantly from Equation 4 is riprap on the nose of a rock dike. The constricting effect of the dike causes the flow to accelerate rapidly around the dike. Because of the short distance, the flow is affected by the dike and the boundary layer has no chance to grow and is continually being reduced by the flow acceleration. Limited tests show that the velocity profile correction to be multiplied by the rock size should be 1.25 for riprap on the nose of a dike.

Stability Coefficient

Stability coefficients defining the onset of unacceptable rock movement were determined from large-scale laboratory tests. These laboratory tests attempted to simulate mechanically placed riprap on a filter fabric without tamping or smoothing after placement. For thickness = $1D_{100}$(max) or $1.5D_{50}$(max), whichever is greater, $C_S = 0.30$ for angular rock. Limited tests show that $C_S = 0.375$ for rounded rock. Note that EM 1110-2-1601 incorrectly gives $C_S = 0.36$ for rounded rock.

Safety Factor

The minimum safety factor to account for nonhydraulic factors and other uncertainties is 1.1. The general tendency in riprap design is to estimate velocity conservatively, which adds in a safety factor. (Figure 2 is generally conservative because the design curve is drawn near the top of the data scatter.) Having to select an available gradation having D_{30}(min) greater than or equal to the computed D_{30} often adds another safety factor. For these reasons, the minimum safety factor is set low, at 1.1. One factor that cannot be easily quantified is the consequence of failure. A larger safety factor should be used for protection works in urban areas than would be used for protection of rural areas.

RIPRAP PACKING

Some Corps districts tamp or pack riprap after placement with a heavy plate or a wide-tracked dozer to achieve increased stability. This action tends to produce a more compact mass of riprap having greater interlock. Limited tests showed that tamping allowed a size reduction 10 percent over normal placement techniques (*3*).

EFFECTS OF FILTER TYPE

The stability tests used in the determination of $C_S = 0.3$ were conducted on a filter fabric. Limited tests showed that place-

ment of riprap on a granular filter allowed a size reduction of 10 percent compared with placement on a filter fabric (*3*). This reduction is considered applicable only to the minimum blanket thickness equal to the maximum stone size ($1D_{100}$). Greater rock thickness would tend to minimize the impact of the filter.

VARIATION OF VELOCITY AND ROCK SIZE UP SIDE SLOPE

In some cases the variation in velocity up the side slope is needed in design, especially when smaller riprap or vegetation is used on the upper slope. Velocity data have been collected in the RTF showing the variation of velocity over the side slope for a bank having the same riprap size from toe of slope to waterline. These data could be used to give an indication of velocities on the upper slope for smaller riprap or vegetation, recognizing that there will be some differences due to the difference in roughness. Figure 5 presents dimensionless depth-averaged velocities over the side slope that were replotted from Maynord for Stations 1+78 and 2+81 in the RTF (*7*). Station 1+78 is at the downstream end of a long straight reach and is unaffected by upstream disturbances. Station 2+81 is at the downstream end of the first bend and is the approximate location of most riprap failures during stability tests in the first bend. Station 2+81 is a severe bend condition because of the large bend angle, large bed roughness, small R/W, and small aspect ratio. These factors combine to produce strong secondary currents that concentrate flow against the outer-bank side slope. Thus Stations 1+78 and 2+81 represent two extremes in terms of secondary current or bend effects. Most bends should fall within these two curves. Figure 5 can be used with Figure 2 to estimate the distribution of maximum depth-averaged side-slope velocity in the bend. The use of depth-averaged velocity distribution given in Figure 5 provides a reasonable estimate of the distribution of forces along the side slope. However, use of the detailed velocity distributions presented in Maynord will provide a better description of forces not only up the side slope but along the bend (*3*).

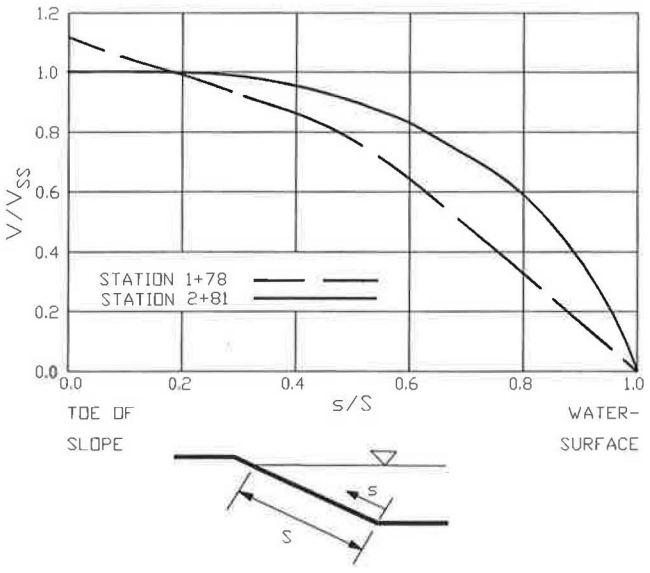

FIGURE 5 Dimensionless side-slope velocity.

EXAMPLE PROBLEMS

The following examples demonstrate the application of the EM 1110-2-1601 procedures. Gradations shown in Table 1 are used for demonstration in some of the examples, but they should not be taken as a recommendation.

Example 1: Bank Protection Only

Problem

Determine stable riprap size for the outer-bank side slope of a natural channel bend in which the maximum velocity occurs at bank-full flow. Water-surface profile computations at bank-full flow show an average channel velocity of 2.2 m/sec (7.1 ft/sec) and a depth at the toe of the outer bank of 4.6 m (15 ft). The channel is wide enough that the added resistance will not significantly affect the computed average channel velocity. A nearby quarry has rock weighing 2643 kg/m^3 (165 lb/ft^3) and can produce the D_{100}(max) gradations of 0.30, 0.38, 0.46, 0.53, and 0.61 m (12, 15, 18, 21, and 24 in.) given in Table 1. A bank slope of 1V:2H has been selected on the basis of geotechnical analysis. A typical blanket thickness of $1D_{100}$(max) will be used in this design with the minimum safety factor of 1.1. Centerline bend radius is 189 m (620 ft), and water-surface width is 61.0 m (200 ft).

Solution

Using Figure 2 with R/W = 189/61 = 3.1 results in V_{ss}/V_{avg} = 1.48 for a natural channel bend. The resulting V_{ss} = 1.48(2.2) = 3.2 m/sec (10.5 ft/sec). Using Equation 1 with C_t = 1, C_V = 1.18 (from Equation 4), K_1 = 0.88, and d = 0.8(4.6) = 3.7 m (12 ft) results in a computed D_{30} = 0.19 m (0.63 ft). Table 1 indicates that of the available gradations, the 0.46-m (18-in.) D_{100}(max) gradation is the smallest, having D_{30}(min) ≥ computed D_{30}. This gradation should be placed to a thickness of $1D_{100}$(max) or 0.46 m (18 in.). This example demonstrates that the actual safety factor is often larger than 1.1 because available gradations are used. In this case the actual safety factor is 0.73/(0.63/1.1) = 1.27.

Example 2: Total Channel Protection

Problem

Determine stable riprap size in a bend of a trapezoidal channel with essentially uniform flow. Bank slope is 1V:2H, and both the bed and banks will be protected with the same size of riprap. The bottom width is 42.7 m (140 ft), channel slope is 0.0017 m/m (0.0017 ft/ft), and the design discharge is 382.6 m^3/sec (13,500 ft^3/sec). Use $1D_{100}$(max) thickness and a nearby

quarry having stone with a unit weight of 2643 kg/m³ (165 lb/ft³) that can produce the D_{100}(max) gradations of 0.30, 0.46, and 0.61 m (12, 18, and 24 in.) given in Table 1. Centerline bend radius is 152.4 m (500 ft).

Solution

In this problem the solution is iterative; flow depth, velocity, and rock size depend on one another because a significant part of the channel perimeter is covered with riprap. Use Strickler's equation $n = 0.036\ [D_{90}(\text{min})]^{1/6}$ from EM 1110-2-1601 to estimate Manning's resistance coefficient. Bend velocity is determined using Figure 2. The solution technique is as follows: assume trial gradation and obtain uniform flow computations in Table 2, and use velocity estimation and riprap size equations to obtain riprap size in Table 3.

This example demonstrates that the increasing rock size for the three trial gradations results in increasing depth and decreasing velocity. The minimum acceptable gradation is the 0.46-m (18-in.) D_{100}(max) gradation placed to a blanket thickness of 0.46 m (18 in.).

Example 3: Design for Thickness Greater Than $1D_{100}$

If a thickness greater than $1D_{100}$(max) is specified, smaller gradations can be used if available. This option frequently requires that the blanket thickness be larger than the thickness for rock placed to $1D_{100}$(max). Using Example 1 and specifying a thickness parameter N of 1.2 in Figure 1 (determined by trial and error) results in a computed D_{30} = 0.18 m (0.59 ft) and an 0.46-m (18-in.) blanket thickness of the Table 1 gradation having a D_{100}(max) = 0.38 m (15 in.). Although both the gradations from Example 1 and this example will remain stable for the design conditions of Example 1, the two gradations are not equal in stability because the real safety factor for the D_{100}(max) = 0.38 m (15 in.) gradation placed to a thickness of 0.46 m (18 in.) is 0.61/(0.59/1.1), or 1.14.

Using Example 1 again, suppose a gradation has a unit weight of 2643 kg/m³ (165 lb/ft³), D_{85}/D_{15} equals 5.2, D_{30}(min) equals 0.12 m (0.40 ft), and D_{100}(max) is 0.43 m (17 in.). Since a D_{30}(min) of 0.12 m (0.4 ft) is less than the required D_{30} of 0.19 m (0.63 ft), a thickness of $1D_{100}$(max) will not be stable. What thickness would be required to maintain stability for the conditions of Example 1? Try various thickness parameters N from Figure 1 to determine the minimum stable thickness. Table 4 gives the results of this trial-and-error analysis. Use of this alternative gradation for Example 1 would require a blanket thickness of 0.76 m (30 in.) because the D_{30}(min) of 0.12 m (0.4 ft) is equal to or greater than the required D_{30} of 0.12 m (0.40 ft). This gradation placed to a 0.76-m (30-in.) thickness satisfies the requirements of Example 1 but is not exactly equal in stability to the previously determined gradations in Table 1 because the actual safety factor is different.

TABLE 2 Uniform Flow Computations

Trial D_{100}(max) (in.)	Manning's n	Normal Depth (ft)[b]	Water-Surface Width (ft)	Average Velocity (fps)[a]	Side Slope Depth, ft
12	0.034	10.6	182.4	7.9	8.5
18	0.036	11.0	184	7.6	8.8
24	0.038	11.3	185.2	7.3	9.0

[a]1 in. = 25.4 mm.
1 ft = 0.305 m.
[b]From iterative solution of Manning's equation $Q/A = (1.49/n)R^{2/3}S^{1/2}$

TABLE 3 Velocity Estimation and Riprap Size

Trial D_{100} (max) (in.)	Thickness (in.)	V_{ss}[b] (fps)	Computed D_{30}[c] (ft)	D_{30} (min) of trial[d] (ft)
12	12	10.8	0.73	0.48
18	18	10.4	0.66	0.73
24	24	10.0	0.59	0.97

[a]1 in. = 25.4 mm.
1 ft = 0.305 m.
[b]From Figure 2 using trapezoidal channel.
[c]From Equation 1.
[d]From gradation information given in Table 1.

TABLE 4 Alternative Thickness Computations

$N = \frac{\text{Thickness}}{D_{100}\text{ (max)}}$	Thickness, (in[a])	C_T from Figure 1	Required D_{30} (ft)
1.5	26	0.76	0.48
1.75	30	0.64	0.40
2.0	34	0.53	0.33

[a]1 in. = 25.4 mm.
1 ft = 0.305 m.

Example 4: Riprap Downstream of Concrete Channel

Problem

The channel shown in Figure 6 suffered riprap failure at Point A and a sediment deposit at Point B. Because the concrete channel is expanding faster than the flow can expand, an eddy formed on the left side of the downstream end of the concrete channel. Observers reported that the left third of the channel had upstream flow. The average velocity (Q/A, where A is total area) at the end of the concrete was 2.4 m/sec (8 ft/sec) and flow was subcritical. Use a unit stone weight of 2643 kg/m^3 (165 lb/ft^3), thickness of $1D_{100}$(max), and flow depth at Point A of 4.6 m (15 ft). Determine stable gradation from Table 1 for riprap placed just downstream and estimate how far to extend downstream.

Solution

The most difficult and uncertain aspect of this problem is estimating the velocity at Point A. Prototype data do not exist, and numerical or physical models cannot be justified. This problem is caused by the flow concentration caused by the eddy, which makes the effective cross-sectional area less than the actual area, and by the abrupt change in roughness from the concrete to the riprap. Assuming that only two-thirds of the channel area at the downstream end of the concrete channel is passing flow, then the average velocity through this effective area will be 2.4/(2/3), or 3.7 m/sec (12 ft/sec). If 3.7 m/sec (12 ft/sec) is the average, then higher velocity should be found near the center of the effective area, which is the location of the previous failure at Point A. A depth-averaged velocity of 4.0 m/sec (13 ft/sec) will be used for this design. Figure 2 does not apply to cases such as this example. Using Equation 1 where $K_1 = 1.0$, $C_t = 1.0$, $C_V = 1.25$, and $d = 4.6$ m (15 ft) results in a required D_{30} of 0.27 m (0.90 ft). This requires the gradation in Table 1 having D_{100}(max) of 0.61 m (24 in.) and D_{30}(min) of 0.30 m (0.97 ft) placed to a thickness of 0.61 m (24 in.). To allow the vertical velocity profile to adjust, the larger rock should be placed 5 to 10 channel depths downstream. To allow the flow to achieve a uniform distribution across the channel, the larger rock should be placed 3 to 5 channel widths downstream. The larger of the two values (5 to 10 channel depths or 3 to 5 channel widths) should be used in design.

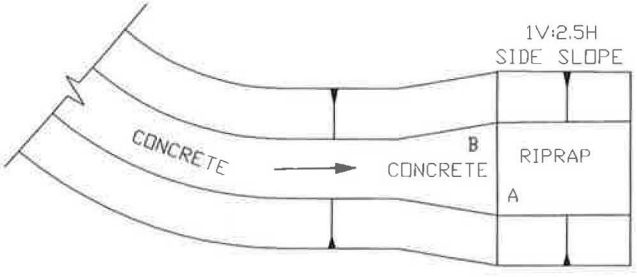

FIGURE 6 Plan view of channel in Example 4: (*a*) riprap failure, (*b*) sediment deposition.

PC PROGRAM

A PC program, RIPRAP15, incorporating these procedures has been developed and is available from the author.

SUMMARY AND CONCLUSIONS

The riprap design procedure presented herein is applicable to bank and channel protection in low-turbulence environments. Local depth-averaged velocity was selected over shear stress as the basis for this procedure because methods are available for estimating depth-averaged velocity and because many designers will not use procedures that are based on shear stress.

This method has several empirical coefficients analogous to the Shields coefficient that take into account the effects of rock shape, blanket thickness, and side-slope angle. The traditional Carter et al. relationship is more conservative than the empirical curve presented herein for side-slope effects (*8*). Another empirical coefficient is used to account for changes in the vertical velocity profile such as those occurring in bendways or downstream of concrete channels. This empirical approach was chosen because a theoretical approach would have been unfriendly to most users of riprap design guidance.

Gradation effects are addressed by using D_{30} as the characteristic particle size in lieu of the commonly used D_{50}. Equation 2 relates D_{50} to D_{30} and D_{85}/D_{15} for designers who prefer to use D_{50}.

Blanket thickness and gradation must both be specified to define the stability of a revetment. A uniform riprap can be placed to a large thickness with only a small increase in stability over the minimum blanket thickness. However, a nonuniform riprap placed to a large thickness will be much more stable than the minimum thickness of the same gradation. The method presented herein defines the stability of a wide

range of gradation and thickness, and design examples show how the method is applied to several cases.

ACKNOWLEDGMENTS

The tests described and the resulting data presented herein, unless otherwise noted, were obtained from research conducted under the Civil Works Investigation "Riprap Design and Cost Reduction: Studies in Near-Prototype Size Laboratory Size Channel" of the U.S. Army Corps of Engineers by the U.S. Army Engineer Waterways Experiment Station. Permission was granted by the Chief of Engineers to publish this information.

REFERENCES

1. *Hydraulic Design of Flood Control Channels*. EM 1110-2-1601. Headquarters, U.S. Army Corps of Engineers, July 1991.
2. Maynord, S. T. *Stable Riprap Size for Open Channel Flows*. Technical Report HL-88-4. U.S. Army Engineer Waterways Experiment Station, Vicksburg, Miss., 1988.
3. Maynord, S. T. *Riprap Stability: Studies in Near-Prototype Size Laboratory Channel*. Technical Report HL-92-5. U.S. Army Engineer Waterways Experiment Station, Vicksburg, Miss., 1992.
4. Maynord, S. T., J. F. Ruff, and S. R. Abt. Riprap Design. *Journal of Hydraulic Engineering*, ASCE, Vol. 115, No. 7, July 1989, pp. 937–949.
5. Bernard, R. S. *STREMR: Numerical Model for Depth-Averaged Incompressible Flow*. U.S. Army Engineer Waterways Experiment Station, Vicksburg, Miss. (in preparation).
6. *Additional Guidance for Riprap Channel Protection*. ETL 1110-2-120. Headquarters, U.S. Army Corps of Engineers, May 1971, Ch. 1.
7. Maynord, S. T. Riprap Stability Results from Large Test Channel. *Proc., 1990 ASCE National Conference on Hydraulic Engineering*, San Diego, Calif., 1990, pp. 257–262.
8. Carter, A. C., E. J. Carlson, and E. W. Lane. *Critical Tractive Forces on Channel Side Slopes in Coarse, Non-Cohesive Material*. Hydraulic Laboratory Report HYD-366. Bureau of Reclamation, U.S. Department of the Interior, Denver, Colo., 1953.

Scour at Bridges on Selected Streams in Arkansas

RODNEY E. SOUTHARD

Scour around bridge piers is a major concern in the design of a new bridge or the evaluation of the structural stability of an existing bridge. Numerous laboratory studies have produced many equations that can be used to estimate local scour at piers. The results of a study to collect scour data at selected bridges in Arkansas are described, the application of several of these local-scour equations to scour at the bridge sites studied is evaluated, and an equation for estimating scour on the basis of data collected at these sites is presented. Scour data were collected at 12 sites on nine streams in Arkansas during 14 floods. The recurrence intervals of the floods ranged from 3 years in the Illinois River basin to 100 years in the Red River basin. Scour holes near bridge piers measured as part of this study and included in the analysis ranged in depth from 0.70 to 4.88 m (2.3 to 16.0 ft). Five local-scour equations were evaluated as to their usefulness in estimating the measured scour at the 12 sites studied. Scour depths estimated using one of these equations had an interquartile range similar in magnitude to the interquartile range of the measured scour depths. A multiple linear regression equation was derived from scour data for the 12 sites. The independent variables are mean bed-material diameter, average velocity, and pier location code, and the dependent variable was measured scour depth. The equation had an average standard error of estimate of ±42 percent.

One of the major concerns in the design of a new bridge or the evaluation of an existing bridge is the susceptibility of the bridge piers to scour. Three types of scour can occur at a bridge: general, contraction, and local. General scour is the progressive degradation or lowering of the streambed through natural or human-induced processes. Channel degradation generally results from increased discharge, decreased bedload, or decreased bed-material size (*1*). Lateral erosion caused by a shift in the flow or meander pattern is also considered as general scour. Contraction scour is streambed erosion caused by increased flow velocity near a bridge or other channel constriction that results from the decrease in flow area at the contracted opening such as that caused by a bridge, approach embankments, and piers. Local scour is erosion caused by local disturbances in the flow, such as vortices and eddies in the vicinity of piers (*2*).

Many investigators have conducted laboratory studies of local scour and have developed a variety of equations that can be used to estimate scour depths. Some of the independent variables used in many of the equations are median bed-material diameter, pier geometry, flow depth, and velocity. When these equations are applied to actual bridge sites, a wide range of estimated scour depths commonly result. One equation may estimate little or no scour at a bridge pier, and another may overestimate scour depth.

U.S. Geological Survey, 2301 Federal Office Building, Little Rock, Ark. 72201.

The need for reliable information and equations to assess the scour potential at bridges has resulted in efforts to collect scour data during floods. Scour depths measured during floods are a result of unique site and flow conditions that are more complex and varied than flows produced in a laboratory. In recent years, several federal and state agencies have been involved in collecting detailed scour data at bridges to develop a national data base that can be used to investigate scour processes and develop scour prediction techniques.

The U.S. Geological Survey (USGS), in cooperation with the Arkansas State Highway and Transportation Department (AHTD), began a study of scour around bridge piers in Arkansas in 1985. The objectives of this study were to (a) collect scour data during flood events, (b) evaluate the usefulness of selected scour equations for estimating local scour, and (c) develop an equation from local scour data collected on Arkansas streams. The scour data collected as part of this study also will be included in the national data base for a study conducted by the USGS and FHWA in 1992.

PURPOSE AND SCOPE

This paper summarizes scour data collected at 12 study sites during 14 high-flow events on 9 streams in Arkansas (Figure 1). The methods used to select the sites are described, and the bridge geometry, hydraulic characteristics, and scour measurements at each site are summarized. Data collected and presented in the paper include (a) pier type and width; (b) flow velocity, depth, and angle; and (c) median bed-material diameter. Existing local-scour equations were selected and evaluated on the basis of their usefulness in estimating the measured scour at the 12 study sites. A multiple linear regression equation also was developed by relating factors such as pier location, flow velocity, and median bed-material diameter to measured scour depths at the study sites. Scour estimates calculated using the various equations were then compared with the scour measurements.

METHODS OF STUDY

AHTD supplied a list of 72 bridges with known scour problems, and 21 sites were selected for additional data collection. The sites were evaluated on the basis of potential for local scour to occur at the bridge and the degree of difficulty in obtaining the scour data.

At the 21 sites, cross sections were obtained along the upstream and downstream sides of the bridge to establish ex-

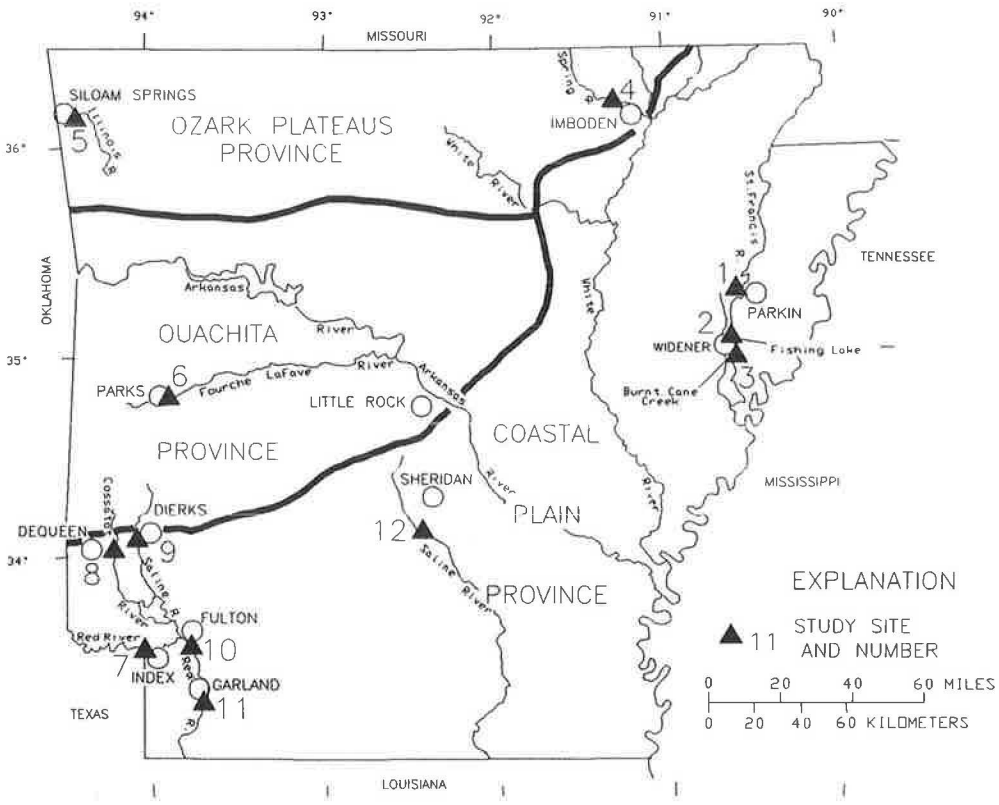

FIGURE 1 Location of study sites and physiographic provinces in Arkansas (7).

isting conditions. Stationing was established on the bridge handrails for horizontal reference. Bed-material samples were collected to determine the representative size and gradation of channel-bed and flood plain material as outlined by Guy and Norman (*3*). The bed-material samples were analyzed using methods described by Guy (*4*). Cross sections were measured during high flows and were plotted to determine the location and depth of the local scour holes. The cross-section measurements included measurements of channel-bed elevations at the end and on each side of the bridge piers.

For historical flood measurements, the maximum depth of a scour hole was assumed to be at the lowest measured channel-bed elevation. For purposes of this paper, the depth of a local scour hole was calculated as the difference between the elevation of the projected channel-bed cross section across the scour hole to the lowest measured channel-bed elevation of the hole. This projected channel cross section represents the concurrent ambient bed level at the scour hole. Flow depth was calculated as the difference between the elevation of the water surface and the elevation of the projected channel-bed cross section at the scour hole.

Discharge and velocity were determined using standard streamflow-gauging procedures described by Rantz et al. (*5*). The velocity variable used in existing local-scour equations is the average velocity of the vertical section immediately upstream or downstream of a pier with local scour. For scour measurements on the downstream side of the bridge, average velocity at the pier was calculated as the average of the velocities of the vertical sections on each side of the pier.

DESCRIPTION OF STUDY SITES

Of the 21 sites where cross-section data were collected, scour around bridge piers was documented at 9 sites. However, scour was also documented at three additional sites on the Red River in southeastern Arkansas during the May 1990 flood. The 12 sites at which scour data were collected are given in Table 1. Six of the study sites are at streamflow-gauging stations where previous discharge measurements have been made during extreme flood events. The scour data collected at these 12 sites formed the data base for the analyses described in this paper.

The 12 study sites are located in three physiographic provinces (Figure 1): the Coastal Plain Province in the southeastern half of Arkansas, the Ouachita Province in west-central Arkansas, and the Ozark Plateaus Province in northwest and north-central Arkansas (*7*). Seven of the study sites are in the Coastal Plain Province, which is underlain by alluvial deposits and other unconsolidated sediments. The composition of the bed material at these sites consists primarily of fine sand, silts, and clays. The remaining five study sites are located in the Ouachita and the Ozark Plateaus provinces, which are underlain by consolidated rocks consisting mostly of limestone, dolomite, sandstone, and shale. The composition of the bed material at these sites consists primarily of coarse gravel and coarse to fine sands.

Drainage areas, discharges, and recurrence intervals for the floods for which scour data were collected are presented for the 12 study sites in Table 1. Drainage areas at the 12 sites

TABLE 1 Summary of Discharge Data at Bridge Sites in Arkansas

Site number	Station number	Station name and location	Drainage area (km^2)	Date of measurement	Measured discharge (m^3/s)	Recurrence interval (years)[a]
1	[b]07047800	St. Francis River at State Highway 64 at Parkin	--[c]	12-28-87	[d]527	25
2	07047908	Fishing Lake at State Highway 70 near Widener	--[c]	12-27-87	484	--[c]
3	07047909	Burnt Cane Creek at State Highway 50 near Widener	--[c]	12-26-87	572	--[c]
4	[b]07069500	Spring River at U.S. Highway 62 at Imboden	[e]3,064	5-23-57	1,260	4
5	07195400	Illinois River at State Highway 161 near Siloam Springs	1,318	11-19-85	688	3
6	07261440	Fourche LaFave River at State Highway 28 near Parks	658	5-03-90	949	6
7	[b]07337000	Red River at U.S. Highway 71 at Index	124,398	5-09-90	7,420	[f]100
8	[b]07340500	Cossatot River at U.S. Highway 71 near DeQueen	932	1-30-69	1,830	12
9	[b]07341000	Saline River at U.S. Highway 70 near Dierks	313	5-06-61	796	10
				5-13-68	1,592	80
10	07341500	Red River at Interstate 30 at Fulton	135,550	5-12-90	7,280	--[c]
11	7342000	Red River at U.S. Highway 82 at Garland	136,428	5-14-90	6,290	--[c]
12	[b]07363200	Saline River at U.S. Highway 167 near Sheridan	2,908	2-01-69	1,900	20
				12-29-87	1,460	9

[a]Recurrence interval from Neely (1987) (6).
[b]U.S. Geological Survey streamflow-gaging station.
[c]Indeterminate.
[d]1 m^3/s = 35.31 ft^3/s.
[e]1 km = 0.62 m.
[f]Record furnished by U.S. Army Corps of Engineers, Little Rock District.

ranged from 313 km^2 (121 mi^2) for the Saline River at U.S. Highway 70 near Dierks to 136 428 km^2 (52,675 mi^2) for the Red River at US-82 at Garland. At sites where the recurrence intervals of the measured floods were determined, the intervals ranged from 3 years for the Illinois River at US-16 near Siloam Springs to 100 years for the Red River at US-71 at Index. The recurrence interval is the reciprocal of the probability of occurrence multiplied by 100 and is the average number of years between exceedances of a given flood magnitude. The occurrence of floods is random in time; no schedule of regularity is implied. A given flood magnitude can be exceeded at any time during a given period.

MEASURED SCOUR DEPTHS

Review of previous measurements made at the six streamflow-gauging stations and measurements made during this study resulted in 22 sets of data describing local scour holes ranging in depth from 0.70 to 4.88 m (2.3 to 16.0 ft) (Table 2). The deepest of these scour holes (4.88 m) was measured during the flood on May 13, 1968, at the US-70 crossing of the Saline River near Dierks just minutes before the failure of a bridge pier. The scour undermined the pier and caused the pier and part of the bridge deck to be lowered by about 0.6 m (2 ft), creating a dangerous road hazard and resulting in the immediate closure of the bridge to traffic.

It should be noted that it was not possible to determine if this scour hole was a result of local scour or a combination of local scour and contraction scour; thus, it was considered to be from local scour only. It is important to determine whether a scour hole develops under live-bed or clear-water conditions. Under live-bed conditions, bed-material is supplied to the hole and scour will occur only if the rate of removal of bed-material exceeds the rate of supply. Clear-water conditions exist if no bed material is supplied to the scour hole. Neill developed an equation to compute the critical velocity necessary to move bed material so live-bed conditions may exist. From these computations, clear-water conditions existed only at Sites 5, 6, and 9 (Table 2).

Scour depths greater than 3.05 m (10 ft) were measured at several sites in the Red River basin during severe flooding in May 1990. Comparison of cross-section data collected before the May 1990 flood and cross-section data collected near the peak of the flood at the US-71, Interstate 30, and US-82 crossings indicates that contraction and local scour processes were prevalent. Scouring at these sites was similar to the scouring at the I-30 bridge shown in Figure 2. The main channel bed at I-30 was lowered 4.57 to 6.10 m (15 to 20 ft), and local scour holes of 2.65 and 4.45 m (8.7 and 14.6 ft) were measured at Stations 176.78 and 238.35 m (580 and 782 ft) from the left abutment. At Station 140.21 (460 ft), the channel bed elevation was approximately the same as the elevation of the bottom of the pier located at Station 118.57 (389 ft).

TABLE 2 Summary of Scour, Pier Geometry, and Hydraulic Data Collected at Study Sites with Measured Scour Depths

Site number	Date of measurement	Measured scour depth (m)	Estimated error of scour depth (±m)	Distance from left abutment (m)	Median bed material diameter (mm)	Pier data				Hydraulic data at scour hole section		
						Type of nose	Width (m)	Width normal to flow (m)	Location code[a]	Flow depth (m)	Average velocity (m/s)	Flow angle (degrees)
1	12-28-87	[b]0.85	0.3	91.4	[c]0.18	square	0.94	0.94	0	9.11	[d]0.76	0
2	12-27-87	1.22	0.3	64.0	0.33	square	0.91	0.91	0	9.45	1.25	0
3	12-26-87	1.92	0.2	101.2	0.28	round	0.46	0.46	1	3.78	1.01	0
3	12-26-87	1.46	0.2	67.0	0.28	round	1.83	1.83	0	8.75	1.28	0
4	5-23-57	1.00	0.2	140.2	3.90	square	1.40	1.40	0	7.25	1.40	0
5	11-19-85	[e]0.98	0.2	233.5	17.00	square	1.22	1.22	0	5.97	0.91	0
5	11-19-85	[e]0.70	0.2	256.0	17.00	square	1.22	1.22	0	5.09	1.10	0
6	5-03-90	[e]1.00	0.2	76.5	21.00	square	2.59	6.46	1	2.38	0.97	37
6	5-03-90	0.94	0.2	100.9	21.00	sharp	0.91	0.91	0	6.10	2.38	0
7	5-09-90	2.32	0.3	219.4	0.12	round	2.13	2.13	0	12.31	2.65	11
7	5-09-90	3.41	0.3	286.5	0.12	round	2.13	2.13	0	13.04	3.90	8
8	1-30-69	1.04	0.2	61.3	0.11	sharp	1.37	1.37	0	6.28	1.31	0
9	5-06-61	1.22	0.2	109.7	18.00	square	0.79	0.79	0	5.79	1.55	0
9	5-13-68	4.88	0.1	36.58	18.00	square	0.79	0.79	1	2.68	3.47	0
9	5-13-68	1.65	0.1	109.73	18.00	square	0.79	0.79	0	6.46	3.35	0
10	5-12-90	4.45	0.3	176.78	0.18	sharp	2.13	2.13	0	10.76	2.90	0
10	5-12-90	2.65	0.3	238.35	0.18	sharp	1.98	1.98	1	8.14	0.73	0
11	5-14-90	4.39	0.3	210.31	0.32	round	3.05	3.05	0	11.73	1.89	0
11	5-14-90	1.80	0.3	271.27	0.32	round	3.05	3.05	0	13.47	2.35	14
11	5-14-90	3.26	0.3	395.02	0.32	round	3.05	3.05	1	9.11	1.46	0
12	2-01-69	1.49	0.2	20.12	0.30	round	0.43	0.43	1	2.56	0.98	23
12	12-29-87	1.52	0.1	55.17	0.30	square	1.16	1.16	1	3.20	0.52	0

[a]0 = pier located on the bed of main channel; 1 = pier located on bank of main channel or on flood plain.
[b]1 m = 3.28 feet.
[c]1mm = 0.003281 feet.
[d]1m/s = 3.28 feet per second.

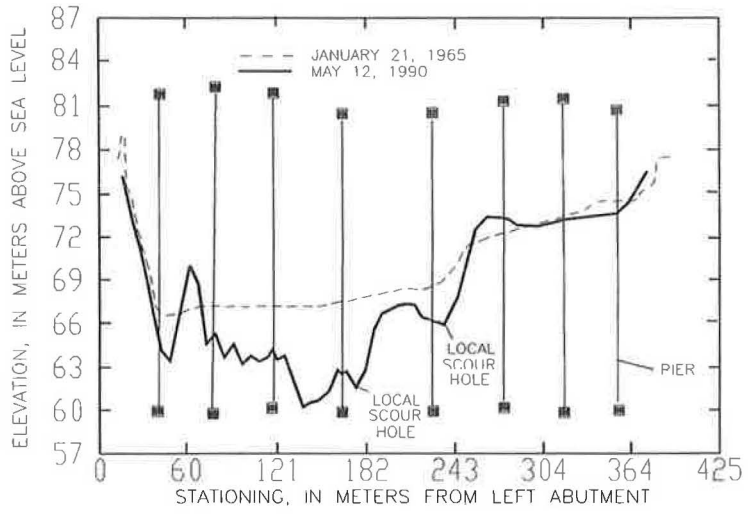

FIGURE 2 Channel cross sections based on data from bridge plans (January 21, 1965) and channel cross section measurements during flood of Red River at I-30 at Fulton, Arkansas (Site 10) along upstream side of bridge (May 12, 1990).

ESTIMATED SCOUR DEPTHS

Several investigators have developed equations to estimate local-scour depths at bridge piers. These equations generally have been based on laboratory studies and commonly yield different estimates of scour depth for the same set of data. To evaluate these equations and their application to streams in Arkansas, five local-scour equations were selected and used to estimate scour depth at the study sites where scour data had been collected. A multiple linear regression equation for estimating scour depth based on the measured scour data at the 12 study sites was also developed.

Selected Local-Scour Equations

The local-scour equations evaluated in this study were the equations developed by Laursen, Chitale, Carstens, Froehlich, and Colorado State University (CSU)—Equations 1 through 5, respectively. The Laursen, Chitale, and Carstens equations are two-variable equations developed from laboratory studies on scour around bridge piers conducted before 1970. The Froehlich and CSU equations are six-variable equations developed since 1987 on larger data bases.

During the 1950s, Laursen conducted some of the first in-depth studies into quantifying the relation between scour depth and streamflow and pier geometry. The graphical relation developed by Laursen and later transcribed to equation form by Neill was widely used during the 1970s.

Chitale's equation is one of the first equations to use the Froude number, which is a function of average velocity and flow depth at a pier, as a variable in determining scour depth. The Froude number is also used in the Froehlich and CSU equations.

Carsten's equation uses the specific gravity of sand, which is a common bed material in channels of many streams in the coastal plain of Arkansas, to calculate estimated scour depth.

As of 1992, the most recently developed equations to compute local scour at piers are the Froehlich and CSU equations. These equations use essentially the same factors to estimate scour depth.

Many other local scour equations exist (*8*), but only the five listed were evaluated as part of this study. These five equations were applied to all of the data collected, and no differentiation was made as to whether the scour holes were derived from live-bed or clear-water conditions. Of the five, the Laursen and Froehlich equations were developed from live-bed scour data, the Chitale and Carstens equations from clear-water scour data, and the CSU equation from both.

These equations were developed for design purposes. They are not a regression "best fit" of their respective data sets; instead, they encompass the data that allow for a factor of safety in the design and analysis of bridge structures. As an example, the Froehlich equation uses a factor of safety of one pier width for design purposes.

The equations used in this study are briefly described in the section that follows. The dates shown indicate the times when the equations were developed.

- Laursen equation—1956 and 1958:

$$D = 1.5B^{0.7} H^{0.3} \quad (1)$$

where

D = local scour depth measured from ambient bed elevation (m),
B = width of pier (m), and
H = flow depth at nose of pier, excluding local scour depth (m).

The Laursen equation was transcribed from its graphical form by Neill (*9*) on the basis of Laursen's basic design curve for a square-nosed pier aligned with the flow, as reported by Laursen and Toch (*10*) and Laursen (*11,12*).

- Chitale equation—1962:

$$D = H[6.65(F) - 5.49(F)^2 - 0.51] \quad (2)$$

where

F = Froude number,
$= V/(gH)^{0.5}$,
V = velocity of flow at end of pier (m/sec), and
g = acceleration of gravity (m/sec^2).

- Carstens equation—1966:

$$D = B\left(0.546\{[(N_s)^2 - 1.64]/[(N_s)^2 - 5.02]\}^{0.83}\right) \quad (3)$$

where

$N_s = V/[(s - 1)gD_m]^{0.5}$,
s = specific gravity of sand
$= 2.65$, and
D_m = median bed-material diameter (m).

- Froehlich equation—1987:

$$D = B[0.32\emptyset(B/B')^{0.62}(H/B)^{0.46}(F)^{0.20}(B/D_m)^{0.08} + 1] \quad (4)$$

where

$\emptyset$ = pier shape correction factor,
B' = pier width projected normal to flow,
$= B \cos \alpha + L \sin \alpha$,
α = flow angle (degrees),
$= 0$ for pier aligned with flow, and
L = length of pier (m).

- CSU equation—1990:

$$D = H[2.0K_1K_2(B/H)^{0.65}(F)^{0.43}] \quad (5)$$

where K_1 is the pier shape correction factor and K_2 is the flow angle correction factor.

The measured scour and estimated local-scour depths calculated using each of these equations are given in Table 3. The pier-shape factors used with the Froehlich and CSU equations are given in the following table:

	Pier-Shape Factor	
Pier Type	*Froelich (Ø)*	*CSU (K_1)*
Square nose	1.3	1.1
Round nose	1.0	1.0
Sharp nose	0.7	0.9

TABLE 3 Measured Scour Depths and Scour Depths Estimated Using Various Equations

Site number	Measured scour depth (meters)	Estimated scour depth calculated using indicated equation (meters): Laursen equation	Chitale equation	Carstens equation	Froehlich equation	Colorado State Universtiy equation	Multiple-linear regression equation (this study)
1	[a]0.8	2.8	--	0.1	2.2	1.6	1.1
2	1.2	2.8	2.4	0.5	2.3	1.9	1.5
3	1.9	1.3	1.6	0.5	1.2	0.9	2.1
3	1.5	4.4	2.7	1.0	3.4	2.7	1.5
4	1.0	3.4	3.2	0.8	2.8	2.5	1.2
5	1.0	3.0	1.2	--	2.2	1.9	0.7
5	0.7	2.8	2.0	--	2.1	3.0	0.8
6	1.0	3.8	1.4	--	4.6	5.6	1.2
6	0.9	2.4	6.2	0.6	1.4	1.9	1.4
7	2.3	5.4	9.5	1.2	4.6	4.3	2.8
7	3.4	5.5	14.7	1.2	4.9	5.1	3.6
8	1.0	3.2	2.8	0.8	2.3	2.0	1.7
9	1.2	2.2	3.6	0.8	1.6	1.8	1.1
9	4.9	1.7	4.0	0.5	1.5	2.3	3.0
9	1.6	2.2	8.5	0.5	1.8	2.5	1.8
10	4.4	5.2	9.9	1.2	5.1	4.4	2.8
10	2.6	4.5	--	1.1	3.1	4.0	1.8
11	4.4	6.9	5.7	1.7	5.6	4.6	1.9
11	1.8	7.1	8.3	1.7	5.9	5.2	2.3
11	3.3	6.3	3.6	1.7	5.3	4.0	2.6
12	1.5	1.1	1.4	0.2	0.8	0.8	2.0
12	1.5	2.4	0.2	0.7	2.1	1.3	1.3

[a]1 m = 3.28 feet.

[--, scour not estimated]

The flow-angle factors used with the CSU equation are given in Table 4.

A method that can be used to summarize the distribution of the estimated scour depths presented in Table 3 is the boxplot. A boxplot displays the symmetry of the distribution of data while using numerical measures of the central tendency and location to provide variability and concentration of data in the tails of the distribution. The box represents the interquartile range (25th to 75th percentile), the horizontal line inside the box represents the median, and the relative size of the box above and below the median represents the skew of the data (a larger box above the median line indicates a right-skewed distribution). The vertical line at the top of the box extends to a depth value less than or equal to the 75th percentile plus 1.5 times the interquartile range, and the vertical line at the bottom of the box extends to a depth value greater than or equal to the 25th percentile minus 1.5 times the interquartile range. Data beyond the vertical lines are individually plotted. Data 1.5 to 3.0 times the interquartile range are "outside values" and occur fewer than once in 100 times for a normal distribution.

TABLE 4 Flow-Angle Factors Used with CSU Equation for Estimating Scour Depth

Flow angle (degrees)	Flow-angle factor (K_2): L/B =4	L/B = 8	L/B =12
0	1.0	1.0	1.0
15	1.5	2.0	2.5
30	2.0	2.5	3.5
45	2.3	3.3	4.3
90	2.5	3.9	5.0

[L, length of pier, in meters; B, width of pier, in meters]

The interquartile range and median were computed for each data set to compare the distribution of the estimated scour depths to the measured scour depths. The interquartile range measures the spread of the data points, and the median measures the location of the distribution. The interquartile range is equal to the 75th percentile minus the 25th percentile. From Table 5, the interquartile range of the measured scour depths is 1.48 m (4.85 ft). The interquartile ranges for values estimated using the Carstens and CSU equations were the next lowest and highest values at 0.67 and 2.33 m (2.20 and 7.65 ft), respectively. The median of the measured scour depths was 1.51 m (4.95 ft). The medians of the scour depths estimated using the Froehlich and Carstens equations were 2.30 and 0.79 m (7.54 and 2.60 ft), respectively. The median of the scour depths estimated using the CSU data was 2.51 (8.25 ft).

Results of a correlation analysis between measured scour depths and estimated scour depths are presented in Table 6. The strongest relation between measured and estimated scour depths was for depths estimated using the CSU equation, with a correlation coefficient of 0.53; this was followed by Chitale's equation, with a correlation coefficient of 0.46. The analysis also indicated that (a) depths estimated using the Chitale equation were only moderately correlated with depths esti-

TABLE 5 Statistical Characteristics of Measured and Estimated Scour Depths

Statistical characteristic	Measured scour (meters)	Estimated scour depth calculated using indicated equation (meters)					
		Laursen equation	Chitale equation	Carstens equation	Froehlich equation	Colorado State University equation	Multiple-linear regression equation (this study)
Mean	[a]2.01	3.66	4.66	0.85	3.03	2.93	1.83
Minimum	0.70	1.10	0.21	0.06	0.80	0.79	0.73
Maximum	4.88	7.13	14.72	1.68	5.90	5.55	3.60
Median	1.51	3.11	3.41	0.79	2.30	2.51	1.75
25th percentile	1.00	2.29	1.80	0.49	1.70	1.81	1.20
75th percentile	2.48	4.88	7.25	1.16	4.60	4.14	2.16

[a]1 m = 3.28 feet.

mated using the other equations, (b) depths estimated using the Chitale equation were more closely correlated with measured scour depths than were depths estimated using the Laursen and Carstens equations, and (c) there are significant relations among scour depths estimated using the Laursen, Carstens, Froehlich, and CSU equations.

Multiple Linear Regression Equation

A multiple linear regression analysis was made on the 22 sets of data available at the 12 study sites to determine which characteristics of bridge geometry, hydraulics, and channel bed were significant on these Arkansas streams. Variables used in the equations and included in the regression analysis are presented in Table 2. The dependent variable of the analysis was measured scour depths, and the independent variables were median bed-material diameter, pier type, pier width, flow depth, Froude number, average velocity, and pier location code. The distribution of the measured scour depths was skewed to the right as indicated by the boxplot of measured scour depths in Figure 3.

To correct for the right-skewness of the data, a log transformation was applied to all variables used in the analysis except the pier location code. The variables that were statistically significant at the 0.05 level were median bed-material diameter, average velocity, and pier location code. Median bed-material diameter and average velocity are commonly used in existing local scour equations, but the pier location code variable is not used in any of the equations studied.

The pier location code identifies whether the pier is located in the main channel or the flood plain. Piers on the banks of the main channel are classified as being on the flood plain. This characteristic was included in the analysis because (a) a large scour hole 4.88 m (16.0 ft) in depth on the flood plain of the Saline River at US-70 crossing was a very influential data point in the initial analysis and was significantly underestimated using any of the five equations, and (b) a scour hole 1.65 m (5.4 ft) in depth was measured at a pier in the main channel during this flood and was overestimated by three of the five equations.

The only difference in the hydraulic characteristics associated with the scour holes was flow depth (Table 2), which was not a statistically significant variable at the 0.05 level in the regression analysis. Further inspection of the data revealed that during the flood of May 3, 1990, at the State Highway 28 crossing of the Fourche LaFave River, two scour holes of nearly equal depth (about 1 m, or 3 ft) developed: one in the main channel and one on the flood plain. The existing equations yielded significantly different estimated

TABLE 6 Correlation Analysis for Measured and Estimated Scour Depths

	Correlation coefficient for scour depths estimated using indicated equation (dimensionless)					
	Laursen equation	Chitale equation	Carstens equation	Froehlich equation	Colorado State University equation	Multiple-linear regression equation (this study)
Measured scour depth	0.31	0.46	0.37	0.41	0.53	0.83
Laursen equation		.51	.94	.97	.89	.29
Chitale equation			.51	.49	.76	.53
Carstens equation				.92	.83	.28
Froehlich equation					.90	.32
Colorado State University equation						.52

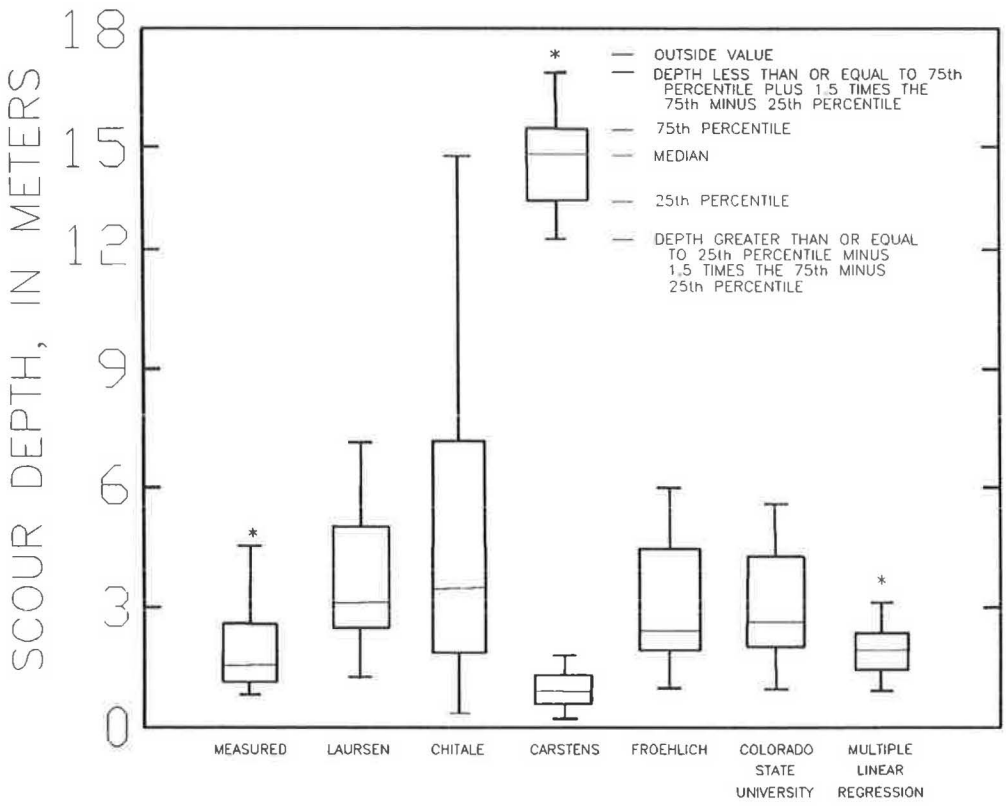

FIGURE 3 Boxplots of distribution of measured and estimated scour depths on data collected in Arkansas.

depths at these two scour holes. For example, the CSU equation indicated an estimated 1.9 m (6.3 ft) of scour in the main channel and 5.6 m (18.2 ft) of scour on the flood plain.

To determine if a significant relationship between scour in the main channel and scour on the flood plain existed, a pier location code of 0 was assigned to piers in the main channel and a value of 1 was assigned to piers on banks of the main channel or on the flood plain. The analysis was computed using a natural log transformation of all variables, except for the pier location code variable. For a pier location code of 0, a factor of 1 was applied to the estimated scour depth. For sites with a pier location code of 1, the factor applied to the estimated scour depth was $e^{0.476}$, or 1.61. The weighting factors assigned to pier location codes indicated that for similar conditions a scour hole that develops at piers on the flood plain will be 1.61 times deeper than one that develops in the main channel.

The significance of the pier location factor may be due to the effect of armoring on the bed of the main channel; nearly clear-water scour conditions in the flood plains; and fine, low-cohesion bed materials on the flood plain. Armoring is the deposition of a layer of larger material on the channel bottom due to suspension and transportation of smaller material during normal flow conditions and on the recession of a flood event. This larger material decreases the susceptibility of bed material in the channel to scour. On the flood plain, the effect of armoring is not a significant factor on scour hole development.

Usually little or no bed material is supplied to a scour hole on a flood plain in comparison with a scour hole in the main channel, thus clear-water scour conditions may be approximated. These conditions would then result in greater scour depths on the flood plain under similar flow conditions.

The equation for scour depth (D) resulting from the multiple linear regression analysis is

$$D = 0.827(D_m)^{-0.117}(V)^{0.684}e^{0.476(c)} \quad (6)$$

where

D_m = median bed-material diameter (m),
V = average velocity (m/sec), and
c = pier location code.

The average standard error of estimate of the multiple linear regression equation is ±42 percent. The equation was developed on a limited data base of 22 scour data sets. The log transformation of the variables used in the development of this equation is similar to that used for the other scour equations, which require the use of log-transformed data. The variables—median bed-material diameter and average velocity—have been shown to be statistically significant on larger data bases (Froehlich and CSU's equations). The scour depths estimated using this equation are presented in Table 3, along with the distribution of estimated depths based on the other equations.

Application of the regression equation is limited to sites with a median bed-material diameter between 0.11 and 21.00 mm (0.00036 and 0.0689 ft) and an average velocity of 0.52 to 3.90 m/sec (1.7 to 12.8 ft/sec). This equation is a regression equation that best fits the data set and has no factor of safety

for design purposes. Scour depths determined using the multiple linear regression equation should not be compared with depths determined using other equations in Table 3. The regression equation was derived from the data and will inherently provide better estimates of scour depth for those data than the other equations, which were based on different data sets.

SUMMARY

Local-channel scour data were collected at 12 sites on streams in Arkansas, 6 of which were at streamflow-gauging stations. Data collected consist of bed-material particle-size data, pier geometry, and hydraulic characteristics during selected flood events. Historic station records and data collected during this study produced 22 sets of scour data during 14 flood events. The recurrence intervals of the floods ranged from 3 to 100 years. Scour holes ranged from 0.70 to 4.88 m (2.3 to 16.0 ft) in depth.

Five local-scour equations were evaluated to determine their usefulness in estimating scour depths at the 12 study sites where scour was measured. The equations were those developed by Laursen, Chitale, Carstens, Froehlich, and CSU. The interquartile range of estimated scour depths using the Carstens and the CSU equations were closest to the interquartile range of the measured scour depths.

The 22 sets of data were used in a multiple linear regression analysis. The variables were log-transformed because the distribution of the measured scour depths were skewed to the right. Analysis of bridge geometry, hydraulic, and channel-bed particle size factors used in the five selected equations indicated median bed-material diameter and average velocity were significant at the 0.05 level. Results of the analysis indicated that a variable identifying the location of the pier was needed. A pier location code was used to identify whether a pier is located in the main channel or on the flood plain. The pier location code was statistically significant at the 0.05 level and was included in the multiple linear regression equation. The resulting equation had a ± 42 percent average standard error of estimate on the limited data base in Arkansas.

REFERENCES

1. Galay, V. J. Causes of River Bed Degradation. *Water Resources Research*, Vol. 19, No. 5, 1983, pp. 1057–1090.
2. Butch, G. K. *Measurement of Bridge Scour at Selected Sites in New York, Excluding Long Island*. Water-Resources Investigations Report 91-4083. U.S. Geological Survey, 1991.
3. Guy, H. P., and V. W. Norman. *Field Methods for Measurement of Fluvial Sediment*. Techniques of Water-Resources Investigations, Book 3. U.S. Geological Survey, 1970, Ch. 2.
4. Guy, H. P. *Laboratory Theory and Methods for Sediment Analysis*. Techniques of Water-Resources Investigations, Book 5. U.S. Geological Survey, 1969, Ch. C1.
5. Rantz, S. E., et al. *Measurement and Computation of Streamflow*, Vol. 1: Measurement of Stage and Discharge. Water-Supply Paper 2175. U.S. Geological Survey, 1982.
6. Neely, B. L., Jr. *Magnitude and Frequency of Floods in Arkansas*. Water-Resources Investigations Report 86–4335. U.S. Geological Survey, 1987.
7. Fenneman, N. M. *Physiography of Eastern United States*. McGraw-Hill Book Co., New York, 1938.
8. Jarrett, R. D., and J. M. Boyle. *Pilot Study for Collection of Bridge-Scour Data*. Water-Resources Investigations Report 86-4030. U.S. Geological Survey, 1986.
9. Neill, C. R. *River-Bed Scour—A Review for Bridge Engineers*. Technical Publication 23. Canadian Good Roads Association, Ottawa, Ontario, 1964.
10. Laursen, E. M., and A. Toch. A Generalized Model Study of Scour Around Bridge Piers andAbutments. *Proc., Minnesota International Hydraulics Convention*, International Association for Hydraulic Research and Hydraulics Division and ASCE, Minneapolis, 1953, pp. 123–131.
11. Laursen, E. M. *Scour at Bridge Crossings*. Bulletin 8. Iowa Highway Research Board, 1958.
12. Laursen, E. M. Scour at Bridge Crossings. *Transactions of the American Society of Civil Engineers*, Vol. 127, Part 1, No. 3294, 1962, pp. 166–209.

Alternatives to Riprap for Protection Against Local Scour at Bridge Piers

LISA M. FOTHERBY

Riprap is the most commonly applied material for protection of bridge piers against local scour. In some locations, however, riprap may be unavailable, costly, or physically untenable for installation. In this laboratory flume study, four alternatives to riprap—mats, grout bags, footings, and tetrapods—were investigated as scour prevention methods around bridge piers. Mats, grout bags, and footings were successful at preventing scour, and recommendations are included for elevating the protection surface in relation to the channel bed and the required size of installation. The method of failure and specific requirements for each material are also presented. The stability of tetrapods was compared with the stability of riprap based on the equivalent spherical diameters of the two materials. Tetrapods exhibited higher stability over riprap on the flat bed of a flume.

Local scour is the erosion of bed material resulting from secondary flows around an obstruction in the flow field. Large financial losses have resulted from local scour at bridge pier foundations. The most prevalent method of preventing local scour is to cover the natural bed around an obstruction with an erosion-resistant material. Riprap is the most commonly applied protection material, and the design process for riprap has been successfully quantified with recommendations for sizing the material, defining the required area of installation, setting the level of installation, and assigning filters.

In many instances, however, riprap cannot be installed or is too costly, depending on size requirements and availability. In contrast to riprap, the design process for alternative protective materials has received little attention and installers are often forced to rely on engineering judgment.

The objective of this study is to evaluate alternative protection materials for their effectiveness in protecting bridge piers from local scour and to provide design information. Many alternative protection materials are available; footings were selected for this study because they are the most prevalent alternative. Mats, grout bags, and tetrapods were chosen because of interest expressed by several state highway departments.

ROLE OF UPFLOW IN MECHANICS OF LOCAL SCOUR

To understand the success or failure of a protective material, it is useful to understand the mechanics of local scour. The primary component of local scour is the horseshoe vortex, but a secondary contributor to erosion is upflow. Upflow was described by Posey in the early 1950s as flow patterns generated by high- and low-pressure points at bridge piers (*1*). The stagnation point upstream of a pier is a high-pressure point, and low-pressure points are found at the upstream corners of the pier where flow accelerates around the pier and maximum velocities occur.

Stream flow enters the channel bed at the high-pressure point, flows underground parallel to the bed surface, and reemerges into the channel at the low-pressure points. The shear created by the upward, reemerging flow carries small particles to the bed surface and is referred to as "piping." In addition to soil piping, the reemerging flow creates a "quick" condition. The upward shear from the upflow counteracts the gravitational force of the particles at the channel bed surface (Figure 1), which allows stream flow passing over the quick particles to induce motion with lower shear forces.

The combination of horseshoe vortex and upflow produces the earliest stages of scour at the corners of a pier. The main scour hole develops from the corner points, which grow to join across the front of the pier. After the main scour hole forms, the erosive action from the horseshoe vortex plays a more significant role than upflow in expanding the scour hole.

If riprap is installed around a bridge pier, it reduces the permeable area of the channel bed. In a low-pressure region, upward flow is restricted to the area between the interstices of the riprap; this concentration of flow produces high shear forces. The preexisting quick condition at the low-pressure region is magnified by the presence of the riprap (*2*). Soil erosion occurs more readily as piping and the quick condition encourage the loss of particles from between the voids in the riprap. The rock settles into the bed of the river as material is eroded out around it. Riprap reduces the maximum depth of scour but does not arrest all scour-hole development. Alternative protection materials will settle in the same manner if they reduce the permeable area of the channel bed. Settling of riprap or other materials in the quick area can be prevented by placing a filter under the riprap layer.

EXPERIMENTAL TESTING

Laboratory testing was conducted at FHWA's Turner-Fairbank Research Center, in McLean, Virginia. A tilting-bed flume, 1.8 m wide × 21.3 m long, was used for all experiments. The pier model was a 1:20 scale rectangular pier, 15.2 cm × 30.5 cm, with the 30.5-cm length aligned with the flow. A sediment recess in the midsection of the flume was 1.3 m long × 0.46 m deep. The sediment recess was filled with a graded sand, D_{50} = 0.3 mm. Flow was supplied by a 0.31-m^3/sec pump and

Colorado State University Engineering Research Center, Fort Collins, Colo. 80521.

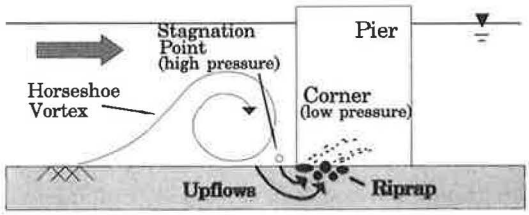

FIGURE 1 Upflows at riprap.

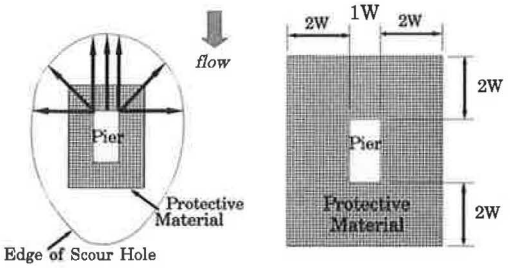

FIGURE 2 Seven locations for measuring lateral extent of scour hole (*left*) and lateral extent of a 2.0*W* protection pad (*right*).

measured by a venturi meter in the supply line. Average approach velocities were calculated from the venturi meter flow value and the flow depth. Point velocities were measured with a spherical, two-dimensional electromagnetic probe 1.3 cm in diameter.

All test runs of piers in a sand bed were conducted for 3.5 hr. Previous testing had established that 95 percent of maximum scour-hole formation, for the given flows and depths, occurred within 3.5 hr. Flow velocity for all tests in a sand bed was held at 0.3 m/sec. A velocity of 0.3 m/sec was just below incipient motion of sand particles in the flume, which afforded a maximum clear-water scour environment. Tests were conducted at flow depths of 0.15 and 0.30 m.

The protective materials were evaluated by comparing the dimensions of a scour hole in a protected bed with the dimensions of one in an unprotected sand bed; the dimensions measured were maximum scour depth and the lateral extent of the scour hole. The lateral extent of the scour hole was characterized by the horizontal distance from the side of the pier to the edge of the scour hole. The value was an average of measurements from seven locations in the front, semicircular area of the scour hole [Figure 2 (*left*)].

The lateral extent (size) of the protection pad for each material was designated by pier widths (W). The largest size tested was 2.0W, or two pier widths. A 2.0W pad of material covered an area around the pier that extended horizontally from the pier, a distance of twice the pier width [Figure 2 (*right*)].

Besides the sand-bed tests, incipient-motion tests were conducted on the mats, grout bags, and tetrapods. Incipient motion is the state at which movement first occurs in the test material. Incipient-motion tests were conducted on a fixed surface and, in most instances, with no pier. The sediment recess in the flume was covered with a sheet of treated plywood to match the elevation of the flume bed surface. The test materials were laid out on the fixed bed. Discharge was held constant throughout the run, but velocity was gradually increased. When a critical velocity was reached, the material "failed" by exhibiting motion. Velocity measurements were recorded for the point of failure.

Testing was conducted in four phases, the sequence of which is presented in Table 1. The first phase established the dimensions of a scour hole in an unprotected sand bed, created by the 15.2- 30.5-cm rectangular pier. This phase also determined the dimensions of a scour hole in a sand bed protected by riprap. Note that all tests of tetrapods (Phase 4) were incipient-motion runs carried out on a fixed, flat bed.

DESCRIPTION OF PROTECTION MATERIALS

Mats

Mats are formed with a double layer of nylon fabric sewn into a checkered series of compartments. The compartments are pumped full of cement grout, and they take on the appearance of pillows. The pillows are interconnected by the fabric and a reinforcing of laced steel cables that pass through them (Figure 3). The flexibility of the pillows within the structure provides tolerance for erosional adjustments in channel bed elevation.

Model mats had rectangular pillows approximately 1.5 × 3 cm. Each pillow was filled with a fine grout of sand and cement, giving the mat a depth of 0.6 cm. Each pillow weighed approximately 2.3 g, and a 1935 cm^2 section of mat weighed 834 g. Mat sizes tested were 1.0W, 1.5W, and 2.0W [see Figure 2 (*right*)].

TABLE 1 Testing Sequence

Phase	Protection Method	Testing Condition
I	Unprotected Sand	Sand Bed w/ Pier
	Riprap (Gravel)	Sand Bed w/ Pier
II	Mats	Sand Bed w/ Pier
	Grout Bags	Sand Bed w/ Pier
	Mats - Incipient Motion	Flat Bed
	Grout Bags - Incipient Motion	Flat Bed
III	Footings	Sand Bed w/ Pier
IV	A. Tetrapods - Incipient Motion	Flat Bed
	B. Tetrapods & Riprap, Side by Side - Incipient Motion	Flat Bed
	C. Tetrapods - Incipient Motion	Flat Bed w/ Pier

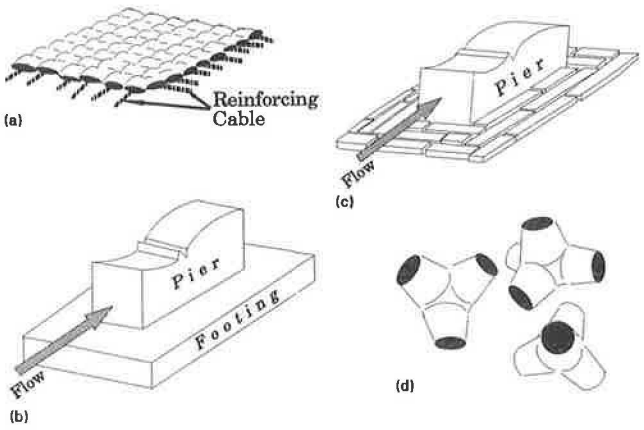

FIGURE 3 Alternative protective materials: (*a*) grout-filled mat, (*b*) footing, (*c*) grout bags, (*d*) tetrapods.

Grout Bags

Grout bags are individual nylon or acrylic bags fabricated from panels of material to create a rectangular block form. Every bag is large enough to resist movement from flows. The bags are positioned like tiles around the pier to form an erosion resistant floor (Figure 3). The bags are pumped full of grout after they have been located on the channel bed. Because the bags are formed in position, they fit snugly against each other. The bags can be installed at a dewatered site, or at a wet site if flow velocities do not inhibit access. There is no suggested or standard manufactured bag size.

The model bags were constructed from the same material used in the prototype bags and filled with a fine sand–cement grout mix. Four sizes of bags were tested. All the bags were roughly 4.3 cm wide and 2.8 cm tall, but lengths included 11.4, 14, 16.5, and 21.6 cm. The average specific gravity of the grout bags was 1.22. Sizes of grout-bag protection pads tested were $0.5W$, $1.0W$, and $1.5W$.

Footings

Four footing sizes were tested: $0.5W$, $1.0W$, $1.5W$, and $2.0W$. The thickness of the footings was 7.6 cm, or half the pier width ($0.5W$) (Figure 3). The footings, like the pier, were constructed from marine plywood.

Tetrapods

Tetrapods are precast concrete forms with extending legs that are randomly placed like riprap for channel protection (Figure 3). The tetrapods considered in this study were modeled after designs presented in the U.S. Army Corps of Engineers *Shore Protection Manual* (*3*).

The size of the model tetrapod was selected to approximate the volumetric size of model riprap: D_{50} = 1.3 cm. Model tetrapods were 1.9 cm tall and were formed from fine cement grout intruded into plastic molds.

RESULTS

Mats

Method of Failure

Mats tested in the flume were susceptible to failure in three ways: rolling, undercutting, and scouring at gaps. Rolling of the mat was the most severe form of failure. Flows passing over the surface of the mat created lift in the same manner as air flows over an airplane wing. Flows over the top of the mat created a lower pressure than found at zero velocities underneath the mat. Once the mat was lifted slightly, the force of the current pushed it loose. At lower velocities, the front end lifted enough to obstruct flows and the mat rolled from front to back. If the lift occurred in the midsection of the mat, the mat lifted slowly until it was abruptly swept out and carried downstream.

Undercutting, the second method of mat failure, proceeded as a gradual erosion process. Undercutting was produced by (a) local scour generated by the edges of the mat, (b) local scour from the movement of bedforms, or (c) scour from the main horseshoe vortex spilling over the edge of the mat. When the mat was loosened by undercutting, it was more susceptible to lift. An eroding vortex generated by the obstruction of the mat edge scoured out channel bed material from under the mat. The trough of a passing dune would also expose the edge of the mat. Local scour was occasionally generated at the exposed edge and would continue to undercut the mat at the same location even after the trough of the dune had migrated. Undercutting also occurred when the horseshoe vortex produced by the pier exceeded the size of the mat. The horseshoe vortex would undercut the edge of the mat where it spilled over.

The final method of failure resulted from a gap between the mat and the pier wall. When a 0.3-cm gap was left between the mat and the front face of the pier, a significant scour hole was found underneath the mat at the front of the pier. A scour hole would also form at the side walls of the pier if a gap was left between the pier walls and the mat. The downflow in the horseshoe vortex worked like a jet against the channel bed below the mat. A 0.3-cm gap in the 1:20 scale model represented a 6.4-cm gap in the prototype. This minor opening allowed one-third of the unprotected scour depth to occur. Therefore, it is important to have a good seal between the pier and the mat at the time of installation.

Lateral Extent of Mat

When a mat was installed, the mean lateral extent of a scour hole was slightly less than $1.5W$. A $2.0W$ mat is, therefore, necessary to protect against the high-end values of scour. A $1.5W$ mat would eventual fail through undercutting.

Elevation of Mat Surface

A mat installed on the surface of the channel (no excavation required because the mat rests on top of the channel bed) was subject to higher velocities from approach flows than a

mat installed at bed level. (The mat is inset so that its top is level with the channel bed.) During testing, the mats installed on the surface required an anchor to hold them in position, whereas mats installed at bed level required no restraint. When the surface mats were anchored adequately, they created a slight increase in the lateral extent of scour but reduced the scour depth by 5 percent of unprotected scour depth, in comparison with the bed level mats. The reduction in scour depth by the surface installation may result from shifting the horseshoe vortex upward, away from the channel bed.

Despite the slight reduction in scour depth, a mat installed at bed level is preferred over a mat installed on the surface, because of the higher susceptibility of a surface installation to lift.

Anchoring Systems

A mat installed on the surface would roll at flow velocities less than 0.3 m/sec. To complete tests with a surface installation, the mat required an anchor system. Two anchor systems were tested. In the first system, the mat was tied down to several deadmen buried in the channel bed. Anchoring the mat to the deadmen was sufficient to retain the mat in position throughout the run; however, the mat was affected by increased undercutting because its edges were exposed to the flow field. In the second system, 2.5 cm of the front and side borders of a 2.0*W* mat was folded down and covered with sand at a 45- to 60-degree angle from the horizontal. After both normal and extended runs, the bottom edge of the toed-in mat was occasionally exposed, but undercutting was minimal.

Toed-in 2.0*W* mats were also tested in incipient-motion runs conducted on fixed beds. Mats that were not toed in failed at lower velocities than those that were. The border of the mat was either laid unrestrained in a recessed slot in the fixed bed or held in place in the recessed slot, with sand packed around the edges. A summary of results from the incipient-motion tests on mats is presented in Table 2.

Results show that toe-ins at the edge of mats are extremely advantageous. Toe-ins significantly increase resistance to rolling failure and prevent undercutting of the mat. For maximum effect, the edges of mats should be buried below the depth of sand dune troughs and predicted depth of channel degradation.

Grout Bags

Method of Failure

If grout bags are undersized, they fail by washing downstream, but the more common form of failure was found to be a gradual erosion process. Erosion failure resulted from three interrelated actions: local scour around the bags, a shift in the grout bags, and undercutting of the filter fabric. If the bags protruded into the flow, they created their own local scour pattern. Local scour uncovered the filter fabric and allowed undercutting of the channel bed material on which the bags rested. As the bags were undercut, they slid sideways into the scour hole, exposing more filter fabric and opening additional areas to attack by scour. High flows would accelerate the process.

Lateral Extent of Protection

Scour-hole depths from grout-bag testing are presented in Table 3. Grout bags were tested as protection pad sizes of 0.5*W*, 1.0*W*, and 1.5*W*. Lateral extent of the scour hole extended to 1.9*W* for grout bags.

If extra precautions are taken with the installation of grout bags, a 1.5*W* area of protection might suffice. Precautions include installing the grout bags at elevations lower than level, using a deep toe-in for the filter fabric, and using massive grout bags to prevent shift. A recommended and more conservative design, however, is to install a grout bag pad of 2.0*W*.

Elevation of Surface of Grout Bags

Model grout bags were tested both with installations on the surface and installations at bed level. Surface installations allowed the bags to rest on top of the channel bed and protrude into the flow field for the full height of the bag. Bed-level installations required excavation, since the tops of the grout bags were installed level with the channel bed. During testing, two disadvantages were noted to placing the grout bags on the surface. The first was that the bags, protruding into the flow, generated a local-scour system that made the filter fabric beneath the bags more susceptible to attack. The second disadvantage was that bags installed on the surface exhibited a higher propensity to movement. In contrast, bed-level installations exhibited little or no movement. An advantage of the surface installation was a slight reduction in maximum scour depth. The reduction in scour depth was not significant enough to override the disadvantage of a decreased life expectancy for the project that would result from the shifting bags.

Filter Fabric

Filter fabric was one of the most significant parameters for grout bags. Without filter fabric, grout bags settled in the

TABLE 2 Incipient Motion Tests for Mats

Size	Number of Runs	Toed-In	Mode of Failure	Average Velocity (mps)
1.0W	3	No	Rolled	0.28
2.0W	3	No	Rolled	0.24
2.0W	2	Yes - Not Packed	Rolled & Lifted Out	0.54
2.0W	2	Yes - Packed	Lifted Out	1.22

TABLE 3 Scour-Hole Dimensions for Grout Bags

Run No.	Lateral Extent of Bags	Elev. of the Top of the Bag	Rigid vs. Loose	Filter Fabric	Max. Depth in Front of the Pier [under blocks] (cm)	Max. Depth at the Edge of the Material (cm)
2.13	0.5W	Level	Loose	No	12.1	8.9
2.14		Surface			8.3	7.5
2.9		Level	Rigid		12.7	10.1
2.10					13.3	11.3
2.11		Surface			12.7	4.5
2.16	1.0W	Level	Loose	No	7.6	4.8
2.21					5.6	5.5
2.29				Yes	0	4.1
2.27					0	2.1
2.15		Surface		No	6.0	2.8
2.20					4.6	2.6
2.30				Yes	0	4.5
2.28					0	4.5
2.23	1.5W	Level	Loose	No	5.1	0.9
2.26				Yes	0	2.1
2.24		Surface		No	6.0	1.4
2.25				Yes	0	1.4

Average velocity for all test runs was 0.3 mps

sand and exhibited scour-hole formation underneath the bags at the front of the pier. Grout bags with no filter fabric could reduce scour depth to approximately one-third of the scour depth observed for an unprotected sand bed. Grout bags with filter fabric could eliminate the scour hole.

A disadvantage of filter fabric was demonstrated when the length of a flume run was extended beyond the 3.5-hr period to promote channel degradation. Although the bed of the channel eroded, the material under the grout bags (and filter fabric) did not degrade. The grout bags and covered material formed a platform in the channel. As a result, the grout bags extended higher into the flow field. If the filter fabric had not been present, the grout bags would have settled with the channel bed. With continued channel degradation, the toe of the filter fabric was undercut and erosion occurred under the platform. Bags on the perimeter of the pad shifted outward by sliding off the platform.

For effective performance of the grout bags, filter fabric should be toed down in the same manner required by mats. The outside edges of the filter fabric should be buried to a depth below the elevation of sand dune troughs and predicted bed degradation. The sides of filter fabric should be overlapped and the fabric sealed around the pier walls to prevent gaps.

Rigidly Connected Grout Bags

Model grout bags in rigid tests were locked together with grout so that the entire system functioned as one footing. The rigid connection of the bags eliminated the adjusting property of the grout bags. Scour from a $0.5W$ size of interconnected bags was the deepest encountered during testing, aside from an unprotected sand bed.

Size of Bags

Optimum grout-bag size was not addressed directly in this study; however, several considerations emerged from testing. The dimensions of a grout bag must be large enough to develop an adequate weight, but the dimensions are limited by the following criteria:

1. A shorter height in a rectangular bag is better able to resist overturning.
2. When a bag is exposed to the flow field, a shorter height produces less scour.
3. Length contributed to failure in the incipient-motion tests when the bags were aligned perpendicular to the flow. The longer bags failed first (Figure 4).
4. Longer bags are less able to adjust to elevation changes and tend to span scour holes rather than conform to the channel bed.
5. A wide bag reduces labor and installation costs when covering a large area.
6. Increased width helps to reduce overturning.
7. A wide bag does not adjust as well to elevation changes and loses its ability to conform to changes in the channel bed.

Footings

Method of Failure

Footings fail when scouring activity undercuts the structure. Undercutting can be a result of the pier-generated horseshoe vortex that spills over the coverage provided by the footing. A second cause of undercutting can be the result of a footing-generated vortex. A vortex off the footing wall develops when

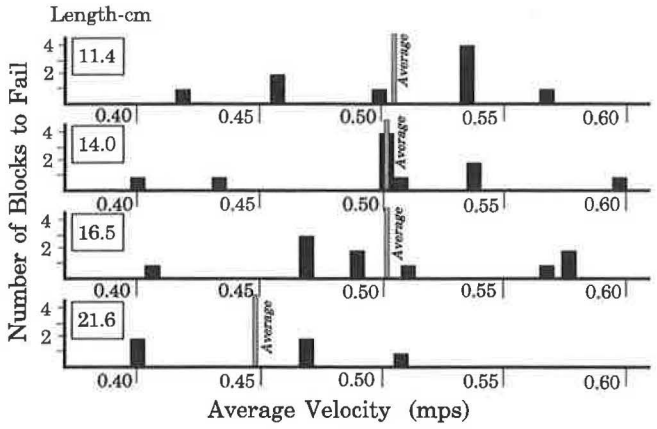

FIGURE 4 Incipient motion, grout blocks.

the footing is exposed to the flow field (*4*). Footing exposure can result from the movement of sand dunes, channel degradation, local scour holes from debris on the channel bed, and a footing installation above the surface of the channel bed. The strength of the footing vortex depends on the vertical distance that the footing extends into the flow field.

Lateral Extent of Coverage

Although a 2.0W size is effective coverage for most materials, a footing must extend 2.5W to completely contain scour from the pier horseshoe vortex. It may not be necessary, however, to completely arrest scour. If the footing can be buried deeper than bed level, or if it is thick enough, it can prevent local scour from undercutting the footing. For either instance, a 2.0W footing may be adequate. In addition, the footing may be able to tolerate a degree of undercutting. The sizing of a footing is primarily dictated by the applied load and by the bearing capacity of the soil. If the lateral extent of the footing is increased from the original geotechnical design to provide scour protection, it may contain some tolerance for loss of bearing area due to undercutting. Consultation with a geotechnical engineer would be required for this consideration.

Elevation of Footing in Relation to Channel Bed

Local scour depth increases as the footing is raised above the channel bed (*5*). The footing may prevent pier scour from undercutting the footing, but the footing can generate enough scour on its own to provoke failure, if it extends far enough into the flow field. Therefore, the optimum placement of a footing is level with the channel bed, or lower. An installation lower than the channel bed allows for channel degradation as well as bed movements due to sand dunes and debris. It also places the footing below the range of undercutting from pier scour.

Footing Thickness (Height)

Structural considerations are a primary factor in determining footing thickness, but scour prevention can provide a secondary consideration. When a footing is installed level with the channel bed or lower, increasing the height dimension of the footing may provide the extra scour protection needed. When the footing is thick, the vortex may expose only a fraction of the footing sidewalls, without undercutting. Burying a footing deeper than level is a more effective solution than increasing footing thickness. If the footing is in danger of becoming exposed to flows, the increased footing thickness will magnify the scour danger.

Tetrapods

Tetrapods were originally designed for shore protection. Tetrapod legs reduced erosional energy by breaking up waves as they approached shore, and they provided high porosity for the release of the wave. The question addressed in this study was whether the interlocking legs of a tetrapod would provide greater resistance to movement than riprap, in a fluvial system. The answer was approached by comparing the incipient-motion velocities for tetrapods with the incipient-motion velocities for an equivalent size of riprap in the flume. For surface runs, tetrapods were placed on top of the flat, plywood flume bed; and for bed level runs, tetrapods were placed in a recessed area (2.4 cm) of the plywood flume bed. The top of the tetrapods was even with the bed of the flume in bed-level runs. In Phase 4, Set B (see Table 1), a pad of tetrapods was tested next to an equal-sized pad of riprap in order to provide a direct comparison. In Phase 4, Set C, a pier was added to the flat bed, and the population of tetrapods per unit area (density) and the size of the protection pad were varied.

Incipient-motion velocities from Sets A and B of Phase 4 were used to compute the stability number, N_s. A comparison was made between tetrapods and riprap by plotting the stability number against the dimensionless parameter l/y, which is the significant length over the flow depth.

Equivalent Sphere

Knowing the specific gravity and mass of the material, the volume of the riprap and the volume of a tetrapod were converted to equivalent average sphere sizes. The diameter of the equivalent sphere was used as the significant length, l, for each particle.

	Tetrapod	*Riprap (average of one particle)*
Mass	3.52 g	5.81 g
Specific gravity	1.83	2.72
Diameter of equivalent sphere (l)	0.0155 m	0.0160 m

The stability number indicates the point at which the drag and inertia forces on a particle are balanced by the body force (weight) of the particle. This balance occurs at incipient motion.

Drag + inertia = weight

$$C_1 l^2(\gamma_w/g)V^2 = C_2 l^3(\gamma_s - \gamma_w) \quad (1)$$

$$N_s = \frac{V^2}{g\,l(SG - 1)} \quad (2)$$

TABLE 4 Stability Numbers for Tetrapods and Riprap

Set Description	Run Number	Ave Vel (mps)	Flow Depth (m)	l/y	Ns
Set A	4.1	0.704	0.131	0.118	3.93
Bed Level	4.2	0.802	0.155	0.10	5.10
Density-2	4.3	0.671	0.188	0.082	3.57
	4.4	0.774	0.163	0.095	4.75
	4.5	0.771	0.166	0.093	4.71
	4.6	0.762	0.166	0.093	4.60
	4.7	0.805	0.183	0.085	5.14
	4.8	0.661	0.210	0.074	3.46
	4.9	0.725	0.193	0.080	4.17
Set A	4.10	0.515	0.169	0.091	2.10
Surface	4.11	0.591	0.152	0.102	2.77
Density-1	4.12	0.558	0.160	0.097	2.47
Set A	4.13	0.546	0.162	0.096	2.36
Surface	4.14	0.631	0.138	0.112	3.16
Density-2					
Set B	4.15T	0.616	0.165	0.094	3.01
Surface	R	0.741	0.135	0.119	2.03
Density-1	4.16T	0.585	0.226	0.069	2.71
	R	0.738	0.177	0.091	2.02
Set B	4.19T	1.119	0.092	0.168	9.92
Bed Level	R	1.152	0.086	0.186	4.92
Density-1	4.20T	0.917	0.143	0.109	6.66
	R	0.945	0.141	0.114	3.31
	4.21T	1.180	0.118	0.132	11.04
	R	1.207	0.113	0.141	5.40
	4.22T	1.237	0.114	0.136	12.13
	R	1.234	0.114	0.140	5.64

Comparison of Stability for Riprap and Tetrapods

Plotting the points of incipient motion allows a comparison between tetrapods and riprap. Table 4 contains incipient-motion data from Phase 4, Sets A and B, and the calculated stability numbers. Figure 5 is a plot of the stability numbers for tetrapods and riprap. The stability of tetrapods in Figure 5, based on the calculated equivalent length, is higher than the stability of riprap for both the recessed and surface installations. If weight is reintroduced into the stability equation by replacing significant length,

$$W = l^3\gamma_s \tag{3}$$

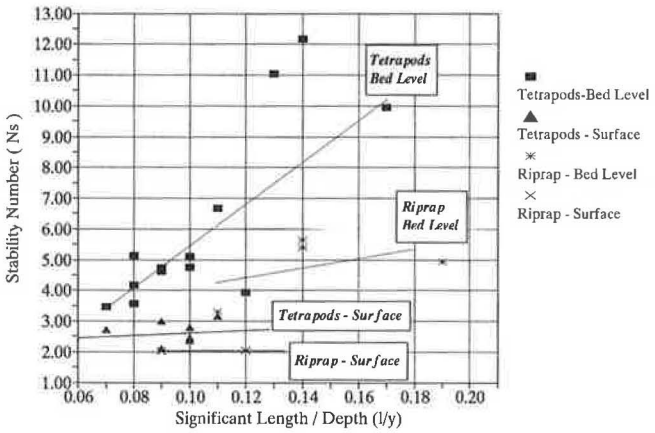

FIGURE 5 Stability numbers for tetrapods and riprap at surface and bed level (*Ns*).

then it can be seen that weight is inversely proportional to the stability number. Tetrapods that are lighter than riprap can provide the same stability. This conclusion is based on the assumption that the significant length of a tetrapod or riprap particle can be represented by an equivalent volumetric sphere. The results, however, are sensitive to the significant length selected. A second limitation is that the materials were tested for a specific situation. They were installed on a level, fixed bed and applied in pad sizes that covered only a limited area of the channel bed.

Table 5 presents results from Phase 4, Set C, in which three densities of material and pad sizes of $1.0W$ and $0.5W$ were tested. The results from Set C indicate that placement density has no significant effect on the stability of tetrapods, but stability appears to increase with the size of the protective pad.

CONCLUSIONS

1. The scour mechanics of upflow play an important role in the effectiveness of scour-protection materials.
2. Installation of mats:
   - Mats should be installed at bed level (top of mat even with the channel bed).
   - Recommended lateral extent of mats is $2.0W$, where W equals the pier width [see Figure 2 (*right*) for explanation of dimensions].
   - Edges of the mat should be toed in below predicted depths for channel degradation, troughs of bedform movements, and local scour holes from debris.

TABLE 5 Set C, Tetrapods

Run Number	Protection Material /Size	No. of Failed Tetrapods	Flow Depth (m)	Average Velocity (mps)	Density[b]
4.23	1.0W	2	0.233	0.430	1
4.24		5	0.224	0.448	
4.25		17	0.265	0.503	
4.26		4	0.293	0.448	
4.27	0.5W	9	0.287	0.354	1
4.28		6	0.279	0.348	
4.29		25	0.293	0.451	
4.30		9	0.323	0.405	
4.31	0.5W	5	0.282	0.366	1.5
4.32		27	0.221	0.448	
4.33		32	0.288	0.460	
4.34		16	0.289	0.460	
4.35	0.5W	8	0.271	0.369	1.75
4.36		12	0.281	0.354	
4.37		110	0.346	0.384	
4.38		12	0.318	0.412	
4.39	1.0W	49	0.171	0.573	1.5
4.40		50	0.171	0.585	
4.41		58	0.213	0.625	
4.42		58	0.221	0.604	

[a] Tetrapods were placed on the surface of the fixed bed.
[b] Density of 1 is equivalent to 3292 tetrapods per square meter.

–The mat must be sealed around the walls of the pier.

3. Installation of grout bags:

–Recommended lateral coverage of grout bags is 2.0*W*, although 1.5*W* may be acceptable, if proper precautions are taken.

–Grout bags should be installed at bed level. If grout bags are installed on the surface, there is slightly less scour, but life expectancy for the project is reduced.

–Filter fabric is an integral part of the system and should be installed.

–Grout bags should not be rigidly connected.

–The sizing of bags should entail a careful comparison of, and balance between, weight and dimensions.

4. Installation of footings:

–A 2.5*W* footing is required to provide complete protection, although a 2.0*W* size is effective if the footing has adequate thickness or can tolerate a minor degree of erosion.

–The footing should be installed level with the channel bed, or lower.

–A lower installation or thicker footing provides some additional measure of scour protection.

5. Tetrapods:

–Tetrapods exhibited a higher stability than riprap, based on calculations using the equivalent spherical diameter of the materials.

–Stability of the tetrapods does not appear to be affected by their placement density.

–Stability of the tetrapods increased with an increase in the lateral extent of their coverage.

ACKNOWLEDGMENTS

Laboratory testing was funded by an FHWA Research Fellowship, whose support is gratefully acknowledged. Special thanks is extended to J. Sterling Jones, FHWA Project Advisor for this study.

REFERENCES

1. Posey, C. J. Some Basic Requirements for Protection Against Erosion. *Proc., Minnesota International Hydraulics Convention*, IAHR and ASCE, Minneapolis, Sept. 1953, pp. 85–88.
2. Koloseus, H. J. Scour Due to Riprap and Improper Filters. *Journal of Hydraulic Engineering*, ASCE, Vol. 110, No. 10, 1984, pp. 1315–1324.
3. *Shore Protection Manual*, Vol. 2. U.S. Army Corps of Engineers Waterways Experiment Station, Vicksburg, Miss., 1984.
4. Jones, J. S. *Laboratory Studies of the Effects of Footings and Pile Groups on Bridge Pier Scour*. Report FHWA-RD-90-035. USGS; FHWA, U.S. Department of Transportation, Oct 1989, pp. 340–360.
5. Fotherby, L. M. *Footings, Mats, Grout Bags, and Tetrapods: Protection Methods Against Local Scour at Bridge Piers*. M.S. thesis. Colorado State University, Fort Collins, July 1992.

Study of Riprap as Scour Protection for Spill-Through Abutments

A. TAMIM ATAYEE

The purpose of the study was to develop empirical design guidelines for riprap protection of spill-through abutments situated in floodplains near channels. Previous laboratory studies have been done for a simple prismatic cross section with spill-through abutments encroaching less than 56 percent of the floodplain width. Previous studies are extended through an experiment with compound channels consisting of a floodplain and a defined main channel encompassing encroachments ranging from 62 to 100 percent of the floodplain. With the benefit of physical models, empirical design guidelines for the protection of spill-through abutments are provided for the broad range of abutment and floodplain configurations. Previous laboratory experiments have been done using the depth-averaged measured approach velocity and Bernoulli's conservation of energy equation to approximate the average contracted velocity. The average contracted velocity is the controlling variable to compute the design grain size, D_{50}, of the riprap. The experiments extend the range of encroachment from 56 to 100 percent of the floodplain width in a physical model composed of a channel, a floodplain, spill-through abutments of various lengths, and riprap (gravel) of various grain sizes. Data from previous laboratory experiments and the current study were used to develop an empirical relationship to size riprap to protect abutments.

Construction of structures within floodplains has significant effects on the hydraulic performance of a stream. These effects are even more pronounced during floods when the majority of the flood flow is in the floodplain overbanks rather than the natural channel. Encroachments onto the floodplain tend to have a contraction effect on the unobstructed approach flow. By introducing an obstruction in the floodplain, the natural flow area is decreased, thus increasing the average velocity.

Obstruction of flows by bridge substructures, such as embankments, abutments, and piers, redirects the natural course of the stream and in doing so accelerates flow and disrupts the streamlines. Residual secondary currents—specifically, vortices and flow separation—are the result. These vortices are rotational currents whose potential to erode the alluvial stream bed increases as the currents grow stronger. The base of the bridge substructures is the most susceptible place for local scour to occur. The unprotected stream bed can experience enough sediment removal to form a scour hole that could potentially undermine the foundation of the bridge substructure. Furthermore, the transport of larger sediment particles impinges the bridge substructures, chips away at the concrete, and poses a threat to the composition of the member. These contributing hydraulic factors that precipitate the scouring at bridge foundations are the leading cause for the bridge failures over streams and rivers.

GKY and Associates, Inc., 5411-E Backlick Road, Springfield, Va. 22151.

COUNTERMEASURES

There are several countermeasures for mitigating local scour caused by encroachment into waterways: for example, relief openings in the bridge substructure, guide banks (spur dikes), channel improvement, and riprap revetment. Rock riprap revetment provides an effective measure to protect streams from the destructive effects of scour. To determine the amount of riprap necessary to adequately protect abutments, the scour potential must be known. The scour potential can be determined if the stream hydraulic characteristics, such as depth and velocity, are known. To dissipate energy effectively, thereby providing erosion protection, the appropriate median grain size and proper gradation and implementation must be employed. Moreover, the particle should be resistant to weathering that may be due to fluid forces, exposure, and abrasion from contact with other particles. One of the goals of this study is to provide a method for determining the appropriate size of riprap for a specified flow condition.

LITERATURE REVIEW

The initiation or threshold of movement of a particle due to the action of fluid flow is defined as the instant when the applied forces due to fluid drag and lift, causing the particle to move, and exceed the stabilizing force due to the particle weight force (*1*). This hydraulic condition is known as incipient motion and the acting forces are depicted in Figure 1, in which L = lift force, W = particle weight, F_D = drag force, F_R = resisting force, and α = angle of contact. These forces are the prevalent forces for grains of noncohesive sediment lying in a bed of similar grains over which fluid is flowing (*2*). The grain is subjected to fluid forces that promote movement and gravitational forces that resist movement. In the presence of these forces, a shear stress forms between the grains on the threshold of motion and the stable grains that compose the stationary boundary.

DIMENSIONAL ANALYSIS

To understand the nature of scour, the mathematical principles describing the bed geometry, capacity, and supply as functions of flow conditions and time must be established.

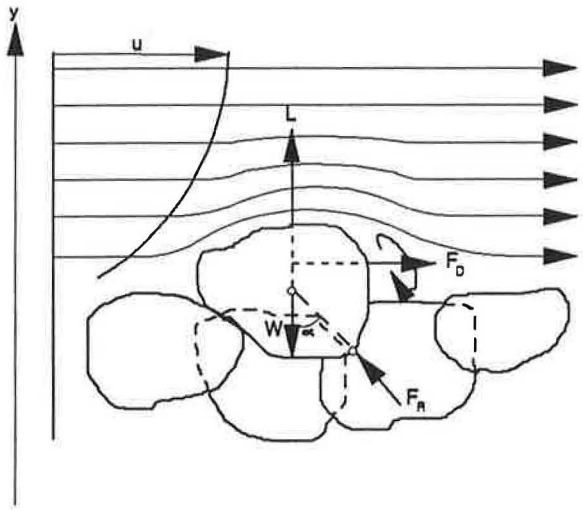

FIGURE 1 Schematic of particle and fluid forces (2).

The following relation describes the contributing factors in the erosion, transport, and deposition of sediment associated with local scour (2):

$$f(B) = \phi_1[g(B),g(S),t] \tag{1}$$

where

$f(B)$ = mathematical description of boundary,
t = time,
$g(B)$ = sediment discharge or transport rate out of scour zone as function of boundary shape and position, and
$g(S)$ = rate of supply to scour zone.

In the absence of the aforementioned mathematical principles, the emphasis must be placed on experiments to determine the functions empirically. After dimensional analysis the bed configuration function becomes a function of average and shear velocities, Reynolds number, and Froude number (2):

$$f(B) = \left[\frac{V}{\sqrt{\frac{\tau_c}{\rho}}}, \sigma, \frac{Vt}{a}, \frac{Va}{\nu}, \frac{V^2}{ga}, \frac{b}{a}, g(S)\right] \tag{2}$$

where

τ_c = critical tractive force for sediment composing bed,
ρ = fluid density,
σ = standard deviation of particle size distribution,
a = characteristic length describing size of system,
ν = kinematic viscosity of fluid,
b = typical length of flow pattern,
V = velocity, and
g = gravitational acceleration.

The use of noncohesive sediments in laboratory studies has been justified as documented by Vanoni:

> Aside from numerous experiments relating to land erosion, the generalized study of scour by flowing water has been limited to studies involving noncohesive soils. Although the property of cohesiveness is of paramount importance in such scour phenomena occurring below conservation and control structures, in bank caving of streams, and in the design of artificial channels constructed in cohesive materials, there are also many problems involving scour of noncohesive soils, e.g., bed scour in natural streams and scour around bridge piers and downstream of outlet works. In addition, considerable progress has been made in the design of stuctures discharging on cohesive soils through model studies using noncohesive sediments. (2)

These experiments are characterized by fully turbulent flow in which the Reynolds number becomes very high (on the order of 10^4 or greater). Since the physical modeling involved only clear-water scour experiments, uniformly graded gravel, and noncohesive soil, and because the experiment was conducted under steady-state conditions, the equation simplifies to a function of relative shear velocity, Froude number, and a dimensionless length ratio:

$$f(B) = \left[\frac{V}{\sqrt{\frac{\tau_c}{\rho}}}, \frac{V^2}{ga}, \frac{b}{a}\right] \tag{3}$$

The length ratio, b/a, has been commonly represented by the relative roughness, D_{50}/y, in scour studies. There exists a relationship between the sediment number, N_{sc}, and the relative roughness. If this relationship is known, a solution for the riprap size, D_{50}, can be achieved. The other hydraulic identities of interest, in the context of this study, derived from dimensional analysis are Shields parameter, sediment number, and Froude number.

SHIELDS PARAMETER

The Shields parameter is a dimensionless hydraulic identity equal to the ratio of the kinematic forces that influence particle motion to the gravitational forces that resist movement (3). This property is a quantitative indication of particle stability. The shear stress due to the kinematic forces of the fluid can be defined by the following equation:

$$\tau_o = \gamma\, d\, S_e = \rho\, u_*^2 \tag{4}$$

where

γ = specific weight of water [N/m³ (lb/ft³)],
d = flow depth [m (ft)],
S_e = energy slope,
ρ = density of water [kg/m³ (slug/ft³)], and
u_* = $(g\, y\, S_e)^{0.5}$
= shear velocity [m/sec (ft/sec)].

The shear stress of the particle to resist movement is represented by the following equation:

$$\tau = \rho g(S_g - 1)D_{50} \tag{5}$$

The Shields parameter, or the critical dimensionless shear stress, is therefore defined as Equation 4 divided by Equation 5:

$$\tau_* = \frac{dS_e}{D_{50}(S_b - 1)} = \frac{u_*^2}{g(S_g - 1)D_{50}} \quad (6)$$

SEDIMENT NUMBER

Like the Shields parameter, the sediment number, N_{sc}, is a ratio of the shear stress due to fluid forces to the shear stress of the particle to resist movement. Furthermore, this property is also an indicator of particle stability. However, the difference between the two stability parameters is that the sediment number is a velocity-based criterion whereas the Shields parameter is a shear stress–based criterion. Hence, the numerator term that defines the fluid shear stress is a function of velocity.

Isbash defined the stability of noncohesive particles on the basis of average velocity criteria. An empirical dimensionless coefficient, E, was determined for the particles (*4*). The sediment number is related to this coefficient as depicted in the following equation:

$$N_{sc} = 2E^2 \quad (7)$$

For loose stones lying on top of other stones, $E = 0.86$, and for stones "seated" among the other stones, $E = 1.20$ (*4*). The higher coefficient value for seated stones than for loose stones reflects the particles' potential to be more resistant to movement. Hence, a higher velocity is associated with the more stable particle. By substituting an average velocity for the shear velocity in Equation 4, the shear stress due to kinematic forces of the fluid as a function of velocity can be defined as

$$\tau_o = \rho V^2 \quad (8)$$

The equation for the sediment number becomes a ratio of Equation 8 to Equation 5:

$$N_{sc} = \frac{V^2}{g(S_g - 1)D_{50}} \quad (9)$$

Comparing Equations 6 and 9 demonstrates the similarities between Shields parameter and the sediment number. These are the two parameters that have historically been used to evaluate incipient motion for sediment in water.

FROUDE NUMBER

The Froude number is a hydraulic identity that is the ratio of the inertial to gravitational forces. This dimensionless property is a disruptive term for the flow field acting on the particles. In this study, the Froude number is a function of the spatially averaged velocity and depth as defined by the following equation:

$$\mathrm{Fr} = \frac{V}{\sqrt{gd}} \quad (10)$$

where Fr is the Froude number.

RELATED LABORATORY EXPERIMENTS

In 1990 laboratory experiments were conducted in the FHWA Hydraulics Laboratory tilting flume to determine the stability of rock riprap protecting abutments in floodplains (*5*). The abutment models were represented by two different shapes: a vertical and a spill-through abutment. These experiments yielded extensive measured data that could be used to interpret the behavior of sediment relative to the prevailing hydraulic characteristics. The results were presented as a relationship between sediment number, N_{sc}, and relative roughness, D_{50}/d_{cc} as depicted in Figure 2. Figure 2 is an illustration of calculated sediment number and calculated relative roughness. The velocity term in Equation 9 is represented by a calculated average constricted velocity, V_{cc}. The relative roughness flow depth term, d_{cc}, is a calculated value along with V_{cc} determined by satisfying the energy equation from the approach section to the constricted section of the laboratory model.

RIPRAP AS COUNTERMEASURE AGAINST SCOUR

Studies have been done to provide rock riprap design guidelines for protecting bridge abutments from erosion. FHWA published design criteria in *Design of Riprap Revetment*, Hydraulic Engineering Circular (HEC) 11 (*6*), which recommends that a rock riprap layer should be extended at least 1.52 m (5 ft) below the stream bed and on a continuous slope with the channel embankment. The design equation for sizing riprap as protection for channels and bridge abutments, as recommended in HEC-11, can be presented in the following form:

$$D_{50} = \left(\frac{0.001\ V_a^3}{d_{\mathrm{avg}}^{0.5}\ K_1^{1.5}}\right) C_{sg} C_{sf} C_{P/A} \quad (11)$$

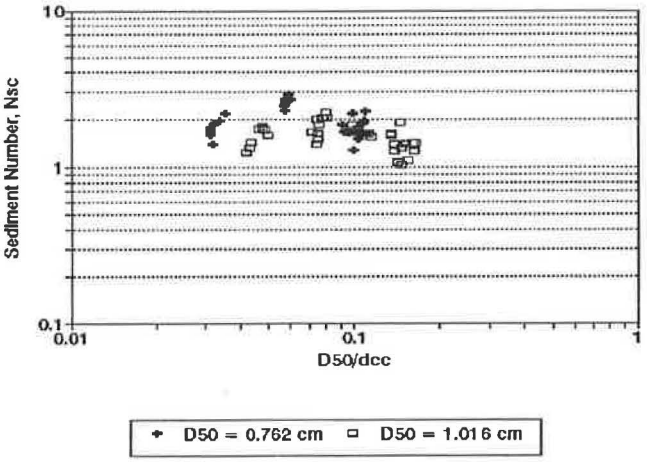

FIGURE 2 Relationship between sediment number and relative roughness for spill-through abutment on floodplain with no channel.

where

V_a = average velocity in main channel (ft/sec),
d_{avg} = average depth in main channel (ft),
K_1 = $\{1 - (\sin^2 \theta / \sin^2 \phi]\}^{0.5}$,
θ = bank angle with horizontal,
ϕ = riprap particle's angle of repose,
C_{sf} = correction factor for stability factor,
C_{sg} = correction factor for specific gravity, and
$C_{P/A}$ = correction factor to account for acceleration of velocities when flow is obstructed by piers or abutments.

In the context of this paper, Equation 11 can apply to the design of riprap on the floodplain and the channel. Since Equation 11 defines D_{50} with a specific gravity of 2.65 and stability factor of 1.2, the following correction factors must be multiplied with Equation 11 to obtain the stable riprap size for different S_g and SF values:

$$C_{sg} = \frac{2.12}{(S_g - 1)^{1.5}} \tag{12}$$

$$C_{sf} = \left(\frac{SF}{1.2}\right)^{1.5} \tag{13}$$

where SF is the stability factor, and $C_{P/A} = (1.5)^3 = 3.38$. HEC-11 recommends that stability factor range of 1.6 to 2.0 should apply for riprap design in the vicinity of bridge abutments (*6*). This criteria in HEC-11 was published as an interim procedure to be used until better criteria could be developed.

Currently, the design equation for sizing riprap for pier protection is a rearranged form of the Isbash equation. Applying the seated dimensionless coefficient to Equation 9 yields the following equation:

$$D_{50} = \frac{0.347\ V^2}{g(S_g - 1)} \tag{14}$$

The Isbash equation has been modified for spill-through abutments on the basis of an experimental study. Previous spill-through abutment laboratory experiments have yielded a design equation for determining stable riprap size (*5*):

$$D_{50} = \frac{0.535\ V_{cc}^2}{g\ (S_g - 1)} \tag{15}$$

where V_{cc} is the computed average velocity at the contraction within the floodplain, in feet per second.

Equation 15 is derived from a relationship between the sediment number and the relative roughness, D_{50}/y. The velocity term is a computed value based on the energy equation applied to the approach and constricted sections.

DESCRIPTION OF EXPERIMENTAL SETUP FOR CURRENT STUDY

The physical scale model is comprised of a spill-through abutment, a floodplain, a channel and a gravel apron. The model was not site-specific, so a scaling ratio is not applicable, but generally, model length dimensions were about 1/50th of the typical prototype dimensions. Figure 3 illustrates a plan view of the physical model.

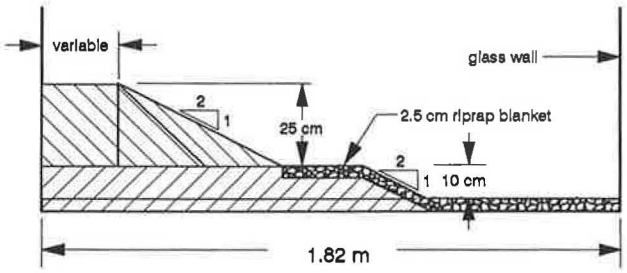

FIGURE 3 Plan view of spill-through abutment, floodplain, and channel.

Spill-Through Abutment

The spill-through abutment model, exhibited in the Figure 4, is comprised of four modular components as follows:

- Two 90-degree-curved embankment faces that make up the upstream and downstream corners of the spill-through abutment,
- Two 51- × 25-cm triangular prisms of variable length that make up the downstream and upstream faces of that are perpendicular to the direction of flow,
- One 15-cm-wide vertical abutment of variable length, and
- 51- × 25- × 15-cm triangular prism that extends from the abutment to the toe of the embankment.

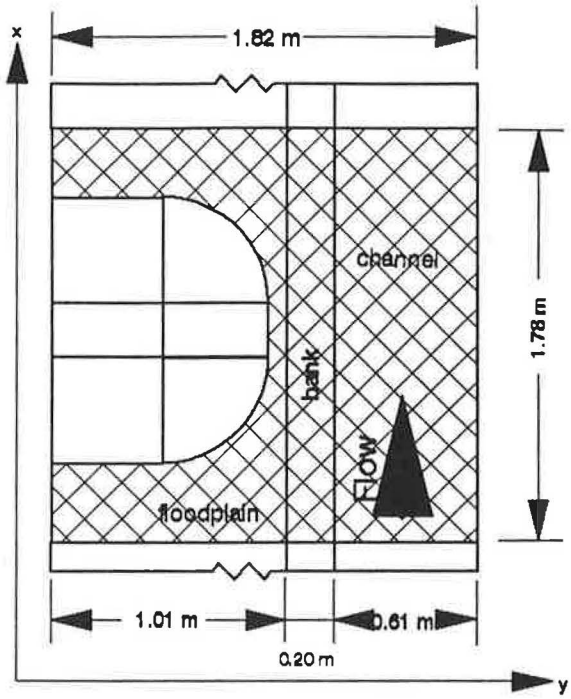

FIGURE 4 Profile view of spill-through abutment, floodplain, and channel.

These units are fastened together and anchored to the test section floor. The exposed surface of all the components are a mixture of fine sand and asphalt to simulate a concrete surface roughness. The spill-through abutment centerline was situated at the 8.12-m (26.63-ft) station from the reference datum at the flume tailbox.

As illustrated in the Figure 4, the dimensions of the spill-through abutment were as follows:

- Abutment length = variable, 13 to 51 cm (5 to 20 in.);
- Abutment width = 15 cm (6 in.);
- Embankment width = 117 cm (46 in.);
- Abutment height = 25 cm (10 in.); and
- Side slopes = 2:1 (horizontal:vertical).

Floodplain and Channel

The stream prototype is simulated as a floodplain and a channel in this study as displayed in Figures 3 and 4. The floodplain and channel were constructed from CDX fir plywood coated with a mixture of sand and asphalt. The spill-through abutment model was placed on the floodplain in the test section. The side slope of the channel was 2:1 (horizontal:vertical), and the channel height was 10 cm (4 in.). Within the test section where the spill-through abutment model was situated, both the floodplain and the channel were lined with riprap.

Riprap Lining

Riprap was modeled in the experiments by two sizes of uniformly graded gravel with D_{50}'s of 7.94 and 11.11 mm (0.31 and 0.41 in.). The smaller gravel represents the geometric mean size of the gravel that passed through the 9.5-mm sieve, was retained by the 6.3-mm sieve, and had a specific gravity of 2.702. The larger gravel passed through the 12.7-mm sieve was retained by the 9.5-mm sieve, and had a specific gravity of 2.709. Since the gravel bed had a thickness of 2.5 cm, two layers of gravel were used to make the riprap apron. Beneath the two layers of gravel is the sand- and asphalt-coated wood surface that was painted neon red in the expected area of failure. The observed area of failure from previous laboratory experiments was consistently at the toe of the embankment on the downstream side of the abutment centerline.

Experimental Plan

The objective of the physical modeling in this study was to simulate the threshold of movement of the gravel material used to protect the floodplain and channel in the vicinity of the spill-through abutment. The experiments were designed to identify the hydraulic conditions that precipitate incipient motion by the process of variation of the following hydraulic properties and model dimensions:

- Tailwater depth,
- Discharge,
- Abutment length,
- Bed slope, and
- Medium grain size, D_{50}, of the gravel.

Velocity is a function of the discharge, flow depth, and bed slope. Hence, it varies as a consequence of the modification to the aforementioned variables. Since the stability of the sediment depends on velocity and flow depth, the stability of the sediment can be modeled for a wide range of scenarios.

The procedure for approaching incipient motion is an iterative experimental process in which the aforementioned hydraulic properties were adjusted by small increments. Generally, when failure was accomplished, discharge was held constant and the tailwater depth, and thus the velocities, were decreased by small increments until incipient motion was "bracketed." By bracketing incipient motion, experiments simulated hydraulic conditions just before and just after the threshold of movement. Conversely, if the experiment did not achieve failure, the tailwater depth was decreased, and thus velocities were increased, by small increments until failure was attained.

Ultimately, the experiments that most closely replicated incipient motion compose the data from which a relationship can be developed. By eliminating the other experiments (i.e., experiments that were not considered to closely simulate incipient motion) from the data analysis, much of the data scatter can be minimized, thereby producing a better correlation.

Location of Data Measurement Stations

In the context of this study, average velocity is defined as a function of time, flow depth, and flow area, respectively, as follows:

- Average point-velocity measurements: orthogonal x- and y-component velocity measurements were made by the electromagnetic current meter at a rate of 10 Hz and averaged over a 30-sec period. These velocity readings were taken at depths of two-, six-, and eight-tenths of the depth and at the bed to give a complete representation of the velocity profile.
- Depth-averaged velocities: the aforementioned average point-velocity measurements taken at various depths at a given station can then be averaged to yield a depth-averaged velocity.
- Spatially averaged velocities: the average point velocity is taken at locations on the floodplain, channel, bank, and abutment to define the average cross-sectional velocities as well as represent the velocity distribution from the approach to the constriction to the exit sections, both with accuracy.

The spatially averaged, or average cross-sectional, velocity is computed for each transect (e.g., approach, centerline, failure, and exit). These velocities can be verified by using the continuity equation to compute the discharge at the cross section and compare it with the flow readings measured by the venturi meter. The general form of the equation would be

$$Q_{ci} = \sum_{j=1}^{n} V_j w_j d_j \tag{16}$$

where

Q_{ci} = computed discharge for Cross Section i [m³/sec (ft³/sec)];
V_j = depth-averaged velocity for Measuring Station j [m/sec (ft/sec)];

w_j = width of flow field represented by measured velocity, V_j [m (ft)]
$= y_{j+1} - y_{j-1}$,
y_j = transverse distance of measurement stations from flume wall [m (ft)]; and
d_j = measured depth of Station j [m (ft)]

Generally, more measuring stations in a transect yield computed flows that are much closer to the measured flow. The error in computed velocity-based flow to measured flow can be represented as follows:

$$\varepsilon_i = \frac{|Q_m - Q_{ci}|}{Q_m} \tag{17}$$

where Q_m equals flow measured by the venturi meter, in cubic meters (or feet) per second, and ε_i is the relative error of computed flow to measured flow.

These computations not only serve to produce averaged one-dimensional hydraulic properties (e.g., average velocity, average depth, and cross-sectional discharge), but also allow for quality assurance and quality control of the data-taking procedures and measuring instruments. Observations from the experiments indicate that accuracy (i.e., the minimization of relative error, ε_i) is highest for transects with more measurement stations and flow regimes resembling uniform flow. Generally, ε_i is less than 0.10 for the approach and contracted centerline sections.

From previous laboratory studies of spill-through abutments, it was observed that the failure zone occurs at the toe of the abutment slightly downstream of the centerline. Furthermore, it was learned tha the local average-point velocity at the failure zone approaches zero because of the turbulent flow that predominates in the flow region. The presence of the turbulent flow is accompanied by rotational flow. Because the measuring instruments can only measure the x- and y-directions, the x- and y-components of velocity that result from rotational flow in the x-y plane cancel each other out to yield an average velocity almost equal to zero.

Representative Discharges

Three different flows were simulated for all the abutment length and gravel sizes. Associated with the three flows are the depths ranging from shallow, medium, and deep flow depth in the floodplain. Generally, as abutment length (i.e., degree of flow obstruction) increased, the backwater effect increased for each of the flow scenarios. For the longest abutment length, the highest flows had to be decreased slightly because the abutment would have been overtopped. Typically, the three modeled flows in these experiments were 0.13, 0.20, and 0.25 m³/sec.

Observed Failure

Similar laboratory studies, as corroborated by this study, consistently developed failure zones located at the toe of the embankment just downstream of the abutment centerline as depicted in Figure 5. Figure 5 shows the typical progression of

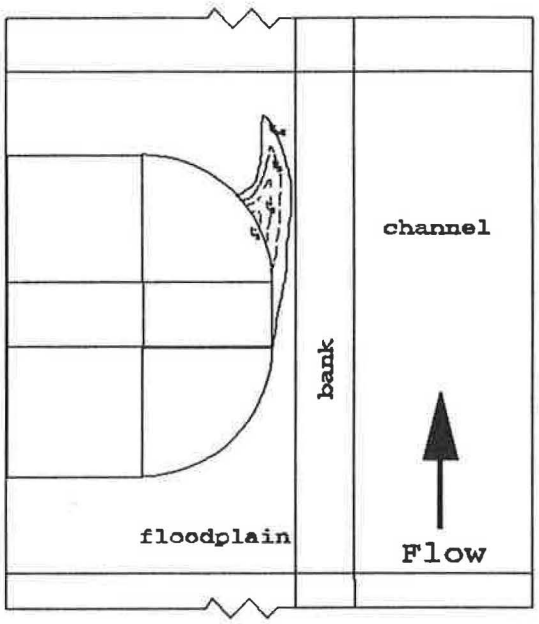

FIGURE 5 Typical riprap failure zone progression as a function of time.

the failure zone with respect to time. The failure zone reaches equilibrium at time, t_{eq} as depicted in Figure 5, which was typically 90 min to 2 hr in these experiments. Moreover, 24-hr experiments were conducted to verify that failure did not proliferate beyond the 4-hr simulation time of the experiments.

In the context of this study, failure was defined as the instantaneous moment when the unprotected surface was clearly exposed. As previously mentioned, a two-layer gravel apron was implemented. Hence, it could be argued that failure could vary for different thicknesses of gravel. Because incipient motion is such an extemporaneous phenomenon, the distinction between stability and failure is very fine. Furthermore, the unprotected surface experiences a change from a two-layer gravel cover to an exposed surface in a matter of seconds. As discussed earlier, incipient motion was approached by such small increments of variation of hydraulic parameters that the relativeness (or arbitrariness) of failure does not affect the hydraulic characteristics of incipient motion significantly.

ANALYSIS OF RESULTS

Surface Roughness Calibration

A series of experiments with just the channel and floodplain configuration were conducted to determine the Manning's roughness coefficient, n, fo the sandy asphalt surface. Manning's equation was rearranged to solve for n:

$$n = \frac{R^{2/3} S_e^{1/2}}{V} \tag{18}$$

where V is the measured depth-averaged velocity in meters (feet) per second, and R is the hydraulic radius (assumed to be depth in open channels) in meters (feet).

The energy gradeline was computed for evenly-spaced stations along longitudinal sections for three flow scenarios:

1. Bank-full flow (i.e., no flow in the floodplain),
2. Shallow floodplain flow, and
3. Deep floodplain flow.

The energy at each measurement station was computed using the energy equation

$$E = \frac{V^2}{2g} + d + z \tag{19}$$

where

V = depth-averaged velocity for the cross section,
d = average cross-sectional flow depth, and
z = vertical distance above reference datum.

From the energy computed in the longitudinal direction of flow, a slope of the energy gradeline can be determined. By applying this energy slope to Equation 18, an average Manning's n-value can be computed. These calibration experiments yielded a Manning's n-value of 0.0112 for the sandy paved wood surface of the floodplain and the channel. The laboratory-derived roughness coefficient is used throughout this study to quantify roughness for the sand and asphalt-coated wood.

Incipient Motion Results

As was the case with the previous spill-through abutment laboratory experiments, these experiments demonstrated that the failure zone develops at the toe of the abutment on the downstream side of the abutment centerline. The failure zone consistently precipitated where the flow separated, as illustrated in Figure 5, downstream of the abutment centerline. Regardless of the abutment length and proximity to the channel, the failure zone location remained constant. Even when the abutment toe was extended completely across the floodplain (i.e., 100 percent encroachment) adjacent to the channel, the gravel failed on the floodplain. The channel remained stable in all cases except when failure was excessive enough to spread to the channel bank. Since the focus of this study is to identify incipient motion (i.e., the moment that gravel begins to fail), the excessive failure that expanded to the channel bank is not relevant to the scope of this study.

Figure 6 illustrates the relationship between the stability of the particle (i.e., dimensionless shear stress) and the flow field (i.e., Froude number) in the constricted floodplain for previous spill-through abutment laboratory studies. Recall that previous laboratory studies represented particle stability with sediment number, N_{sc}, as a function of the relative roughness, D_{50}/d_{cc}, as exhibited in Figure 2. However, that relationship did not yield a good correlation. Figure 6 depicts a relationship that describes particle stability with Shields parameter is a better correlation.

Similarly, these laboratory experiments assume a relationship much like the one illustrated in Figure 6. By eliminating experimental data points that represent excessive failure (i.e., well beyond incipient motion) and non-failure well before incipient motion and considering the local (i.e., floodplain) hydraulic conditions, a good correlation between Shields parameter and the Froude number in the constricted floodplain can be developed, as illustrated in Figure 7.

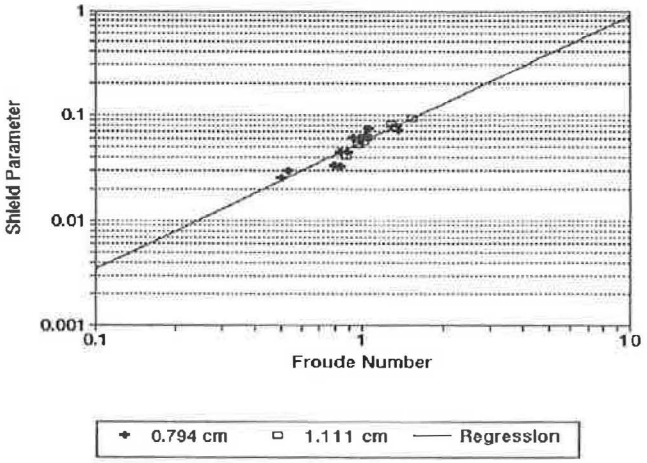

FIGURE 6 Relationship between Shields parameter and Froude number for spill-through abutments situated in floodplain with no channel.

A regression analysis yields a line, as depicted in Figure 7, that can be represented by the following equation:

$$\tau_* = 0.0556\ \mathrm{Fr}^{1.1997} \tag{20}$$

where τ_* is the Shields parameter, and Fr is the Froude number.

Substituting Equations 6 and 10, Equation 21 becomes

$$\frac{d_{fp}\, S_e}{D_{50}(S_g - 1)} = 0.0556\left(\frac{V_{fp}}{\sqrt{g d_{fp}}}\right)^{1.1997} \tag{21}$$

where

V_{fp} = depth-averaged velocity in the contracted floodplain (m/sec), and
d_{fp} = average floodplain flow depth in the contraction, in m.

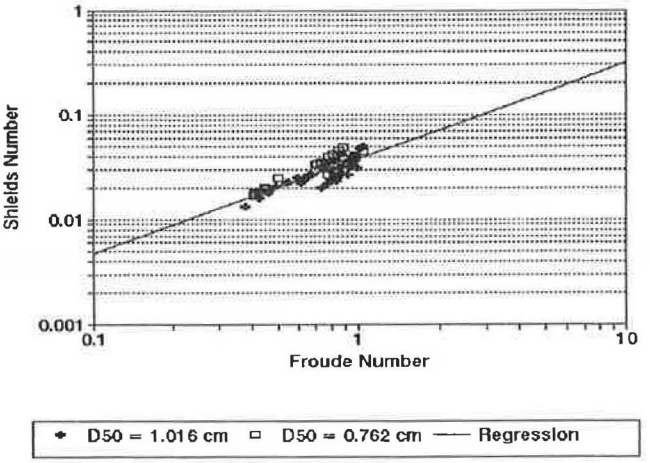

FIGURE 7 Relationship between Shields parameter and Froude number for contracted section of spill-through abutment floodplain.

Because of the limitations of these experiments, an energy slope, S_e, could not be measured accurately. The rapidly varied unsteady flow occurring at the toe of the abutment made accurate measurement very difficult Therefore, a theoretical approximation of the energy slope was made by rearranging Equation 19, which is a form of Manning's equation. The assumptions of Manning's equation is steady uniform flow, whereas these experiments demonstrated rapidly varied unsteady flow at the toe of the abutment and steady uniform flow everywhere else. However, the Manning equation is meant to provide a theoretical approximation of a hydraulic property that could not be measured experimentally. To obtain the Shields parameter, τ_*, from the experimental data, S_e was expressed in terms of the Manning equation, as follows:

$$S_e = \frac{V_{fp}^2 n^2}{d_{fp}^2} \tag{22}$$

Substituting into Equation 21 and rearranging to solve for D_{50} yields the following relationship:

$$D_{50} = \frac{17.988 n^2 V_{fp}^{0.8} g^{0.6} d_{fp}^{0.27}}{(S_g - 1)} \tag{23}$$

where D_{50} is the geometric mean grain size of the riprap in meters.

Because n is a function of D_{50}, either from experimental or theoretical derivation, it may be necessary to perform a few iterations before arriving at a solution for Equation 23. Furthermore, since Equation 23 defines the regression line that passes through the data points, the application of a factor of safety may be necessary. The selection of an appropriate factor of safety is left to the discretion of the designer. This linear relationship for floodplain with channel is comparable to the previous experimental studies of spill-through abutments with a floodplain and no channel. Since the data exhibited in Figure 7 represent local (i.e., spatially averaged in the floodplain only) hydraulic conditions and the previous experimental studies employed floodplains only, good agreement between the data from the two studies is the result, as demonstrated in Figure 8. Recall that the D_{50} sizes 0.794 and 1.111 cm were used for the experiments in this study, and 0.762 and 1.016 cm were used for the previous spill-through abutment experiments. The similarity shown in Figure 8 implies that a universal relationship can be developed to describe spill-through abutments in floodplains regardless of proximity to channels and varying abutment lengths, flows, flow depths, and velocities in the contraction.

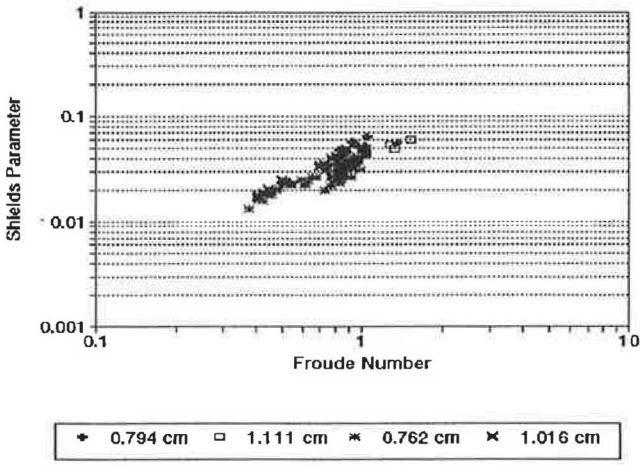

FIGURE 8 Comparison of spill-through abutments situated in floodplains near channels and spill-through abutments situated in floodplains with no channels.

CONCLUSIONS

This study established the following observations and relationships:

- The local Shields parameter correlates well with the local Froude number.
- There is good agreement between the results of this study and previous spill-through abutment studies in floodplains without a channel.
- A linear regression with a high coefficient of determination describes the experimental data points. From this linear relationship between the local Shields parameter and the local Froude number, the geometric mean grain size, D_{50}, of the riprap can be determined.
- Since failure always occurred on the floodplain initially, the stability of the riprap-lined channel is not undermined until failure is so excessive that it spreads to the channel.
- The failure zone always developed at the downstream side of the spill-through abutment toe regardless of the degree of encroachment or proximity of the spill-through abutment with respect to the channel. The location of the failure zone maintained consistency with previous studies.
- The progression of the failure zone is consistent for all the flow scenarios. Furthermore, the failure zone consistently reached equilibrium shortly after incipient motion.
- This study dovetails with previous spill-through abutment studies by proliferating the degree of encroachment on the floodplain. This study demonstrated that the design guidelines presented in this study is universally applicable for the entire range of encroachment simulated in this study and previous studies.
- The location of the spill-through abutment on the floodplain with respect to the channel did not affect the local hydraulic conditions that caused the riprap to fail at the abutment toe.
- Other references such as HEC-11 should be used for guidance in designing riprap revetment for the channel and bank, because this study revealed that the channel riprap stability was not affected by the proximity of the channel to the spill-through abutment. Therefore, the channel riprap can be treated as a separate design.

ACKNOWLEDGMENTS

The author would like to express his sincerest appreciation to Roy Trent of FHWA for his patience, guidance, and support throughout the course of the research project. The author extends gratitude to J. Sterling Jones of FHWA, whose guid-

ance, technical support, and expertise in hydraulic modeling contributed a great deal to efforts in this study.

The author also wishes to thank everyone at the National Highway Institute, especially Ilene Payne, for the opportunity to be part of the Grants for Research Fellowships (GRF) program. Her willingness to accommodate the author under the unusual circumstances of this GRF project is sincerely appreciated.

REFERENCES

1. Raudkivi, A. J. *Loose Boundary Hydraulics*. University of Auckland, New Zealand.
2. *Sedimentation Engineering*, (V. A. Vanoni, ed.) ASCE Manuals and Reports on Engineering Practice 54. ASCE, New York, 1975.
3. Shields, A. *Application of Similarity Principles and Turbulence Research to Bedload Movement*. California Institute of Technology, Pasadena, 1936 (English translation by W. P. Ott and J. C. van Uchelon).
4. Isbash, S. V. Construction of Dams by Depositing Rock on Running Water. *Trans. 2nd Congress on Large Dams*, Vol. 5, Washington, D.C., 1936, pp. 123–135.
5. Pagán-Ortiz, J. E. *Stability of Rock Riprap for Protection at the Toe of Abutments Located at the Floodplain*. FHWA, U.S. Department of Transportation, 1991.
6. *Design of Riprap Revetment*. Hydraulic Engineering Circular 11; FHWA-IP-89-016. FHWA, U.S. Department of Transportation, 1989.

Methodology for Investigation of Inappropriate Pollutant Entries into Storm Drainage Systems

DONALD E. BARBÉ, ROBERT PITT, MELINDA LALOR, D. DEAN ADRIAN, AND RICHARD FIELD

A summary is presented of the user's guide that was the result of a series of research projects sponsored by the Environmental Protection Agency to develop a procedure to investigate non-stormwater entries into storm drainage systems. Previous projects have found that dry-weather flows discharging from storm drainage systems can contribute significant pollutant loadings to receiving waters. If only wet-weather stormwater runoff is considered, little improvement in the conditions of receiving water may occur with many stormwater control programs. These dry-weather flows may originate from many sources; the most important sources are sanitary wastewater from separate sanitary collection systems or failing septic tank systems and industrial or commercial pollutant entries from vehicle maintenance facilities and the like. After the outfalls affected by polluted dry-weather flows are identified, additional survey activities are needed to locate and correct the non-stormwater entries into the storm drainage systems. The user's guide contains information on conducting local investigations to identify the types and estimate the magnitudes of these non-stormwater entries.

Urban stormwater runoff is the portion of precipitation that drains from urban surfaces such as roofs, streets, parking lots, and garages. Current interest in illicit or inappropriate connections to storm drainage systems is an outgrowth of investigations into the larger problem of determining the role of urban stormwater runoff as a contributor to problems with the quality of receiving water. An urban stormwater drainage system also conveys waters and wastes from many other sources. For example, Montoya found that slightly less than half the water discharged from Sacramento's stormwater drainage system was not directly attributable to precipitation (*1*). Sources of some of this water can be identified and accounted for by examining current permit records from the National Pollutant Discharge Elimination System (NPDES) for permitted industrial wastewaters that can be discharged to the storm drainage system. However, most of the water comes from other sources, including illicit and inappropriate entries to the storm drainage system. These entries can account for a notable amount of the pollutants discharged from storm drainage systems (*2*).

D. E. Barbé, Department of Civil Engineering, University of New Orleans, New Orleans, La. 70148. R. Pitt and M. Lalor, Department of Civil Engineering, University of Alabama at Birmingham, Birmingham, Ala. 35294. D. D. Adrian, Department of Civil Engineering, Louisiana State University, Baton Rouge, La. 70803. R. Field, Storm and Combined Sewer Program, Water and Hazardous Waste Treatment Division, Environmental Protection Agency, Edison, N.J. 08837.

The Storm and Combined Sewer Pollution Control Program of the Office of Research and Development, Environmental Protection Agency (EPA), and the NPDES Program Branch have supported the development of a user's guide (*3*) for the investigation of inappropriate entries to storm drainage systems. The user's guide is designed to provide information and guidance to local agencies by meeting the following objectives: (a) identify and describe the most common potential sources of inappropriate pollutant entries into storm drainage systems, and (b) describe a procedure that will allow a user to determine whether significant inappropriate pollutant entries are present in a storm drainage system and, if any, to identify the type of source, as an aid to finding the ultimate location of the source.

The user's guide (*3*) was prepared in conjunction with a background study by Pitt and Lalor (*4*) that examined three categories of non-stormwater outfall discharges:

1. Pathogenic and toxic pollutants,
2. Nuisances and threats to aquatic life, and
3. Clean water.

The most important category is that of outfall discharges containing pathogenic or toxic pollutants. The most likely sources for this category are sanitary or industrial wastewaters. The outfall analysis procedure described in the user's guide has a high probability of identifying all of the outfalls in this most critical category. High probabilities of detection of other contaminated outfalls are also likely when using the procedures. After identification of the contaminated outfalls, their associated drainage areas can be subjected to a detailed source identification investigation. The identified pollutant sources can then be corrected.

ROLE OF DRY-WEATHER FLOWS IN URBAN STORMWATER RUNOFF ANALYSES

EPA's Nationwide Urban Runoff Program (NURP) highlighted the significance of pollutants from inappropriate entries into urban storm drainage (*4*). Such entries may be evidenced by flow from storm drain outfalls following and during substantial dry periods. Such flow, frequently referred to as "baseflow" or "dry-weather flow," could be the result of direct "illicit connections" as mentioned in the NURP final

report (*4*) or of indirect connections (e.g., leaky sanitary sewerage contributions through infiltration). Many of these dry-weather flows are continuous and would therefore also occur during rain-induced runoff periods. Pollutant contributions from the dry-weather flows in some storm drains have been shown to be high enough to degrade water quality significantly because of their substantial contributions to the annual mass pollutant loadings to receiving waters.

Dry- and wet-weather flows have been monitored during several urban runoff studies. These studies have found that discharges observed at outfalls during dry weather were significantly different from wet-weather discharges. Data collected during the 1984 Toronto Area Watershed Management Strategy Study monitored and characterized both stormwater and baseflows (*2*). The Toronto project involved intensive monitoring in two test areas (a mixed residential and commercial area and an industrial area) during warm and cold weather and during wet and dry weather. The annual mass discharges of many pollutants were found to be dominated by dry-weather processes.

During the mid-1980s, several individual municipalities and urban counties initiated studies to identify and correct illicit connections to their storm drain systems. This action was usually taken in response to problems with receiving water quality or information noted during individual NURP projects. Data from these studies indicate the magnitude of the cross-connection problem in many urban areas. From 1984 to 1986, Washtenaw County, Michigan, dye-tested 160 businesses in an effort to locate direct illicit connections to the county stormwater drainage. Of the businesses tested, 61 (38 percent) were found to have improper storm drain connections (*5*). In 1987 the Huron River Pollution Abatement Program dye-tested 1,067 commercial, industrial, and tax-exempt businesses and buildings, and 154 (14 percent) were found to have improper connections to storm drainage (*6*). Commercial car washes and other automobile-related businesses were responsible for most of the illicit connections in both studies. Discharges from commercial laundries were also noted.

An investigation of outfalls from the separate storm drain systems in Toronto, Canada, revealed 59 percent with dry-weather flows. Of these, 84 (14 percent of the total outfalls) were identified as grossly polluted, on the basis of the results of a battery of chemical tests (*7*). In 1987 an inspection of the 90 urban stormwater outfalls draining into Inner Grays Harbor in Washington revealed 29 (32 percent) flowing during dry weather (*8*). A total of 19 outfalls (21 percent) were described as suspect on the basis of visual observation or anomalous pollutant levels as compared with those expected in typical urban stormwater runoff characterized by the EPA 1983 NURP report.

CURRENT LEGISLATION

The Clean Water Act of 1987 contained provisions specifically addressing discharges from storm drainage systems. Section 402(p)(3)(B) provides that permits for such discharges

> i. May be issued on a system or jurisdiction-wide basis.
> ii. Shall include a requirement to effectively prohibit non-stormwater discharges into the storm drains, and
> iii. Shall require controls to reduce the discharge of pollutants to the maximum extent practicable, including management practices, control techniques and system design and engineering methods, and such other provisions as the Administrator or the State determines appropriate for the control of such pollutants.

In response to these provisions, EPA issued a final rule to begin implementation of Section 402(p) of the Clean Water Act on November 16, 1990 (*9*). A screening approach that includes chemical testing of outfalls or storm drainage with dry-weather flow (defined by a 72-hr antecedent dry period) was adopted. The parameters to be tested are a combination of several pollutants of concern and tracers that may be used to help identify contaminated outfalls and predict the source of illicit discharges.

Section 122.26(d)(1)(iv)(D) of the rule applies specifically to the user's guide (*3*). EPA requires an initial screening program to provide a means of detecting high levels of pollutants in storm sewerage. Minimum requirements are

> a narrative description . . . of visual observations made during dry weather periods. If any flow is observed, two grab samples shall be collected during a 24 hour period with a minimum period of four hours between samples. For all such samples, a narrative description of the color, odor, turbidity, the presence of an oil sheen or surface scum as well as any other relevant observations regarding the potential presence of non-stormwater discharges or illegal dumping shall be provided. In addition, a narrative description of the results of a field analysis using suitable methods to estimate Ph, total chlorine, total copper, total phenol, and detergents (or surfactants) shall be provided along with a description of the flow rate. Where the field analysis does not involve analytical methods approved under 40 CFR Part 136, the applicant shall provide a description of the method used including the name of the manufacturer of the test method along with the range and accuracy of the test.

The protocol of the user's guide seeks to determine whether non-stormwater flows are causing problems (e.g. pathogenic, toxic, threat to aquatic life, nuisance) and to provide additional detail with respect to the source. It accomplishes this by outlining an effective screening methodology to identify storm drainage system outfalls contaminated by illicit or inappropriate discharges and to determine specifically how the likely sources can be identified. This protocol is supported by a research report containing the results of a demonstration project using these procedures and much more detailed information.

POTENTIAL DRY-WEATHER DISCHARGE SOURCES

The user's guide is directed to the identification and location of non-stormwater entries into storm drainage systems. It is important to note that for any effective investigation of pollution within a stormwater system, all pollutant sources must be included. Prior research has shown that for many pollutants, stormwater may contribute the smaller portion of the total pollutant mass discharged from a storm drainage system. Significant pollutant sources may include dry-weather entries occurring during both warm and cold months and snowmelt runoff, in addition to conventional stormwater associated with rainfall. Consequently, much less benefit in reducing pollution

will occur if only stormwater is considered in a control plan for controlling storm drainage discharges. The user's guide contains a protocol to identify sources of inappropriate entries to storm drainage systems. The investigations presented in the user's guide may also identify illicit point source outfalls that do not carry stormwater. Obviously, these outfalls also need to be controlled and permitted.

Table 1 presents a summary of the potential sources of contaminated entries into storm drainage systems, along with their probable flow characteristics. The following subsections summarize these sources.

Residential and Commercial Sources

The most common potential non-stormwater entries, which have been identified by a review of documented case studies for commercial and residential areas, are

- Sanitary wastewater sources:
  - –Raw sanitary wastewater from improper sewerage connections, exfiltration, or leakage; and
  - –Effluent from improperly operating, designed, or nearby septic tanks.
- Automobile maintenance sources:
  - –Car-wash wastewaters,
  - –Radiator flushing wastewater,
  - –Engine degreasing wastes,
  - –Improper oil disposal, and
  - –Leaky underground storage tanks.
- Irrigation sources:
  - –Lawn runoff from overwatering, and
  - –Direct spraying of impervious surfaces.
- Clean sources:
  - –Infiltrating groundwater,
  - –Water routed from preexisting springs or streams, and
  - –Infiltrating potable water from leaking water mains.
- Other sources:
  - –Laundry wastewaters,
  - –Noncontact cooling water,
  - –Metal plating baths,
  - –Dewatering of construction sites,
  - –Washing of concrete ready-mix trucks,
  - –Sump-pump discharges,
  - –Improper disposal of household toxic substances, and
  - –Spills from roadway and other accidents.

From this list, sanitary wastewater is the most significant source of bacteria, and automobile maintenance and plating baths are the most significant sources of toxicants. Waste discharges associated with the improper disposal of oil and household toxicants tend to be intermittent and low in volume. These wastes may therefore not reach the stormwater outfalls unless carried by higher flows from another source or by stormwater during rains.

Industrial Sources

Industries can produce dry-weather entries to storm sewers in several ways. Common examples include the discharge of cooling water, rinse water, other process wastewater, and sanitary wastewater. Industrial pollutant sources tend to be related to the raw materials used, final product, and the waste or byproducts created. Guidance on typical discharge characteristics associated with common industries is given in Sections 3 and 4 of the user's guide.

There is also a high potential for unauthorized connections within older industries. One reason for this is that at the time of an industry's development, sanitary sewers may not have been in existence, since early storm drains preceded the development of many sanitary sewer systems. A lack of accurate maps of sanitary and storm drain lines may lead to confusion as to their proper identification. In addition, when the activ-

TABLE 1 Potential Inappropriate Entries into Storm Drainage Systems

	Storm Drain Entry		Flow Characteristic		Contamination Category		
Potential Source	Direct	Indirect	Continuous	Intermittent	Pathogenic/Toxic	Nuisance	Clear
Residential area							
Sanitary wastewater	X	x	X	x	X		
Septic tank effluent		X	X	x	X		
Household chemicals	x	X		X	X		
Laundry wastwater	X			X		X	
Excess landscaping watering		X		X	x	x	X
Leaking potable water pipes		X	X				X
Commercial area							
Gasoline filling station	X	x		X	X		
Vehicle maintenance/repair	X	x		X	X		
Laundry wastwater	X		X	x	x	X	
Construction site dewatering		X	X	x		X	
Sanitary wastewater	X	x	X		X		
Industrial area							
Leaking tanks and pipes	x	X	X	x	X		
Many process waters	X	x	X	x	X	x	x

NOTE: X: most likely condition
x: may occur
blank: not very likely

ities within an industry change or expand, there is a possibility for illicit or inadvertent connections (e.g., floor drains and other storm drain connections receiving industrial discharges that should be treated before disposal). Finally, industries that process large volumes of water may find the carrying capacity of sanitary sewer flow to be inadequate, leading them to remove the excess water improperly through the storm drain system.

Continuous processes (e.g., industrial manufacturing) are important potential sources because any waste streams produced are likely to be constantly flowing. Detection of dry-weather discharges from these sources is therefore made easier, because the continuous and probably undiluted nature of these discharges is more noticeable (e.g., odors produced will be stronger and colors more intense).

Intermittent Sources

The presence of regular, but intermittent, flows will usually be a good indication of contaminated entries to the storm drains and can usually be distinguished from groundwater infiltration flows. However, as drainage areas increase in size, many intermittent flows will combine to create a continuous composite flow. Examples of situations or activities that can produce intermittent dry-weather flows are

- Wash-up operations at the end of a work shift or job activity,
- Wash-down following irregular accidents and spills,
- Disposal of process batches or rinse water baths,
- Overirrigation of lawns, and
- Car maintenance (e.g., automobile washing, radiator flushing, and engine degreasing).

Industries that operate on a seasonal basis, such as fruit canning and tourism, can also be a source of longer-duration intermittent discharges.

Direct Connections to Storm Drains

Direct connections refer to physical connections of sanitary, commercial, or industrial piping that carry untreated or partially treated wastewaters to a separate storm drainage system. These connections are usually unauthorized. They may be intentional or accidental, due to mistaken identification of sanitary sewer lines, and they represent the most common source of entries to storm drains by industry.

Direct connections can result in continual or intermittent dry-weather entries of contaminants into the storm drain. Some common situations are

- Sanitary sewer lines that tie into a storm drain;
- Foundation drains or residential sump-pump discharges that are frequently connected to storm drains—although this practice may be quite appropriate in many cases, it can be a source of contamination when the local groundwater is contaminated (e.g., by septic tank failures); and
- Commercial laundries and car-wash establishments that may route process wastewaters to storm drains rather than sanitary sewers.

Infiltration to Storm Drains

Infiltration into storm drains most commonly occurs through leaking pipe joints and poor connections to catch basins, but it can also be due to other causes, such as damaged pipes and subsidence.

Storm drains, as well as natural drainage channels, can therefore intercept and convey subsurface groundwater and percolating waters. In many cases, these waters will be uncontaminated and have variable flows due to fluctuations in the level of the water table and percolation from rainfall events.

Breaks of underground potable water mains are another potential clean source of releases to storm drains. Although such occurrences are not a direct pollution source, obviously they should be corrected.

Groundwater may be contaminated, either in localized areas or on a relatively widespread basis. In cases where infiltration into the storm drains occurs, it can be a source of excessive contaminant levels in the storm drains. Potential sources of groundwater contamination include, but are not limited to,

- Failing or nearby septic tank systems,
- Exfiltration from sanitary sewers in poor repair,
- Leaking underground storage tanks and pipes,
- Landfill seepage,
- Hazardous waste disposal sites, and
- Naturally occurring toxicants and pollutants due to the surrounding geological or natural environment.

Leaks from underground storage tanks and pipes are a common source of soil and groundwater pollution and may lead to continuously contaminated dry-weather entries. These situations are usually found in commercial operations such as gasoline service stations or industries involving the piped transfer of process liquids over long distances and the storage of large quantities of fuel (e.g., petroleum refineries).

INVESTIGATION METHODOLOGY

The methodology presented in the user's guide can determine if a storm drain outfall (and drainage system) is affected by pronounced non-stormwater entries. In many cases, the information to be collected following this methodology will also result in a description of the most likely sources of these discharges. Several aspects of the methodology were derived from the experience of many municipalities that have previously investigated inappropriate entries into storm drainage systems.

The methodology establishes priorities to identify the areas with the highest potential for causing problems. The investigative procedures then separate the storm drain outfalls into three general categories (with a known level of confidence) to identify which outfalls (and drainage areas) need further analyses and investigations. These categories are outfalls affected by non-stormwater entries from pathogenic or toxic pollutant sources, nuisance and aquatic life–threatening pollutant sources, and unpolluted water sources.

The pathogenic and toxic pollutant source category should be considered the most severe because it can cause illness upon water contact or consumption as well as significant water

treatment problems for downstream consumers, especially if the pollutants are soluble metal and organic toxicants. These pollutants may originate from sanitary, commercial, and industrial wastewater non-stormwater entries. Other residential area sources (besides sanitary wastewater)—for example, inappropriate household toxicant disposal, automobile engine degreasing, and excessive use of fertilizers and pesticides—may also be considered in this most critical category.

Nuisance and aquatic life–threatening pollutant sources can originate from residential areas and may include laundry wastewaters, lawn irrigation runoff, automobile washwaters, construction site dewatering, and washing of concrete ready-mix trucks. These pollutants can cause excessive algal growths, tastes and odors in downstream water supplies, offensive coarse solids and floatables, and noticeably colored, turbid, or odorous waters.

Clean water discharged through stormwater outfalls can originate from natural springs feeding urban creeks that have been converted to storm drains, infiltrating groundwater, infiltrating domestic water from waterline leaks, and such.

An outline of the major topics presented in the user's guide follows:

1. Initial mapping (Section 3).
   a. Identify receiving waters.
   b. Locate all outfalls.
   c. Compile area and land use data for each drainage area.
2. Design of initial field survey (Section 4).
   a. Select tracer parameters (visual and chemical).
   b. Develop local library of likely source flow characteristics.
3. Field screening sampling activities (Section 5).
   a. Select sample analysis procedures (detection limits, repeatability, etc.).
   b. Conduct field screening survey for both intermittent and continuous flows.
4. Data analysis (Section 6).
   a. Use simple procedures (negative indicators).
   b. Employ checklist for major flow components.
   c. Quantify major sources with flow-weighted procedures.
   d. Use matrix algebra procedures to quantify many flow components.
5. Locate inappropriate pollutant sources (Section 7).
   a. Conduct drainage surveys using tracer parameters in critical watersheds.
   b. Use flow mass balances, dye studies, and smoke tests in isolated drainage areas.
6. Correct inappropriate pollutant sources (Section 8).
   a. Use public education and zoning ordinances.
   b. Treat widespread sanitary sewerage failures possibly as a combined sewer overflow.
   c. Require regional solutions possibly for failing septic tanks.
   d. Prevent industrial and commercial area pollution.

Figure 1 is a simplified flow chart for the detailed methodology. The initial phase of the investigative protocol includes the initial mapping and field surveys. These activities require minimal effort and result in little chance of missing a seriously contaminated outfall. The initial activities are followed by more detailed watershed surveys to locate and correct the sources of the contamination in the identified problem areas. After corrective action has been taken, repeated outfall field surveys are required to ensure that the outfalls remain uncontaminated. Receiving water monitoring should also be conducted to analyze improvements in water quality. If expected improvements are not noted, then additional contaminant sources are probably present, and additional outfall and watershed surveys are needed.

RECOMMENDATIONS

The user's guide should be used as part of a comprehensive stormwater management plan that addresses all sources of stormwater pollution. The correction of pollutant entries identified only by the use of the user's guide is unlikely to achieve a significant improvement in the quality of stormwater discharges or receiving waters.

A municipality will need to plan its investigation of inappropriate entries to a storm drainage system to suit local conditions. The guide describes the issues in sufficient depth and provides examples only to enable the design of a local investigation.

The full use of all of the applicable procedures described in the user's guide is probably necessary to identify pollutant sources. Attempting to reduce costs—by, for example, examining only a certain class of outfalls or using inappropriate testing procedures—will greatly reduce the utility of the testing program and result in inaccurate data. Cursory data analysis is also likely to result in inaccurate conclusions.

Consideration should be given to any economic and practical advantages of designating the storm drainage system as a combined sewer and applying end-of-pipe treatment during investigations of non-stormwater entries to storm drainage systems.

It is also recommended that the methodology (appropriately modified) be applied to other types of sewer systems, such as combined and separate sanitary sewer systems, to locate inappropriate entries (e.g., untreated or toxic industrial wastewaters and wastes).

It is recommended that the user's guide be updated and refined by incorporating experience gained in its application. Incorporation of information from a wide variety of test locations (e.g., lake and large river receiving waters, tidal receiving waters, areas experiencing long dry periods, areas having short summers, areas having unusual groundwater characteristics, areas where the stormwater is pumped for discharge, etc.) will improve the testing and data analysis protocols described.

ACKNOWLEDGMENTS

This paper is a summary of research sponsored by the Risk Reduction Engineering Laboratory, Office of Research and Development, EPA; the Center of Environmental Research Information, EPA; and the Urban Waste Management and Research Center, University of New Orleans.

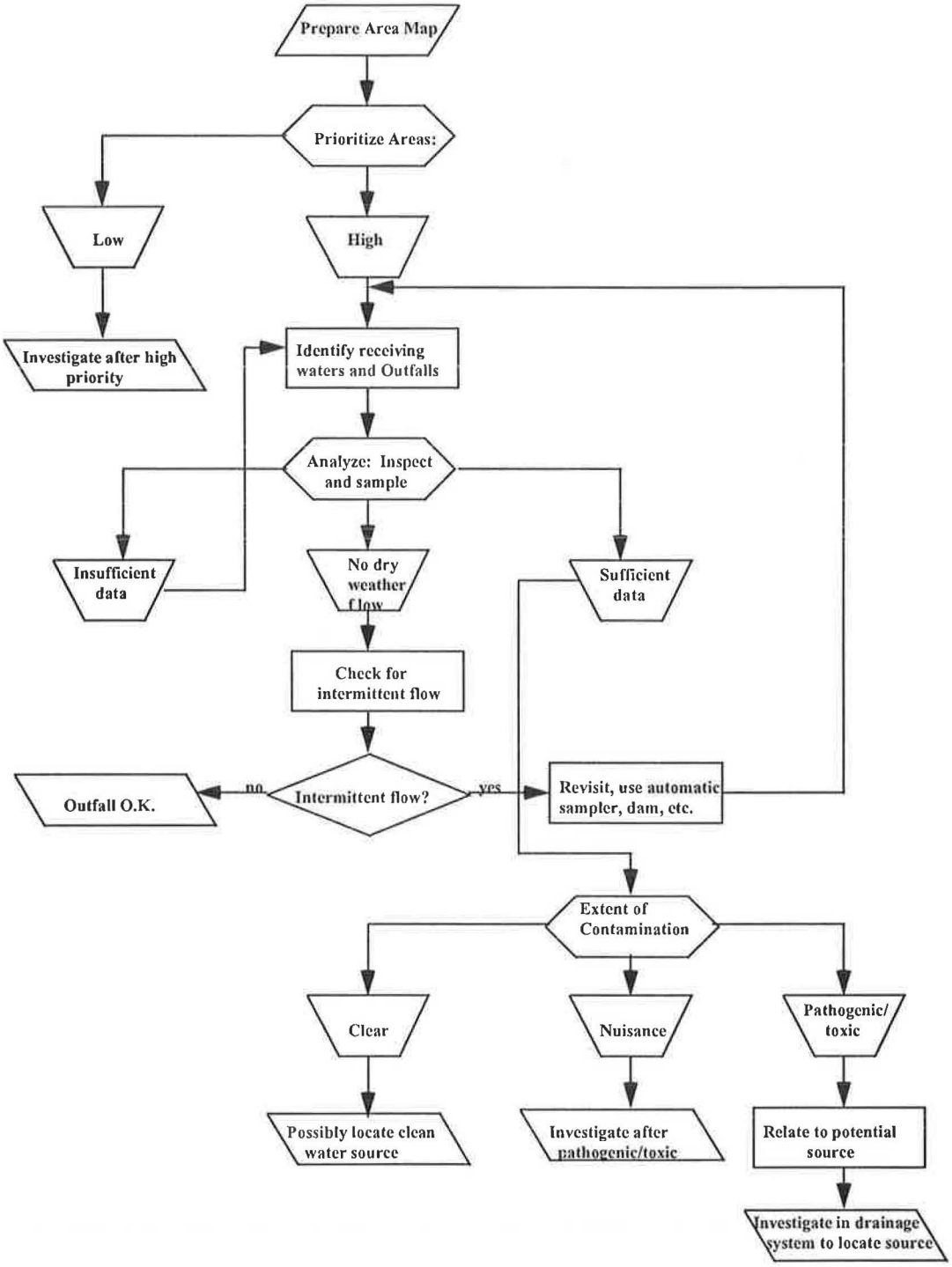

FIGURE 1 Flow chart for investigative procedures.

REFERENCES

1. Montoya, B. L. *Urban Runoff Discharges from Sacramento, California*. Report 87-1SPSS. Central Valley Region, California Regional Water Quality Control Board, 1987.
2. Pitt, R., and J. McLean. *Toronto Area Watershed Management Strategy Study; Humber River Pilot Watershed Project.* Final Report. Ontario Ministry of the Environment, Toronto, Canada, 1986.
3. Pitt, R., M. Lalor, D. Barbé, D. Adrian, and R. Field. *Investigation of Inappropriate Pollutant Entries into Storm Drainage Systems—A User's Guide*. Research Report 92-09. Urban Waste Management and Research Center, University of New Orleans, Louisiana, 1992.
4. *Results of the Nationwide Urban Runoff Program*. PB 84-185552. Water Planning Division, Environmental Protection Agency, Dec. 1983.
5. Schmidt, S. D., and D. R. Spencer. The Magnitude of Improper Waste Discharges in an Urban Stormwater System. *Journal of the Water Pollution Control Federation*, July 1986.

6. *Huron River Pollution Abatement Project*. Summary. Washtenaw County Drain Commissioner, Michigan, 1988.
7. Gartner Lee and Associates, Ltd. *Toronto Area Watershed Management Strategy Study: Humber River and Tributary Dry-Weather Outfall Study*. Technical Report 1. Ontario Ministry of the Environment, Toronto, Canada, Nov. 1983.
8. Pelletier, G. J., and T. A. Determan. *Urban Storm Drain Inventory, Inner Gray Harbor*. Water Quality Investigations Section, Washington State Department of Ecology, Olympia, 1988.
9. Environmental Protection Agency. *National Pollutant Discharge Elimination System Permit Regulations for Storm Water Discharges*. Final Rule. 40 C.F.R., Parts 122, 123, and 124, 1990.

Effectiveness of Highway Drainage Systems in Preventing Road-Salt Contamination of Groundwater: Preliminary Findings

PETER E. CHURCH AND PAUL J. FRIESZ

A study to determine the relative effectiveness of four highway drainage designs in preventing the contamination of groundwater by road salt is being conducted by the U.S. Geological Survey in cooperation with the Massachusetts Highway Department and FHWA. Four test sites, each representing a specific highway drainage design, are located along a 5-km section of Route 25 in southeastern Massachusetts. The drainage designs being tested are open drainage, closed drainage, closed drainage with snow berm, and full-snow-berm drainage. Preliminary comparisons of the effectiveness of the highway drainage systems are based on computations of chloride loads from road salt in groundwater and chloride loads from road salt discharged through the highway-drainage monitoring stations at each test site. A comparison of monthly chloride loads from November 1990 through May 1992 shows that chloride loads in groundwater at the closed drainage site, the closed drainage site with snow berm, and the full-snow-berm site are about 40, 50, and 20 percent, respectively, of the chloride load in groundwater at the open drainage site. The chloride load discharged through the full-snow-berm drainage site, and thus prevented from entering groundwater, is twice that discharged from the closed drainage site and from the closed drainage site with snow berm. Evaluation of the effectiveness of these drainage systems will be refined as additional data are collected and analyzed. Results from this study should also be applicable to the transport of other conservative chemical constituents in highway runoff.

Road-salt contamination of public and private water supplies has become a serious and costly problem, particularly in the northeast and midwest United States. For example, the Massachusetts Highway Department (MHD) received complaints of road-salt contamination from 100 of the 341 municipalities in the state from 1983 through 1990. MHD spent about $1.2 million to investigate and remediate road-salt contamination complaints during this period (*1*). Nationally, state and local governments spend about $10 million each year to prevent and remediate problems of road-salt contamination (*2*).

One method that state highway agencies use to reduce road-salt contamination of public water supplies is that of diverting highway runoff from sections of highway that pass near public supplies to less sensitive areas. Four types of highway drainage systems were incorporated into the design of an 11-km, six-lane section of Route 25 in southeastern Massachusetts completed in 1987. Three of these drainage systems—two of which are new, untested designs—divert highway runoff away from adjacent public water supplies. The methods by which the diverted highway runoff is collected (and, correspondingly, the cost of highway construction) differ between drainage systems. The most expensive, and potentially the most effective, drainage system added about $1.6 million/km to construction costs for that section of highway (*2*). However, the relative effectiveness of the individual drainage systems in preventing road-salt contamination of the public water supplies is not yet known.

An investigation of the relative effectiveness of these highway drainage designs in preventing groundwater from being contaminated by road salt is being conducted by the Water Resources Division of the U.S. Geological Survey (USGS) in cooperation with MHD and FHWA, U.S. Department of Transportation. Four test sites, each representing one of the highway drainage designs, are located along a 5-km section of Route 25 (Figure 1). Data collection for analysis and comparison of the effectiveness of the drainage designs began in November 1990 and is planned to continue through December 1995.

PURPOSE AND SCOPE

The purpose of this paper is to describe the highway drainage systems being tested, discuss the general hydrogeology of the study area, define the methodologies by which the drainage systems are being evaluated, and present preliminary findings of the effectiveness of the highway drainage systems in preventing road-salt contamination of groundwater. These findings are based on computations of chloride loads from road salt in groundwater and chloride loads from road salt discharged through the highway drainage systems from November 1990 through May 1992.

STUDY APPROACH

Networks of observation wells were installed at each test site to enable the comparison of water samples collected from wells upgradient (background) and downgradient (potentially contaminated) from Route 25. Water samples from the wells are analyzed for concentrations of dissolved sodium, calcium, and chloride to determine the amount of road salt entering

U.S. Geological Survey, Water Resources Division, Massachusetts–Rhode Island District, 28 Lord Road, Suite 280, Marlborough, Mass. 01752.

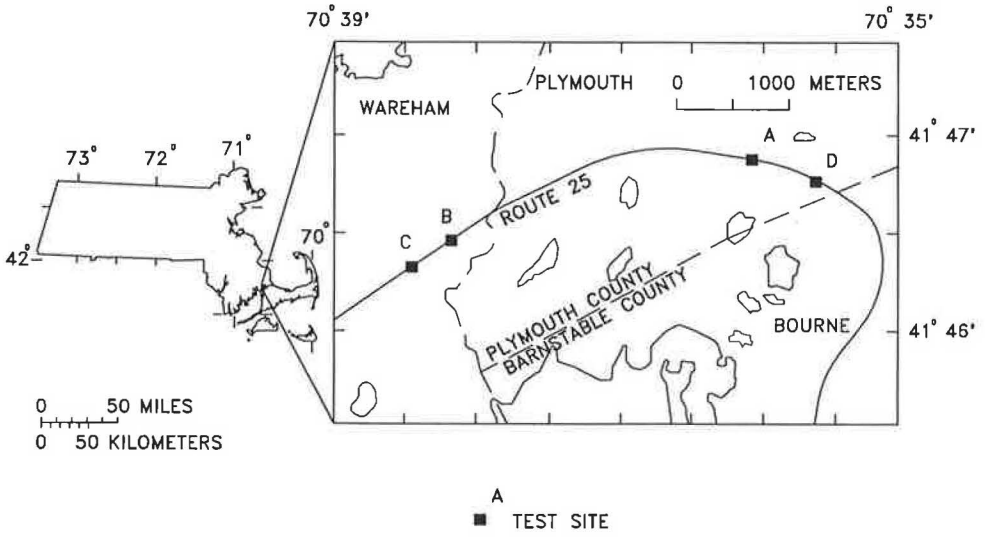

FIGURE 1 Location of study area in southeastern Massachusetts and Test Sites A, B, C, and D along Route 25.

groundwater at each test site. Highway-drainage monitoring stations were installed within the drainage systems to measure continuous records of stage and specific conductance of the runoff. Samples of runoff are analyzed for concentrations of dissolved sodium, calcium, and chloride. Relations between stage and discharge and between specific conductance and chloride concentration are used to determine the amount of chloride discharged through each monitoring station.

MHD monitors the application of road salt to the highway. Department records indicate the amount of road salt applied to the entire 11-km section of Route 25 along which the test sites are located and are not specific to each test site. Therefore, it is assumed that road-salt application is equal at all test sites.

HIGHWAY DRAINAGE SYSTEMS

The four types of highway drainage system incorporated into the construction of Route 25 each represent a different method of control of runoff from the highway surfaces, shoulders, and median strip. Test sites designated A, B, C, and D, in order of increasing highway runoff control, are representative of each drainage system (Figure 1). Test Sites A and B represent standard drainage designs, whereas Test Sites C and D represent new, untested designs.

The roadway surface at all test sites is crowned to allow highway runoff to flow toward the highway shoulders and the median strip. The top 2.5 cm of the highway pavement is composed of an open-graded friction coarse bituminous concrete, referred to as "popcorn pavement," to limit ponding of water on the highway surface. This permeable layer is underlain by a 20-cm-thick layer of consolidated asphalt estimated to be at least 95 percent impervious (L.C. Stevens, Jr., MHD, personal communication, 1990). Rainfall and salt-laden water from melting snow and ice easily penetrate the 2.5-cm-thick popcorn pavement and then flow laterally to the edges of the roadways. The extent to which the water flows onto the shoulders or the median strip is controlled by the drainage systems, as described later. The quantity of salt-laden water percolating through the 20-cm-thick consolidated asphalt is assumed to be small and uniform at all test sites.

Site A represents an open drainage system, where local groundwater is unprotected from contamination by road salt (Figure 2). Runoff collected in catch basins on the pavement surface and drop inlets in the median strip is discharged lo-

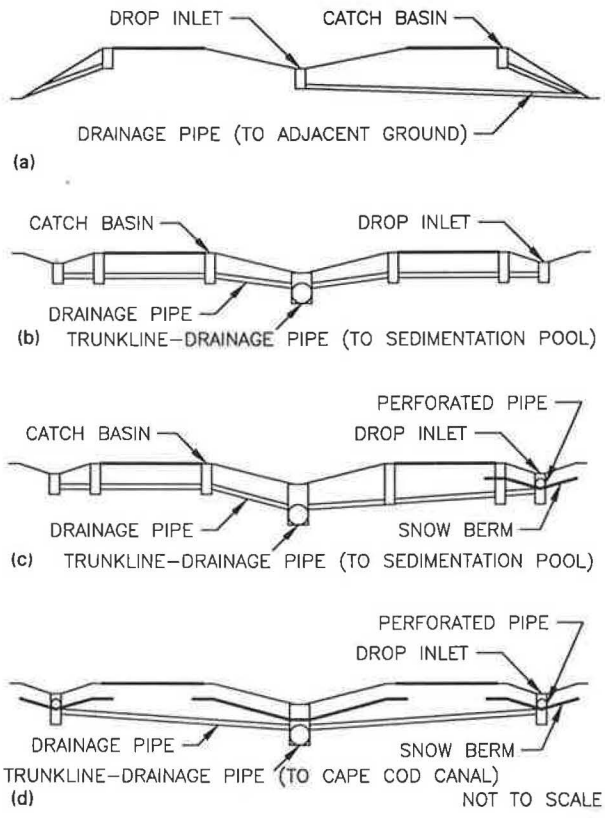

FIGURE 2 Sections of highway drainage designs: *a*, open drainage; *b*, closed drainage; *c*, closed drainage with snow berm; *d*, full snow berm drainage.

cally. In effect, all highway runoff—whether from direct overland flow, melting of snow plowed from the highway surface, or spray caused by vehicular traffic—is allowed to infiltrate the soil and percolate through the unsaturated zone to the water table.

Site B is a closed drainage system, where catch basins are installed every 90 to 180 m on both edges of both roadways (Figure 2). Highway-surface runoff collected in these catch basins is piped beneath the highway to a trunkline drainage pipe beneath the median strip and is then discharged into a sedimentation pool. Outflow from the pool enters a local stream about 1.6 km upstream of a coastal bay. Additional runoff from the highway shoulders and the median strip can enter the trunkline drainage pipe through drop inlets; however, the bulk of runoff from the shoulders and the median strip (snow plowed from the road surface and spray caused by vehicular traffic) is uncontrolled and is allowed to infiltrate the soil and percolate to the water table.

The highway drainage system at Site C contains elements of two distinct overlapping designs (Figure 2). Site C represents a closed drainage system as described for Site B but also incorporates a 5-cm-thick layer of bituminous concrete buried about 1 m beneath the eastbound roadway shoulder. This snow berm is sprayed with a seal coat during construction to make it 100 percent impervious (L.C. Stevens, Jr., MHD, personal communication, 1990) and is then covered with a 1-m-thick layer of well-sorted permeable sand. The snow berm is shaped as a channel running parallel to the highway. Drop inlets in the center of these channels are sealed to the snow berm about every 90 m along the highway. Perforated pipes on the snow berm are connected to the drop inlets immediately above the snow-berm seal. Highway runoff can enter the drop inlets directly as overland flow and indirectly by percolation through the sand to the snow berm and eventually draining into the drop inlet through the perforated pipe. Highway runoff from the drop inlets is then piped to the trunkline drainage pipe beneath the median strip of the highway. The drainage system at Site C is designed so that highway-surface runoff from both roadways and runoff from the eastbound roadway shoulder is diverted from the site and thus is prevented from percolating through the unsaturated zone to groundwater. Captured highway runoff at Site C enters the same trunkline drainage pipe that passes through Site B.

Site D is a full-snow-berm drainage system, where both highway shoulders and the median strip are underlain by snow berms (Figure 2). Highway-surface runoff is allowed to flow onto the shoulders and the median strip where it either enters drop inlets as overland flow and is channeled directly to the trunkline drainage pipe or percolates to the impervious snow berms. Runoff captured by the snow berms enters drop inlets from below the land surface through perforated pipe and is then directed to the trunkline drainage pipe. This trunkline drainage pipe under the median strip of the highway discharges into the Cape Cod Canal, a coastal waterway about 3 km east of the test site.

HYDROGEOLOGY OF STUDY AREA

The study area is in a rural area of southeastern Massachusetts in the towns of Wareham and Plymouth (Figure 1). This area is part of a coastal outwash plain bounded by till and bedrock hills to the north and west and by saltwater bays of the Atlantic Ocean to the south and east. In general, the test sites selected along Route 25 are underlain by a layer of fine to coarse sand with gravel ranging in thickness from about 9 m at Site D to about 27 m at Site C. A lower unit of fine to coarse sand with silt is present at Sites A, B, and C. The sand with gravel unit at Site D is underlaid by fine to coarse sand with gravel and silt. Considerable small-scale vertical and lateral variations in grain-size distribution, typical of sand and gravel deposits, are present in the upper and lower layers at all test sites.

Few streams drain the area because precipitation infiltrates easily into the sandy soils. Depth to the water table below the highway ranges from 6 m at Site B to 18 m at Site A. Compared with land-surface topography, the water table is relatively flat. The saturated zone is more than 15 m thick at all test sites. Groundwater flow is generally to the south, nearly perpendicular to the highway. Water-table gradients are less than 0.006, and annual ranges in water-table altitudes vary from year to year in response to precipitation but are normally from 0.5 to 1.5 m.

Horizontal hydraulic conductivity of the upper 7.5 m of the saturated zone at each test site was estimated by use of borehole permeability tests (slug tests). Hydraulic conductivities of 67, 33.5, 30.5, and 33.5 m/day were measured at Sites A, B, C, and D, respectively.

Background concentrations of sodium, calcium, and chloride in groundwater and background specific conductance of groundwater were monitored before construction and before operation and salting of Route 25. Typical background concentrations of sodium ranged from 5 to 10 mg/L, calcium from 1 to 5 mg/L, and chloride from 5 to 20 mg/L at Sites A, B, and D. Background concentrations of these constituents were generally higher at Site C, where sodium concentrations ranged from 5 to 20 mg/L, calcium concentrations from 3 to 15 mg/L, and chloride concentrations from 10 to 30 mg/L. Background specific conductance ranged from 40 to 70 μS/cm (25°C) at Sites A, B, and D. At Site C, specific conductance ranged from 50 to 250 μS/cm. Background chemical data at Site C are probably higher than at the other test sites because of the former presence of a pig farm approximately 0.8 km upgradient from the test site, which is now an unpaved lot where many used buses are stored.

METHODOLOGY

Preliminary comparisons of the effectiveness of the highway drainage systems are based on computations of chloride loads from road salt in groundwater and chloride loads from road salt discharged through the highway-drainage monitoring stations. The constituents of road salt—primarily sodium chloride and secondarily calcium chloride—ionize when dissolved in water. Chloride, a nonreactive ion with little affinity for the sands and gravels that make up the surficial and aquifer materials in the study area, is easily transported in groundwater and in highway surface and shoulder runoff. Transport of sodium and calcium, however, is more likely than chloride to be attenuated because of exchange with other ions. Therefore, chloride loads can be used as a measure of road-salt contamination of groundwater and road salt discharged through the drainage systems for comparisons between test sites.

Monitoring Road-Salt Chloride Loads in Groundwater

Water samples are collected from wells upgradient and downgradient from Route 25 to monitor the quantity of chloride from road salt entering groundwater at each test site. Clusters of wells with screens of 5-cm inside diameter and 1.5-m length were installed in a line parallel to the direction of groundwater flow at the four test sites (Figure 3). Well clusters about 60 m upgradient from the median strip of the highway contain three wells, two of which together fully screen the upper 3 m of the aquifer. The third well is screened at about 15 to 18 m below the water table. Well clusters about 60 m downgradient from the median strip of the highway include six wells, five of which together fully screen the upper 7.5 m of the aquifer. The sixth well is screened at about 18 to 21 m below the water table. An additional well was installed about 120 m downgradient from the median strip and is also screened at about 18 to 21 m below the water table at each test site.

Water samples are collected monthly from the two wells screened immediately below the water table upgradient from the highway and from the five wells screened immediately below the water table downgradient from the highway at each test site. These samples are analyzed for dissolved concentrations of sodium, calcium, and chloride. Borehole electromagnetic-induction (EM) logs are taken from the deep wells at each well cluster and the deep wells about 120 m downgradient from the highway concurrently with water sample collection. EM logs are performed to monitor the vertical distribution of salt-contaminated groundwater at the well sites to verify that the zone of aquifer in which the contaminated groundwater is transported is fully screened.

Because hydraulic gradients and hydraulic conductivities of the aquifer differ between test sites and hydraulic gradients change with time, comparison of the amount of road-salt chloride (chloride from road salt only) entering groundwater requires that the mass flux of road-salt chloride through a specific vertical section within the aquifer downgradient from the highway be computed at each test site. Road-salt chloride concentrations are calculated by subtracting chloride concentrations at wells upgradient from the highway (background-chloride concentration) from concentrations at wells downgradient from the highway. The mass flux of road-salt chloride through the aquifer (QC_d), in kilograms per day, is then computed as follows:

$$QC_d = K \times I \times A \times \mathrm{Cl} \times C \quad (1)$$

where

K = estimated horizontal hydraulic conductivity of aquifer (m/day),
I = water-table gradient (dimensionless),
A = area of vertical section through which groundwater flows (m^2),
Cl = road-salt chloride concentration (mg/L), and
C = constant 0.001 (kg-L/m^3-mg) (conversion of units m^3-mg/day-L to kg/day).

Monthly loads of road-salt chloride transported past the downgradient wells are calculated by summing the daily flux of chloride determined by Equation 1 over 1 month. Monthly chloride loads are then converted to chloride loads, in kilograms per lane-kilometer of highway, for comparison between test sites.

Monitoring Road-Salt Chloride Discharged from Highway Drainage Stations

Highway-drainage monitoring stations were installed in the trunkline drainage pipes of the highway drainage systems at Sites B, C, and D (Figure 4). Design of the monitoring stations was adapted from that of Kilpatrick et al. (*3*). Each moni-

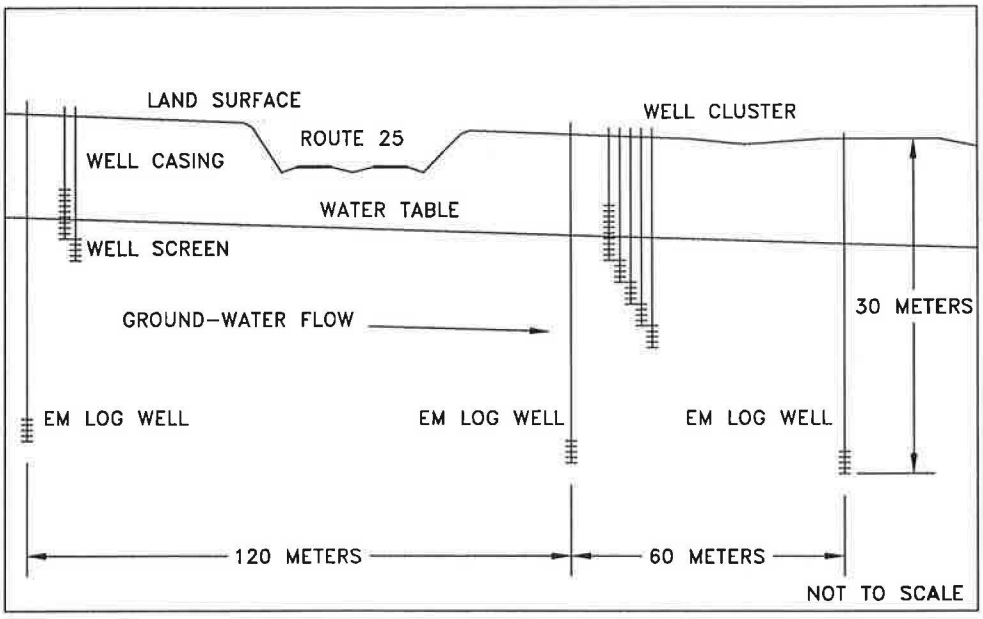

FIGURE 3 Section of well network at test sites.

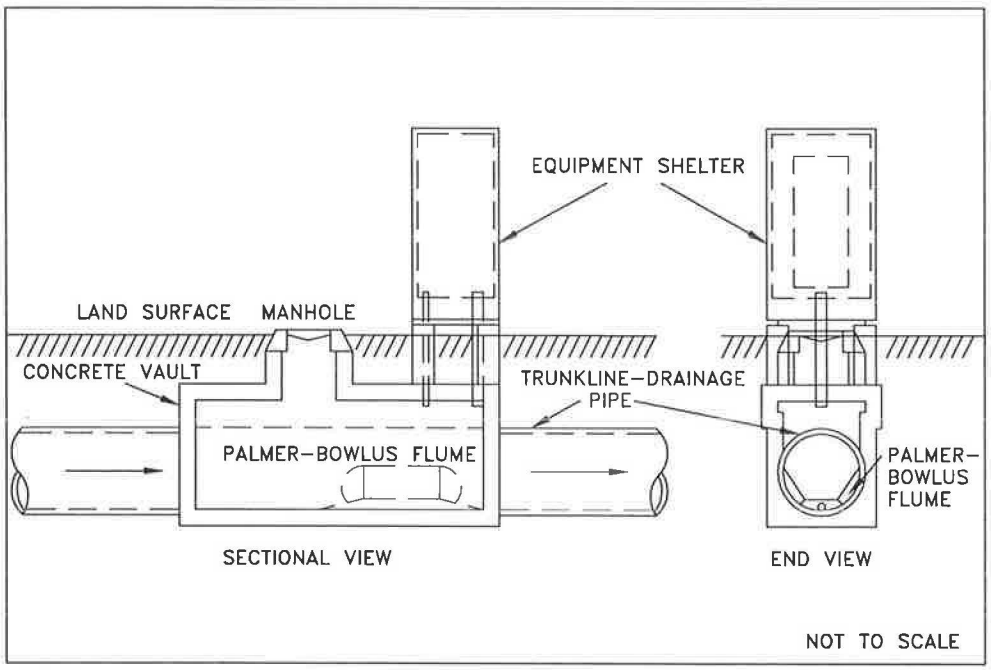

FIGURE 4 Sections of highway-drainage monitoring station.

toring station consists of a calibrated Palmer-Bowlus flume (*4*) cast into a reinforced-concrete vault. The concrete vaults containing the flumes were installed during highway construction.

Instrumentation for monitoring discharge of road salt through the flumes is contained in equipment shelters on top of the concrete vaults. Stage is measured by use of pressure transducers, and specific conductance is measured with USGS Minimonitors. Water samples for analysis of chloride concentrations are collected by automatic water samplers during runoff to establish a relation between chloride concentration and specific conductance. Stage, specific conductance, and the dates and times of water-sample collection are recorded in digital data loggers. The data loggers are programmed to control the frequency of recording and water-sample collection. Stage thresholds are entered whereby recording and sampling frequencies are increased in steps as stage rises and decreased as stage falls. The frequency of baseline data collection is set at 6 hr at all stations; however, stage thresholds and recording and sampling frequencies are set independently for each station on the basis of diameter and slope of the pipe in which the flume is installed. Stage thresholds of 0.03 m and recording and sampling frequencies of 5 and 15 min, respectively, are typical. These stage thresholds and sampling frequencies are adjusted seasonally to account for differences in flow regimes and to ensure the recording of stage and specific-conductance and collection of water samples during runoff and to prevent the collection of voluminous data at times of little or no flow.

Theoretical stage-discharge relations for each highway-drainage monitoring station have been developed by use of the Bernoulli total energy equation, as described by Kilpatrick and Schneider (*5*). Discharge at each station is determined from the recorded stage data and these theoretical relations. The relation between specific conductance and chloride concentration is used to determine chloride concentrations from recorded specific-conductance data. A chloride load is computed for every stage and specific-conductance measurement. Chloride load (QC_{TI}), in kilograms per time interval since last measurement, is computed as follows:

$$QC_{TI} = Q \times Cl \times TI \times C \quad (2)$$

where Q is the discharge of water (m^3/sec) and TI is the time interval since last measurement in seconds.

The values calculated in Equation 2 are summed over a monthly period to provide chloride loads, in kilograms per month. Monthly chloride loads are then converted to chloride loads, in kilograms per lane-kilometer of highway, for comparison between test sites.

RESULTS AND DISCUSSION OF RESULTS

Comparison of road-salt chloride loads in groundwater at each test site from November 1990 through May 1992 shows that the various highway drainage systems differ in effectiveness. This interpretation is confirmed by chloride loads discharged through the highway-drainage monitoring stations during the same period.

Road-Salt Chloride Loads in Groundwater

Examination of the computed monthly road-salt chloride loads in groundwater from November 1990 through May 1992 shows that chloride loads differ between test sites (Figure 5). Monthly chloride loads at the open drainage site are generally much higher than those at the other drainage sites throughout the 19-month period. This is particularly apparent in the late winter/early spring of 1991. The chloride loads at the closed

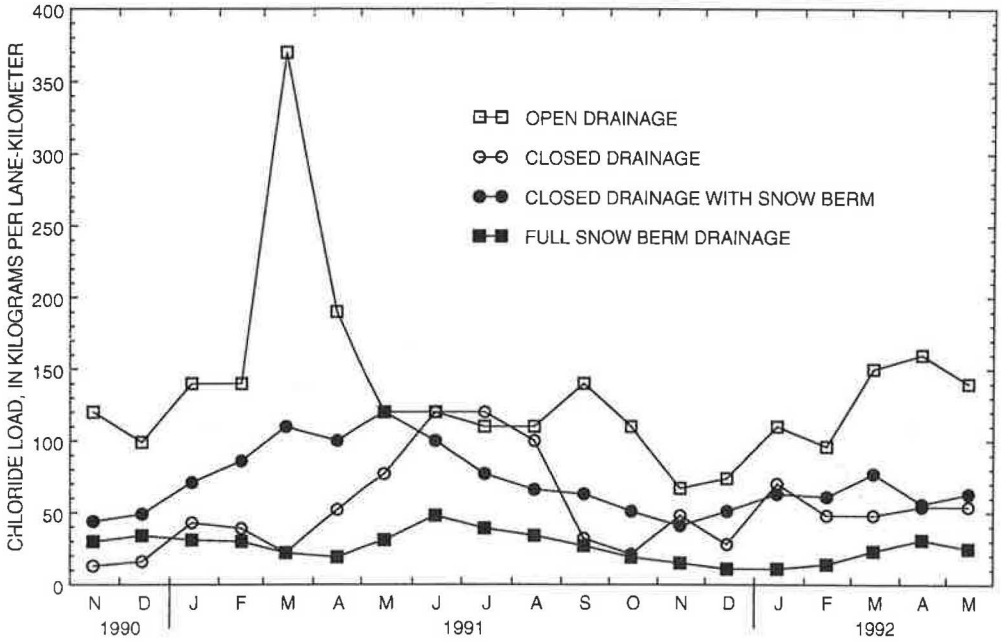

FIGURE 5 Monthly road-salt chloride loads in groundwater at test sites, November 1990 through May 1992.

drainage site and the closed drainage site with snow berm appear similar except for an approximate 2-month delay in maximum chloride loads at the closed drainage site. Chloride loads at the full-snow-berm drainage site vary little with time and are generally much lower than those at the other drainage sites.

Monthly and total chloride loads in groundwater at each test site over this 19-month period are given in Table 1. Total chloride loads at the closed drainage site, the closed drainage site with snow berm, and the full-snow-berm drainage site are about 40, 50, and 20 percent, respectively, of the chloride load at the open drainage site.

These relative differences in chloride loads in groundwater are likely to change as more data are collected. Chloride load data from 1991 show that annual plumes of salt-contaminated groundwater develop in response to annual application of road salt to the highway. Maximum loads occurred in March at the open drainage site, in May at the closed drainage site with snow berm, and in June at the closed drainage and full-snow-berm drainage sites. Minimum chloride loads occurred in the late fall and early winter of 1991 at each test site. Because the 1992 chloride loads are only through May and a large amount of road salt was applied in late March, these data do not represent the entire road-salt plumes developed from salt applied during winter 1991–1992.

Data collection is planned to continue through December 1995. Monthly data will be accumulated over the entire data collection period so as to determine the effectiveness of the drainage systems. Comparisons between test sites on an annual or biannual basis can be biased because of the difficulty in matching chloride loads in groundwater at each test site with chloride from road salt applied to the highway in the same winter. Monthly chloride loads in groundwater from November 1990 through May 1992 appear to represent chloride from road salt applied from two winters, 1990–1991 and 1991–1992. However, it is uncertain whether some of this chloride represents the trailing edges of road-salt plumes developed from salt applied in winter 1989–1990. It is also uncertain whether the chloride loads in the late fall and early winter of 1991 represent the trailing edges of the 1990–1991 plumes, the leading edges of the 1991–1992 plumes, or composites of both. Considering that road salt is applied intermittently to this six-lane highway, which is approximately 80 m wide (including shoulders and median strip), over a 5-month period each year, it is reasonable to assume that the leading edge of one year's plume could combine with the trailing edge of the previous year's plume. The extent to which these annual road-salt plumes overlap is likely to vary between test sites because of the differing hydraulic conductivities, hydraulic gradients, and unsaturated zone thicknesses between test sites. These differences in aquifer properties result in differing times of travel of road salt through the unsaturated zone and the rates of transport of annual road-salt plumes between test sites. Such overlapping of annual road-salt plumes can be further complicated because the total amount of salt applied and the time at which it is applied varies significantly from year to year. The accumulation of monthly data over several years reduces the bias introduced by the inability to account fully for what portion of a road-salt plume is related to which salting season at each test site because this potential bias would occur only in the first and last years of data collection.

Road-Salt Chloride Discharged from Highway Drainage Stations

Examination of road-salt chloride loads discharged through the highway-drainage monitoring systems from November 1990 through May 1992 shows that most of the chloride captured in the drainage systems is discharged in the winter and spring;

TABLE 1 Monthly and Total Chloride Loads in Groundwater at Test Sites, November 1990 Through May 1992 (kg/lane-km)

Year/ month	Open drainage	Closed drainage	Closed drainage with snow berm	Full-snow-berm drainage
1990				
November	120	13	44	30
December	99	16	49	34
1991				
January	140	43	71	31
February	140	39	86	30
March	370	22	110	22
April	190	52	100	19
May	120	77	120	31
June	120	120	100	48
July	110	120	77	39
August	110	100	66	34
September	140	32	63	27
October	110	21	51	19
November	67	48	41	15
December	74	28	51	11
1992				
January	110	70	63	11
February	96	48	61	14
March	150	48	77	23
April	160	54	56	31
May	140	54	63	25
TOTAL	2,600	1,000	1,300	490

[data rounded to two significant figures]

discharge of chloride in the summer and fall is negligible (Figure 6). Chloride discharged from the full-snow-berm drainage site is much greater than that from the close-drainage site and the closed drainage site with snow berm.

Monthly and total chloride loads discharged through the highway-drainage monitoring stations at each test site over this 19-month period are presented in Table 2. Total chloride load at the closed drainage site is similar to that at the closed drainage site with snow berm. However, the chloride load at the full-snow-berm drainage site is twice that of the closed drainage and closed drainage with snow berm sites.

Discharge of chloride through the drainage system at the full-snow-berm drainage site was not monitored from May through September 1991 while a related investigation was being conducted at this site. Chloride loads during these 5 months are assumed to fall between the April and October values of 73 and 39 kg/lane-km, respectively; however, these estimated values are not used in the current analysis. Even though road salt was not applied from the middle of March to early December 1991, October and November values of 39 and 25 kg/lane-km were measured. These elevated values, relative to those at the other drainage systems, are probably due to retention and slow release of salt-laden water from the approximately 1-m-thick layer of sand fill overlaying the snow berm.

SUMMARY

Four test sites, each representing a separate highway drainage system designed for a different amount of highway runoff control, were selected and instrumented to determine their relative effectiveness in preventing groundwater from becoming contaminated by road salt. These distinct designs were incorporated into the construction of an 11-km section of Route 25 in southeastern Massachusetts, completed in 1987. Preliminary comparisons of the effectiveness of the highway drainage systems are based on computed chloride loads in groundwater and computed chloride loads discharged through highway-drainage monitoring stations.

The test sites are designated Sites A, B, C, and D in order of increasing highway runoff control. Site A is an open drainage design where highway runoff collected in catch basins on the roadway surface is discharged locally. Sites B, C, and D,

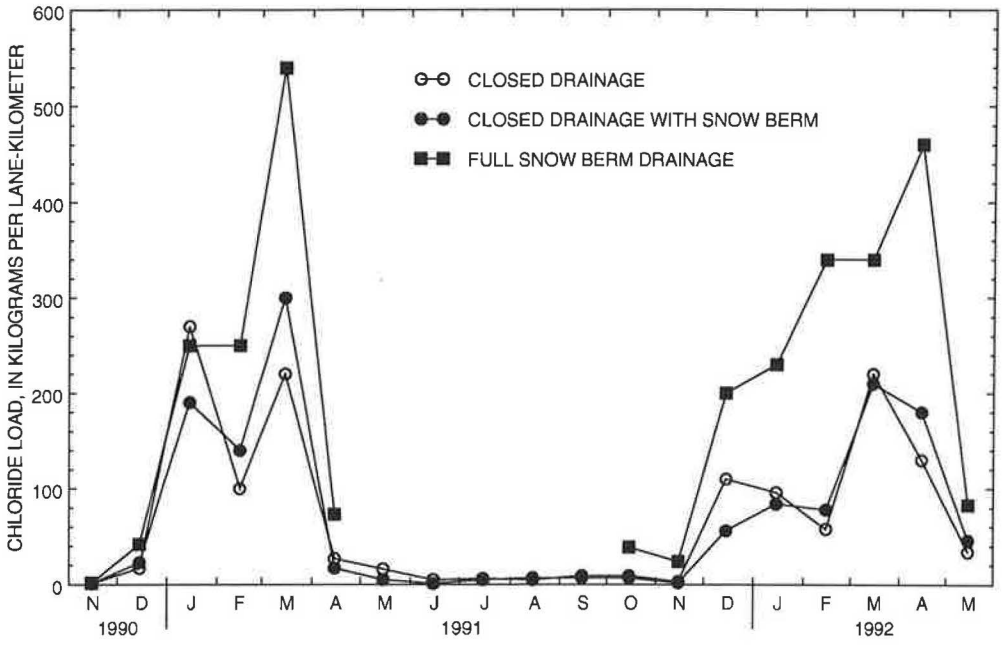

FIGURE 6 Monthly road-salt chloride loads at highway-drainage monitoring stations, November 1990 through May 1992.

TABLE 2 Monthly and Total Chloride Loads Discharged Through Highway-Drainage Systems, November 1990 Through May 1992 (kg/lane-km)

Year/ month	Closed drainage	Closed drainage with snow berm	Full-snow-berm drainage
1990			
November	1	1	2
December	17	23	42
1991			
January	270	190	250
February	100	140	250
March	220	300	540
April	27	17	73
May	16	5	--
June	5	1	--
July	6	5	--
August	5	7	--
September	9	7	--
October	9	7	39
November	3	2	24
December	110	56	200
1992			
January	96	84	230
February	58	78	340
March	220	210	340
April	130	180	460
May	34	46	83
TOTAL	1,300	1,400	2,900

[data rounded to two significant figures; -- denotes no data collected during this period]

however, contain trunkline drainage pipes beneath the median strip through which captured highway runoff is carried away and discharged into a nearby stream or coastal waterway. These drainage designs differ only in the way in which highway runoff is captured. At Site B, the closed drainage design, highway runoff is collected in catch basins on the roadway surface and is then piped beneath the highway to the trunkline drainage pipe. The drainage design at Site C, closed drainage with snow berm, is similar to that of Site B; however, the eastbound roadway shoulder is underlain with an impervious layer of bituminous concrete (snow berm) from which highway runoff is piped to the trunkline drainage pipe. Both roadway shoulders and the median strip are underlain with snow berms at Site D, a full-snow-berm drainage design. This type of drainage system is designed to capture all highway runoff and pipe it to the trunkline drainage pipe.

Test sites are on a coastal outwash plain bounded to the north and west by till and bedrock hills and to the south and east by the saltwater bays of the Atlantic Ocean. The study area is directly underlain by a layer of fine to coarse sand with gravel that varies in thickness from 9 to 27 m. Fine to coarse sand with silt is present below this layer. Depth to the water table below the highway ranges from about 6 m at Site B to 18 m at Site A, and annual water-table fluctuations are less than 1.5 m. Estimated hydraulic conductivity of the aquifer ranges from 30.5 m/day at Site C to 67 m/day at Site A. Background concentrations of sodium, calcium, and chloride—the primary constituents of road salt—generally range from 5 to 10 mg/L, 1 to 5 mg/L, and 5 to 20 mg/L, respectively, in groundwater.

Groundwater samples are collected from clusters of wells with 1.5-m-long screens upgradient and downgradient from the highway. The monthly mass flux of road-salt chloride is computed by use of chloride concentrations, water-table gradients, and hydraulic conductivities at each test site. Highway-drainage monitoring stations at Sites B, C, and D consist of Palmer-Bowlus flumes within trunkline drainage pipes from which stage and specific conductance are continuously monitored and recorded. Monthly chloride loads discharged through the highway drainage systems are computed by use of relations between stage and discharge and between specific conductance and chloride concentration.

A comparison of accumulated monthly chloride loads in groundwater from November 1990 through May 1992 shows that chloride loads at the closed drainage site, the closed drainage with snow berm site, and the full-snow-berm drainage site are about 40, 50, and 20 percent, respectively, of the chloride load at the open drainage site. The chloride load discharged through the full-snow-berm drainage site, and thus prevented from entering groundwater, is twice that discharged from the closed drainage site and from the closed drainage with snow berm site.

These preliminary findings show that the effectiveness of the highway drainage systems in preventing road-salt contamination of groundwater varies widely. However, it is premature to use these data for quantitative evaluation of the effectiveness of the drainage systems. The 1992 chloride load data through May at each site do not represent the entire road-salt plumes developed from salt applied during winter 1991–1992, and they do not represent the total discharge of road salt through the highway-drainage monitoring stations. Additionally, difficulties in matching the leading and trailing edges of annual road-salt plumes in groundwater with road salt applied in the same winter at each test site introduces some uncertainties in the analysis that can be reduced by collection of more data. Data collection is planned to continue through 1995 to reduce uncertainties that might occur in the analysis of the effectiveness of the highway drainage systems.

ACKNOWLEDGMENTS

This paper was prepared in cooperation with MHD and FHWA. The authors thank the Research and Materials Section and the District 5, Wareham Office of MHD for providing ongoing logistical support during this study, including drilling and well installation, surveying, and recording of road-salt application. The authors also thank those in the MHD Research and Materials Section and FHWA for their comments and suggestions in the development of the study approach.

REFERENCES

1. Pollock, S. J. Remediating Highway Deicing Salt Contamination of Public and Private Water Supplies in Massachusetts. *Proc., Focus Conference on Eastern Regional Groundwater Issues*, National Water Well Association, Portland, Maine, 1991, pp. 347–368.
2. *Special Report 235: Highway Deicing: Comparing Salt and Calcium Magnesium Acetate*. TRB, National Research Council, Washington D.C., 1991, pp. 108–110.
3. Kilpatrick, F. A., W. R. Kaehrle, J. Hardee, E. H. Cordes, and M. N. Landers. *Development and Testing of Highway Storm-Sewer Flow Measurement and Recording System*. Water-Resources Investigation Report 85–4111. U.S. Geological Survey, U.S. Department of the Interior, 1985.
4. Palmer, H. K., and F. D. Bowlus. Adaptation of Venturi Flumes to Flow Measurements in Conduits. *Transactions, American Society of Civil Engineers*, Vol. 101, 1936, pp. 1195–1216.
5. Kilpatrick, F. A, and V. R. Schneider. *Use of Flumes in Measuring Discharge*. Techniques of Water-Resources Investigations, Book 3. U.S. Geological Survey, U.S. Department of the Interior, 1983, Ch. A14.

Transport of 2,4-D in Soil as Affected by Aggregation and Organic Matter Content

C. HINZ, S. KALLUR, D. D. ADRIAN, AND D. ROY

The transport of 2,4-dichlorophenoxy acetic acid (2,4-D) in the Ap (surface) and Bt (subsurface) horizons of an acid silt loam has been examined using batch and miscible displacement experiments. The batch experiments revealed that the sorption is linear for the Ap horizon and nonlinear for the Bt horizon. The miscible displacement experiments were carried out on soil aggregate whose diameters ranged from 2 to 4.8 mm and on soil without any significant aggregation. Miscible displacement experiments with Cl as a tracer in the well-aggregated soil showed typical nonequilibrium effluent concentration curves. The two-region model was adequate to describe the data. Breakthrough curves in soil without well-defined aggregates were described well by the classical convective-dispersive equation. The 2,4-D breakthrough curves in the aggregated Ap horizon exhibited typical nonequilibrium shape, but the experimental data were not well-described by the two-region model when the batch equilibrium sorption data were applied. However, the two-region model successfully predicted the breakthrough curves in the aggregated Bt horizon. The convective-dispersive equation did not accurately predict the 2,4-D breakthrough curves in the soils without aggregates. It can be concluded that under different flow regimes, different physicochemical processes may control the transport behavior of 2,4-D at high concentrations.

Declining water quality caused by the excessive use of herbicides and insecticides has become an important environmental issue. A potential source of groundwater contamination is the application of herbicides on roadsides to prevent excessive growth of brush and other plants. The soil texture of the roadside environment consists generally of coarse particles, resulting in hydraulic properties that enhance fast flow. Depending on the pesticide application and rainfall events, applied herbicides may move quickly into the soil profile and possibly into the groundwater.

To simulate such conditions on a laboratory scale, soil column experiments were designed to mimic preferential or bypass flow through large pores and flow through the soil matrix. In addition, the effect of high and low contents of soil organic matter on the herbicide sorption and transport was investigated because surface soils contain larger amounts of organic matter than subsoils. Preferential flow and low herbicide adsorption capacity of a subsoil imply low residence time for pesticides and hence greater potential for subsurface contamination.

The objectives of this study were to (a) determine experimentally the transport behavior of 2,4-dichlorophenoxy acetic acid (2,4-D) in soils with and without bypass flow, (b) determine the effect of organic matter content on the transport of 2,4-D, and (c) describe the observed phenomena with the two-site/two-region model.

Department of Civil Engineering, Louisiana State University, Baton Rouge, La. 70803.

THEORETICAL

The fate and transport of herbicides in the subsurface environment should be identified in terms of chemical, physical, and biological processes. The fate of pesticides in particular can be characterized by the simultaneous occurrence of transport, sorption, and both chemical and biological degradation. More precisely, when a pesticide molecule enters the soil matrix, it first is translocated primarily by convection through the large pores. Then the solute diffuses through a thin film (film diffusion) into the small pores (particle diffusion) and is finally adsorbed onto the surface of the solid phase. If the solid is made of organic matter, the solute may undergo intraorganic matter diffusion (*1*). Alternatively, the organic compound may be adsorbed first and then diffuses along the surfaces to other adsorption sites (surface diffusion). If diffusion is rate limiting, then the time-dependent sorption process is generally described as being in a physical nonequilibrium state.

In contrast to these physical processes, chemical reaction mechanisms range from low-energy London-van der Waals bonding, hydrogen bonds, and cation and water bridging to high-energy covalent bonding and ligand exchange, among others (*2*). Considering the chemical heterogeneity of soils, it is most likely that several of the aforementioned mechanisms may control the sorption of pesticides. Besides the purely chemical processes, organic molecules may be trapped so that the desorption may be incomplete and the reaction may be viewed as irreversible for the time frame of interest. This trapping may be attributed to herbicide sorption onto the interlayer of montmorillonite (*3*) or to molecular sieves formed by humic acids (*4*). Besides the chemical and physical processes of dislocation and accumulation, abiotic and biological degradation is one of the most important aspects of pesticide fate in the environment. In the case of soil decontamination, degradation is a process that should be enhanced. In general, heterogeneous physical, chemical, and biological properties of soil often prevent the identification of all processes involved. Hence, model development may be restricted to the use of lumped parameters. In this context the two-site/two-region model is applied in this paper.

The two-site/two-region model is based on a one-dimensional solute differential mass balance with either two reaction sites or a mobile and an immobile fluid phase. The first approach may be interpreted as chemical equilibrium and nonequilib-

rium, whereas the second may describe physical nonequilibrium. Detailed derivations of these models have been presented by van Genuchten and Wagenet (*5*). Since the two-region model is more applicable to aggregated soils, only this model is presented:

$$(\theta_m + f\rho k)\frac{\partial c_m}{\partial t} = \theta_m D_m \frac{\partial^2 c_m}{\partial x^2} - \theta_m v \frac{\partial c_m}{\partial x} - \alpha(c_m - c_{im}) - (\theta_m \mu_{lm} + f\rho k \mu_{sm})c_m \quad (1)$$

$$[\theta_{im} + (1 - f)\rho k]\frac{\partial c_{im}}{\partial t} = \alpha(c_m - c_{im}) - [\theta_{im}\mu_{lim} + (1 - f)\rho k \mu_{sim}]c_{im} \quad (2)$$

where

ρ = bulk density (M L^{-3}),
θ_m = water content of mobile phase (L^3 L^{-3}),
θ_{im} = water content of immobile phase (L^3 L^{-3}),
D = dispersion coefficient (L^2 T^{-1}),
α = mass transfer coefficient (T^{-1}),
v = average pore water velocity (L T^{-1}),
k = distribution coefficient describing adsorption of pesticide to the solid phase,
f = fraction of sorption sites directly in contact with mobile phase,
μ_{lm} = degradation rate coefficient of mobile liquid phase (T^{-1}),
μ_{lim} = degradation rate coefficient of immobile liquid phase (T^{-1}),
μ_{sm} = degradation rate coefficient for mobile sorbed phase (T^{-1}),
μ_{sim} = degradation rate coefficient for immobile sorbed phase (T^{-1}),
x = distance (L), and
t = time (T).

The following dimensionless groups have been derived for the two-region model:

$$P = v_m L/D_m \quad (3a)$$

$$R = 1 + \rho k/\theta \quad (3b)$$

$$\beta = \frac{\theta_m + f\rho k}{\theta + \rho k} \quad (3c)$$

$$\omega = \frac{\alpha L}{\theta_m v} \quad (3d)$$

$$\psi = \frac{\mu L}{v} = \frac{\mu L}{\theta_m v_m} \quad (3e)$$

where

P = Peclet number,
R = retardation factor,
L = column length,
ω = dimensionless rate coefficient,
ψ = dimensionless degradation rate constant, and
β = dimensionless parameter.

Furthermore, it should be noted that the two-region model without degradation is obtained when the degradation constants (μ) are 0. The convective-dispersive equation is also a special case of Equation 1 when the mass transfer to the immobile liquid phase is negligibly small. The solutions of the two-region models as well as the convective-dispersive equation with the appropriate boundary and initial conditions can be found elsewhere (*5*,*6*).

Furthermore, the degradation within the different phases cannot be distinguished, and therefore the degradation should be lumped into one degradation rate constant as demonstrated by Gamerdinger et al. (*7*). More precisely, the degradation is

$$\mu = \mu_{lm} = \mu_{sm} = \mu_{lim} = \mu_{sim}$$

It should be noted that the sorption of a solute is often described by a nonlinear isotherm; hence the model requires modification. Generally, the Freundlich isotherm is assumed to describe a nonlinear isotherm appropriately. Van Genuchten (*6*) described a procedure by which the Freundlich equation is linearized so that the model introduced is applicable. The Freundlich isotherm can be given as

$$s = Kc^n \quad (4)$$

where K and n are empirical coefficients. To use this linear model, the distribution coefficient can be approximated by (*6*)

$$k = Kc_0^{n-1} \quad (5)$$

where c_0 denotes the pulse concentration.

MATERIALS AND METHODS

The Ap (surface) and the Bt (subsurface) horizons of the Loring silt loam were sampled on the Baton Rouge campus of Louisiana State University. The soil was air-dried and sieved through 4.8- and 2-mm mesh so that aggregates with diameters from 2 to 4.8 mm were separated. The soil was then analyzed for exchangeable cations, organic matter, and pH. The Ap horizon had an organic matter content of 3.04 percent, a pH of 5.65, a sum of exchangeable cations of 5.25 cmol(+) kg^{-1}, whereas the Bt had an organic matter content of 0.67 percent, a pH of 5.15, and a sum of exchangeable cations of 3.40 cmol(+) kg^{-1}.

Batch experiments were performed to obtain sorption isotherms for the Ap and Bt horizons. Portions of 5 g of soil were added to 15-mL glass test tubes with screw caps. Then 5 mL of solutions containing 10, 20, 50, 75, 100, or 150 mg L^{-1} of 2,4-D with 0.005 *M* $Ca(NO_3)_2$ background solute were added to the tubes so that a solution:soil ratio of approximately 1:1 was maintained. The test tubes were vortex-mixed, agitated in a shaker for 24 hr, and placed in a centrifuge to separate the solid and liquid phases. The supernatant aqueous phase was removed and analyzed for 2,4-D by high-pressure liquid chromatography. The experiments for each concentration were triplicated. The amount of sorbed 2,4-D was calculated by the difference of the initial and final solution con-

centration. The isotherm data were used to determine the distribution coefficient and the Freundlich parameter using a nonlinear least-squares procedure similar to that presented by van Genuchten (*6*).

Solute transport experiments were carried out using glass columns with a length of 15 cm and an inner diameter of 4.8 cm (Kontes chromaflex chromatographic columns). Soil aggregates of size ranging from 2 to 4.8 mm as well as soil with aggregates smaller than 2 mm were packed into the columns. The soil was saturated with 0.005 *M* $Ca(NO_3)_2$ solution. Then a pulse of approximately 48 mg L^{-1} of 2,4-D in 0.005 *M* $Ca(NO_3)_2$ was passed through the column. Thereafter, the 2,4-D solution was leached out with the $Ca(NO_3)_2$ solution. The effluent was collected with a fraction collector and analyzed for 2,4-D. The parameters describing the experimental conditions for all miscible displacement experiments are presented in Table 1.

The use of the two-region model requires at least three parameters that are difficult to measure independently: the dispersion coefficient D, the dimensionless rate coefficient ω, and the dimensionless parameter β that combines the mobile and total water content (θ_m,θ) with the mass fraction of the solid phase in direct contact with the mobile liquid (f) (see Equation 3). To get an estimate for the immobile water content, aggregates of the Ap and Bt horizons were placed on a stainless steel screen. The screen was then placed on water-saturated filter paper. The aggregates were wetted for approximately 24 hr and then dried at 105°C for 24 hr.

To estimate the hydrodynamic dispersion, tracer breakthrough experiments were performed using 0.1 *M* $CaCl_2$ solutions. The Cl was analyzed with an ion-selective microelectrode, and the program CXTFIT was then applied to obtain numerical values for the hydrodynamic dispersion coefficient (D) (*8*).

RESULTS AND DISCUSSION OF RESULTS

The isotherm for the Ap horizon is best described by the linear isotherm. The value of the distribution coefficient k is 0.572 ± 0.0100 with a correlation coefficient of r^2 = .999. In contrast, the Bt horizon follows the Freundlich isotherm best, which is clearly demonstrated in Figure 1. The value for Freundlich parameters were K = 1.142 ± 0.2545 and n = 0.75 ± 0.069 with a correlation coefficient of .985. Applying Equation 5 and the Freundlich parameters with a c_0 value equal to 50 mg L^{-1} yields a value of 0.429 for the distribution coefficient k. In addition to the average experimental values of the sorption isotherms, the sample standard deviations were denoted with the error bars. At high concentrations some data scatter was noted; however, for the lower concentrations, data from triplicate runs of batch experiments clearly demonstrate good reproducibility. The difference in sorption behavior between the two soil horizons can be attributed to the considerably higher organic matter content of the Ap horizon relative to the Bt horizon.

The Cl breakthrough curves show considerable difference between the aggregates and the nonaggregated soil (Figure 2). The results of the column experiment for the aggregated soil exhibit an asymmetrical shape, indicating an early breakthrough. Since the breakthrough curves of the nonaggregated soil are symmetrical, bypass flow appears to dominate the aggregated soil. On the basis of the shape of the breakthrough curves of the aggregated soil, the parameters for the nonreactive two-region model (R = 1) were determined using CXTFIT and are presented in Table 2 along with the standard error of estimates and the correlation coefficients. To avoid meaningless parameter values, the dimensionless rate coefficient was approximated by the method outlined by Rao et al. (*9,10*). The authors assumed an average aggregate radius of 0.17 cm and a tortuosity factor of 0.4 so that the mass transfer coefficient ranged from 0.9 to 1.2 h^{-1}. The values of the corresponding dimensionless variable are given in Table 2. The results of the immobile water content measurement yielded a value of 0.3 for β, assuming that the retardation factor (R) equals 1 (Equation 3).

Since at least three parameters are needed to determine the transport behavior of solutes using the two-region model, the parameter estimation was performed by optimizing the dispersion coefficient with the approximations of the dimensionless rate coefficient ω and the dimensionless parameter β constant. The correlation coefficients of all parameter optimizations of the same column run are very similar, but some of the parameters change drastically when incorporated into the optimization (Table 2). This was especially true for the slow-velocity experiment of the Ap horizon, where the dispersion increases from 0.001 to 12.47 cm^2 h^{-1} associated with an increase of β from 0.3 to 0.91. Even though the model is physically meaningful, the parameters do not appear to behave independently during the parameter optimization. Also, when all three parameters are optimized, the ratio of mobile to total water content appears to be overestimated. Nevertheless, the parameters may be viewed as empirical coefficients that describe the mixing behavior of nonreactive solutes in soil columns.

TABLE 1 Experimental Conditions for Miscible Displacement Experiments of Cl^- Tracer and 2,4-D in Loring Silt Loam, With and Without Aggregates

Experimental parameters	Experiments			
	Ap - soil	Ap - aggr.	Bt - soil	Bt - aggr.
ρ (g cm^{-3})	1.16	0.95	1.32	1.04
θ (cm^3 cm^{-3})	0.567	0.589	0.502	0.608
% saturation	89.2	98.9	91.4	92.5
v (cm h^{-1})	2.98	3.04	3.88	3.11
Tracer pulse (V V_0^{-1})	2.00	1.81	2.09	1.61
2,4-D pulse (V V_0^{-1})	8.86	8.09	11.2	8.62

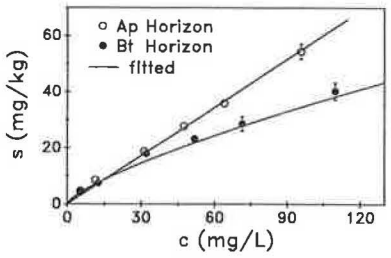

FIGURE 1 Isotherms of 2,4-D in Ap and Bt horizons of Loring silt loam measured using batch experimental techniques.

Using the parameters obtained from the Cl breakthrough curves and assuming that the sorption is well-described by the retardation factor (R), the breakthrough curves of 2,4-D were predicted. Even though the shape of the breakthrough curve of the aggregated Ap horizon closely resembles the experimental data, the curve is more retarded (Figure 3). Hence, the retardation coefficient of the Ap horizon determined from the batch experiment appears to overestimate the retardation. However, the prediction for the aggregated Bt horizon shows excellent fit with the experimental data (Figure 4). Since the organic matter content of the Ap horizon is considerably higher than that of the Bt, the authors assume that the aforementioned breakthrough phenomenon may be attributed to this difference.

The 2,4-D breakthrough curves in the soils with particles and aggregates below 2 mm in diameter show tailing phenomena. In addition, this effect is observed to a lesser extent for the breakthrough curves in the aggregated soils of the Ap horizon. To eliminate sorption nonlinearity as a cause for this phenomenon, the convective-dispersive equation with the Freundlich isotherm was solved numerically for the Bt horizon. The result is plotted as the dashed-dotted line in the upper graph of Figure 4. The tailing is more pronounced for the prediction when the linear sorption breakthrough simulation is used but deviates substantially from the experimental data. Also, the breakthrough front is steeper and the deviation

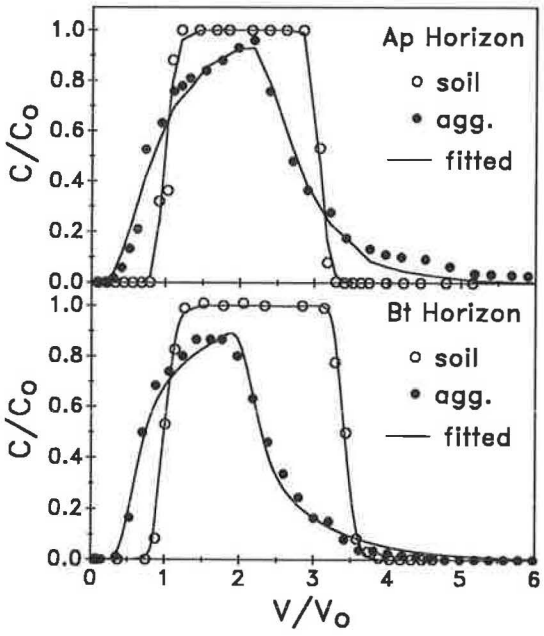

FIGURE 2 Cl breakthrough curves in soil columns with samples from Ap and Bt horizons of Loring silt loam, with and without distinct aggregates.

from the data points increased in comparison with the analytical solution of the linear convective-dispersive equation.

To ensure that the linear equilibrium sorption cannot describe the data adequately, the authors used the transport parameter from the two-region model and the convective-dispersive equation to optimize the retardation factors R for all pesticide breakthrough curves. The results are shown in Figures 3 and 4 as the dashed lines. The curves are shifted toward the origin, especially for the Ap horizon. As indicated in Table 3, the retardation coefficients determined from the transport data are approximately 14 to 36 percent lower than those estimated from the batch experiment. The only exception is the retardation factor of the aggregate's Bt horizon, which is higher than the batch-determined value. However,

TABLE 2 Parameter Estimates of D, β, and ω With Standard Error of Estimate from Cl^- Breakthrough Experiments for Ap and Bt Horizons, With and Without Aggregates

Exper.	r^2	D	SE	$\beta^\dagger$	SE*	$\omega^\dagger$	SE*
		---- $cm^2\ h^{-1}$ ----					
Ap soil	0.983	0.237	0.0627	-	-	-	-
Ap aggr.	0.961	0.001	2.167	0.3	-	1.8	-
Ap aggr.	0.979	12.47	3.034	0.915	0.0848	1.8	-
Ap aggr.	0.968	8.629	1.456	0.766	0.0337	1135.	183.5
Bt soil	0.995	0.471	0.0580	-	-	-	-
Bt aggr.	0.969	0.250	1.867	0.3	-	1.8	-
Bt aggr.	0.986	0.540	0.8325	0.457	0.0348	1.8	-
Bt aggr.	0.991	2.179	0.9108	0.629	0.0444	0.59	0.159

* Blank entries for the standard errors (SE) of either β or ω indicate that the parameter were estimated independently.

† Blank entries for β and ω indicate that the classical convective-dispersive equation was fitted instead of the Two-Region model.

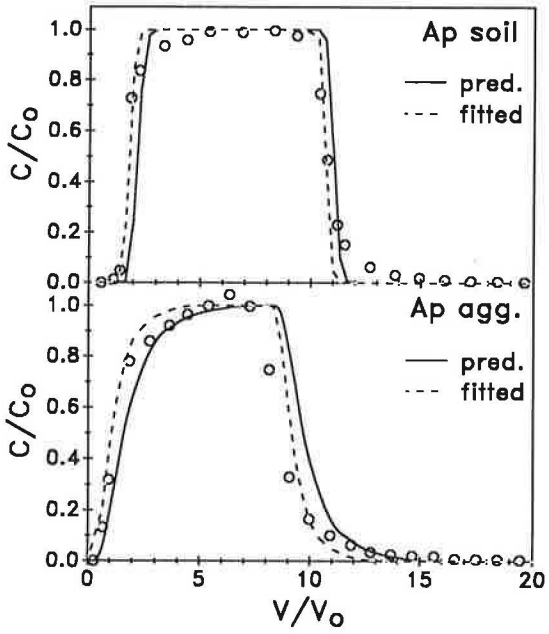

FIGURE 3 2,4-D breakthrough curves in soil columns containing soil and aggregates of Ap horizon of Loring silt loam.

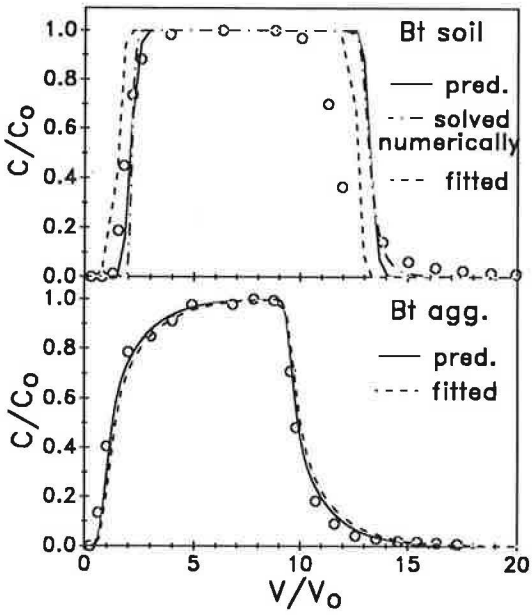

FIGURE 4 2,4-D breakthrough curves in soil columns containing soil and aggregates of Bt horizon of Loring silt loam.

the fitted and the predicted breakthrough curves show great similarities. This indicates that for the aggregated Bt horizon, the physical flow regime dominates the overall effluent concentration so that the breakthrough is relatively insensitive toward the retardation factor (R).

Since the two-region model seems to describe adequately only the nonreactive tracer transport, possible mechanisms explaining the deviation of the predicted and the experimental pesticide data need to be addressed. Nonequilibrium processes are most likely to occur since neither linear nor nonlinear isotherms can explain these findings. Also, the higher organic matter content of the Ap horizon may cause the difference between the breakthrough curves of the aggregated Ap and Bt horizons. Hence, higher organic matter contents seem to pronounce the observed effects that may be attributed to intraorganic matter diffusion as reviewed by Brusseau and Rao (*1*). The underlying concept of intraorganic matter diffusion is that the organic matter consists of polymeric materials so that solutes can diffuse through a mesh-like structure of organic matter. To describe the breakthrough data of the aggregated Ap horizon, an additional kinetic rate equation should be invoked.

The results of this research may be related to practical problems. First, surface soils are usually richer in organic matter than subsoils and hence the distribution coefficient k is expected to be higher in surface soils. Also, high organic matter content is associated with well-structured and highly permeable soils. High distribution coefficients and permeability affect each other adversely—that is, the solute is more retarded whereas the mean pore water velocity is high and therefore the mean residence time is decreased.

Besides the hydraulic properties, well-defined large aggregates as well as macropores caused by biological activity enhance bypass flow. As the depth increases, the organic matter content decreases, as do the aggregation, number, and size of macropores. Hence, the hydraulic properties increase the mean residence time of the solute, but the decreased retardation factor may enhance the transport of pesticides into groundwater. Applying this argument to the Loring silt loam implies that the danger of groundwater contamination is in-

TABLE 3 Parameter Estimates of Retardation Factor from Miscible Displacement Experiments Compared with Retardation Factor from Batch Experiments

Experiment	r^2	R	SE	R*
Ap soil	0.970	1.806	0.03079	2.171
Ap aggr.	0.972	1.264	0.08014	1.922
Bt soil	0.997	1.531	0.02265	2.118
Bt aggr.	0.969	2.064	0.04157	1.725

* Retardation factor determined from batch experiments

creased when the pesticide concentration is very high since the retardation of 2,4-D decreases in the Bt horizon considerably in comparison with the Ap horizon. Discrepancies between Ap and Bt should be most pronounced especially at concentrations above 75 mg L^{-1}. This also implies that the results are applicable to point source pollution such as accidental spills where the pesticide concentration is very high, rather than to non–point source pollution with low-concentration contamination.

SUMMARY AND CONCLUSIONS

Miscible displacement and batch experiments were performed to determine the effect of sorption and bypass flow on the transport of 2,4-D. The early breakthroughs of Cl in soil made of aggregates 2 to 4.8 mm in diameter showed a typical shape of physical nonequilibrium. These breakthrough curves are well described by the two-region model. In contrast, Cl breakthroughs of the soil that had been passed through a 2-mm sieve were adequately described by the classical convective-dispersive equation. However, the convective-dispersive equation did not provide a good fit for the 2,4-D data for both the Ap and Bt horizons. This deviation could not be attributed to the nonlinearity of the isotherm of the Bt horizon.

In addition, the predicted breakthrough curves for the aggregated Ap horizon were more retarded, which implies that the batch experiments overestimated the retardation. Adjustment of the retardation factors resulted in a shift in breakthrough curves, bringing them closer to the experimental data, but the tailing effect was still underestimated. In contrast, the predicted breakthrough curve of the aggregated Bt horizon agreed well with the experimental data. Increased bypass flow may control the overall effluent concentration in the aggregated Bt horizon, whereas additional chemical processes influence the breakthrough curves of the aggregated Ap horizon. An additional chemical process causing the deviation may be intraorganic matter diffusion, which also may cause the failing of the convective-dispersive model to predict the breakthrough curves in the soil without distinctive aggregates.

ACKNOWLEDGMENT

This research was partially funded by the Louisiana Transportation Research Center.

REFERENCES

1. Brusseau, M. L., and P. S. C. Rao. Sorption Kinetics of Organic Chemicals: Methods, Models and Mechanisms. In *Special Publication 27: Rates of Soil Chemical Processes* (D.L. Sparks and D.L. Suarez, eds.), Soil Science Society of America, Madison, Wis., 1991, pp. 281–302.
2. Koskinen, W. C., and S. S. Harper. The Retention Process: Mechanisms. In *Pesticides in the Soil Environment: Processes, Impacts, and Modeling* (H. H. Cheng, ed.), Soil Science Society of America Book Series 2, Soil Science Society of America, Madison, Wis., 1990, pp. 51–77.
3. Weber, J. B., P. H. Shea, and S. B. Weed. Fluridone Retention and Release in Soils. *Journal of the Soil Science Society of America*, Vol. 50, 1986, pp. 582–588.
4. Khan, S. U. Distribution and Characteristics of Bound Residues of Prometryn in an Organic Soil. *Journal of Agricultural and Food Chemistry*, Vol. 30, 1982, pp. 175–179.
5. Van Genuchten, M. T., and R. J. Wagenet. Two-Site/Two-Region Models for Pesticide Transport and Degradation: Theoretical Development and Analytical Solutions. *Journal of the Soil Science Society of America*, Vol. 53, 1989, pp. 1303–1310.
6. Van Genuchten, M. T. *Non-Equilibrium Transport Parameters from Miscible Displacement Experiments*. Research Report 119. U.S. Salinity Laboratory, Science and Education Administration, U.S. Department of Agriculture, Riverside, Calif., 1981.
7. Gamerdinger, A. P., R. J. Wagenet, and M. T. van Genuchten. Application of Two-Site/Two-Region Models for Studying Simultaneous Nonequilibrium Transport and Degradation of Pesticides. *Journal of the Soil Science Society of America*, Vol. 54, 1990, pp. 957–963.
8. Parker, J. C., and M. T. van Genuchten. *Determining Transport Parameters from Laboratory and Field Tracer Experiments*. Bulletin 84-3. Virginia Agricultural Experiment Station, Blacksburg, 1984.
9. Rao, P. S. C., D. E. Rolston, R. E. Jessup, and J. M. Davidson. Solute Transport in Aggregated Porous Media: Theoretical and Experimental Evaluation. *Journal of the Soil Science Society of America*, Vol. 44, 1980, pp. 1139–1146.
10. Rao, P. S. C., R. E. Jessup, D. E. Rolston, J. M. Davidson, and D. P. Kilcrease. Experimental and Mathematical Description and Nonadsorbed Solute Transfer by Diffusion in Spherical Aggregates. *Journal of the Soil Science Society of America*, Vol. 44, 1980, pp. 684–688.

Grassy Swales To Control Highway Water Quality Runoff

STUART M. FINLEY AND G. KENNETH YOUNG

The authors propose grassy swales for roadsides for new or upgraded highway facilities to provide water quality benefits. The proposal applies to state and local agencies responsible for highway infrastructure development, restoration, and maintenance. The concept is to incorporate grassy swales into land development street design and into highway repair activities. Vegetated side ditches are known to provide significant suspended solids and phosphorus reductions. Within urban to suburban developments, the tendency has been to require relatively expensive curb-and-gutter street cross sections from developers. Curbs and gutters concentrate storm flow and its suspended sediments, including phosphorus, and this contributes to non–point source pollutant loadings from developed areas. Providing grassy swale shoulders with underground storm drains to pick up flows that are on erosion thresholds may be an attractive alternative for new projects or for curb and gutter replacement if right-of-way costs are not a major factor. Concentrated flows would be slowed and subject to sediment deposition in swales. Highway, road, and particularly local street developments could cost less, be more attractive, and provide water quality benefits for nutrient and suspended solids removal with the use of grassy swales.

The objectives are to propose and justify the use of grassy swales as the preferred method of handling pavement drainage. Rural highway and road systems typically have such vegetated side treatments, but other systems—including Interstate, federal aid, and local streets in settled areas—are usually designed with paved ditches or curb-and-gutter systems, both with possible storm sewers, to accept pavement drainage and to cope with erosive velocities.

Consider Fairfax County, Virginia, as a well-organized example of a densely settled, nonincorporated region of 1 million inhabitants. The county's public infrastructure, including streets and drainage, has been installed by land developers who must comply with local regulations (*1*). These regulations are included in a county public facilities manual that provides comprehensive street and drainage design details. The local regulations are in accordance with Virginia Department of Transportation (VDOT) (and hence federal) design standards (*2,3*) and with the county zoning ordinance. Taken together, the federal and state design standards and the local zoning requirements led to developments in Fairfax County that provide curb-and-gutter streets for densities greater than one dwelling unit per acre. Also, most development occurred in the last half of the 20th century and can be expected to need repair and replacement during this generation.

This documented pressure in Fairfax County to give curb-and-gutter sections to local streets in highly populated regions is believed to be typical of urban and suburban developments across the country and to apply to higher-class road facilities as well. The influence is seen to be widespread and has resulted in an existing urban and suburban street system infrastructure that efficiently drains pavement and quickly moves the runoff away from the roads and developments. Pollution prevention was not a past concern. Road infrastructure generally preceded the nation's pollution control system (Pub. L. 92-500). Massive inputs of public money developed both. Now it appears that pollution control and road development policies may interact as we close out the 20th century.

The initial mid-century focus of pollution control was the collection and purification of sewage and industrial wastes—the so-called point sources. As this effort resulted in more and more success, the focus has now shifted. The present end-of-century focus is the control of the pollutants contained in land washoff—the so-called non–point sources (NPS). The control of NPS has led the federal government to expand the National Pollutant Discharge Elimination System (NPDES) to include the discharge from storm sewers. Jurisdictions are engaged in acquiring federal permits for their stormwater systems. The policy is clear: reduce NPS. Specific methods to implement the policy are in a state of flux and are being defined as part of the process of implementing the policy. State highway departments are engaged in these efforts.

Why highway departments? Because pavement drainage collects pollutants and may be considered to be an NPS. Regulators are looking for ways to control NPS, the term "control" meaning to impose best management practices (BMP) to runoff. BMP is a term that originated in a farming context and applied to the minimization of soil loss and the efficient use of agricultural chemicals, fertilizers, and pesticides to avoid their loss to runoff waters. The BMP concept translates to urban settings with the following practices: zoning modifications, detention ponds with or without permanent pools (wet or dry), intermittent wet ponds (extended detention), infiltration pits, grassy swales, biofiltration swales, buffer areas, and street cleaning.

The concepts espoused herein are

1. Pavement systems transport NPS pollution deposited on them by the NPS contributions of adjacent property.
2. Sooner or later, policies will develop to use highway BMPs to mitigate NPS.
3. Infrastructure maintenance and repair affords an opportunity to supply BMPs.
4. Future development can be reregulated so that new construction includes appropriate BMPs.
5. A very promising BMP is the grassy swale.

S. M. Finley, Lake Barcroft Watershed Improvement District, 3428 Mansfield Road, Falls Church, Va. 22041. G. K. Young, GKY & Associates, 5411-E Backlick Road, Springfield, Va. 22151.

6. The grassy swale has technical and policy barriers to implementation in urban settings where it would be beneficial as a BMP.

The benefits of grassy swales are that they remove silts and fines from the stormwater; they do so by slowing the flow and allowing deposition to occur. Not only is a portion of the suspended solids removed, but the phosphorus that is sorbed to soil fines or is in a precipitate state is removed. The removal of phosphorus is beneficial ecologically and is the subject of additional regulation in regional settings.

For example, the states that drain into the Chesapeake Bay have agreed to a policy to remove 40 percent of the nutrients to the bay using BMPs. This is accomplished with buffers, swales, detention ponds, and the like being applied to development and redevelopment. Legislation has been enacted to achieve this policy in Virginia (*4*).

Another example is the provision of "ecology ditches" by Washington State Department of Transportation to respond to the Puget Sound regional planning manual (*5*). Puget Sound, like the Chesapeake Bay, is being managed to control phosphorus inputs. The ecology ditch is a biofiltration swale that, in the context of this paper, is a grassy swale with an underdrain, bedded in porous backfill, that provides biotic action on the storm waters. In the Puget Sound manual, the term "biofiltration" describes the more-or-less simultaneous processes of filtration, infiltration, adsorption, and biological uptake of pollutants in storm water that takes place when runoff flows over and through vegetated treatment facilities.

This paper discusses adapting the geometrics of 50-ft rights of way, typically found in urban and suburban settings, to the incorporation of swales. The principal reason for considering grassy swales is to acquire water quality benefits for street projects. A major hurdle is that with any topographic relief, streets achieve grades that cause road-side drainage to flow with erosive velocities; thus the erosion issue requires more detailed roadside design considerations.

GRASSY SWALE CROSS SECTIONS

The typical curb-and-gutter cross section for areas with high population densities is shown in Figure 1 for a 50-ft right of way. There is a minimum of 30 ft from curb to curb for two traffic lanes. The gutters are extended from the curbs with a 1 to 2 percent cross slope. Curb, grate, or combination inlets admit the pavement drainage to storm sewers. The water is quickly removed, and velocities in the gutters and storm sewers are sufficient to transport suspended materials. A design criterion of typical storm sewers is to ensure sufficient velocity, typically greater than 1 ft/sec, to transport any suspended particles and to avoid deposition.

Alternatively, Figure 2 presents a ditch section cross section with a 50-ft right of way. The site treatments for this design are paved ditch, grassy swale, or earthen ditches, depending on erosive stability. This ditch section can also have underground storm sewers to pick up surface water before it floods the traveled way or achieves erosive velocities.

Within the present regulations in Fairfax County, Virginia, the ditch section would be acceptable only if zoning was a density of one dwelling unit per acre or less. This is a local requirement—VDOT enables ditch sections across the board but the county opted for a more stringent standard. Ditch cross sections require load-bearing shoulders for parking. Paved ditches would be provided when flow velocities in the side channels become erosive. Unless the street is nearly flat, paved ditches tend to prevail over grassy swales or earthen ditches.

Curb, gutter, paved ditch, and storm drain calculations can be accomplished using the HYDRAIN computer system (*6,7*). Key design elements are inlet spacings to avoid gutter spread, types of inlet, and sizing of storm drains.

For streets with mild grades, the ditch section shown in Figure 2 reduces to the alternative grassy swale section shown in Figure 3. Because erosive velocities are avoided with flat or nearly flat grades, the side drainageways can be vegetated ditches. Such ditches move water slowly, so particles have opportunity to settle out. Keeping suspended solids in the side ditches provides benefits to water quality.

Technical difficulties that arise with the grassy swale section are those of keeping velocities low and removing water when the ditch fills up. A secondary issue is the integration of a shoulder into the swale that will support parked vehicles. However, if the technical difficulties can be overcome, the more widespread use of grassy swales in new and retrofit situations will provide a BMP to address the NPS concerns associated with pavement drainage.

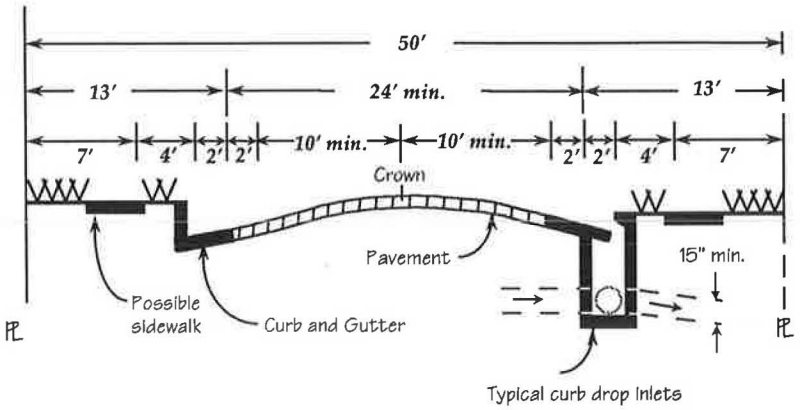

FIGURE 1 Cross section of typical urban local street, curb-and-gutter section (not to scale).

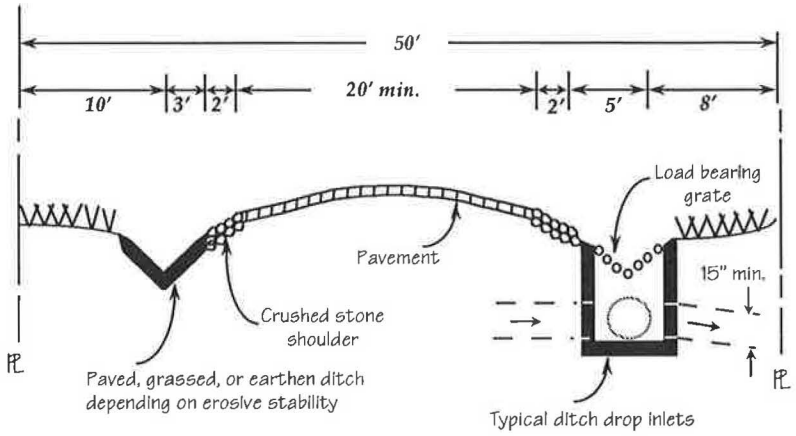

FIGURE 2 Cross section of typical urban local street, ditch section (not to scale).

The design of roadside channels having dirt, grass of various types, and riprap is also facilitated by HYDRAIN (*8,9*). Tractive force theory is used to size swales and grades to avoid erosion and to promote deposition. This latter design objective—the encouragement of siltation in roadside channels, in other words—is new. However, reflection indicates that a design to avoid erosion is also a design to encourage deposition. Furthermore, a new set of design concepts is needed to extend the grassy swale cross section from mild street grades to steeper grades in order to achieve more widespread benefits for water quality.

Consider the journey of NPS silt and pollutants in surface washoff. The NPS materials are added to the drainage from the pavement, roadsides, and adjacent property. They proceed in roadside conveyance channels (gutters and paved or unpaved ditches) to storm inlets and then to the storm sewer itself. The sewer outfall moves the NPS materials to downstream receiving waters and may damage them or their riparian property owners.

The objective is to reduce the NPS materials, which is what a BMP does. Grassy swales can retain NPS material near to the location where it starts its journey. It seems reasonable to let it settle out there before it accumulates and becomes a progressively larger amount within a converging storm water pipe system. The chore of maintaining swales becomes one of cleaning, regrading, and reseeding ditches and not one of maintaining detention ponds or other downslope facilities, which may require costly space that the right-of-way engineer must acquire.

DISCUSSION OF DESIGN DIFFICULTIES

Consider a parabolic grassy swale with a ½-ft depth at a full width of 15 ft. Such a swale could be provided on both sides of a ditch section street with 50-ft right of way. Figure 4 shows slopes calculated by HYDRAIN that are possible for this swale at various nonerosive velocities. At a 3 percent grade, the swale can convey 3.5 ft^3/sec at a nonerosive velocity of 0.7 ft/sec. Once the swale fills up or achieves erosive velocities, a stormwater pickup to a storm sewer is needed.

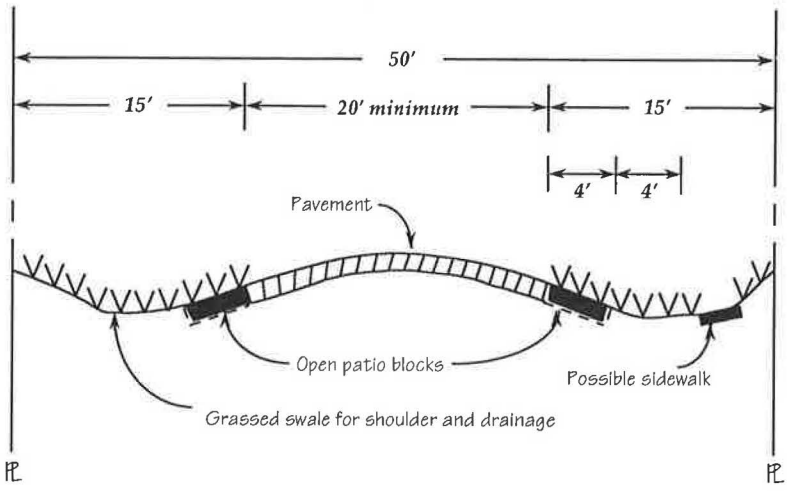

FIGURE 3 Cross section of grassy swale roadside improvement (not to scale).

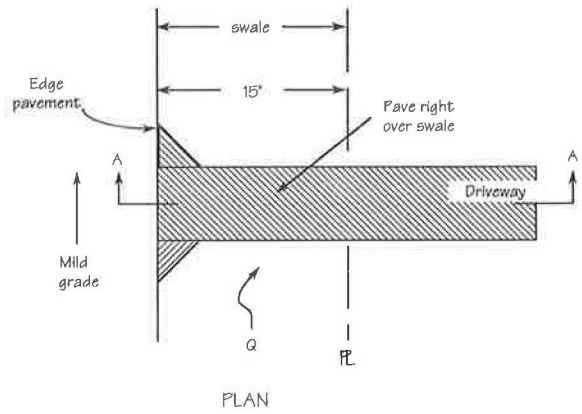

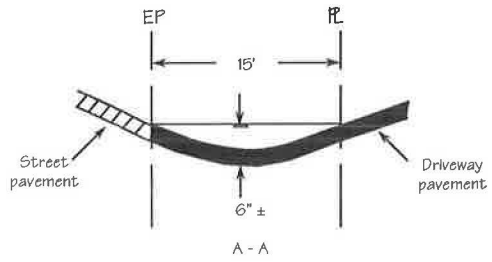

S Swale Slope	Q (cfs)	V (f/s)	Non-errosive
.5%	.35	.07	yes
1%	.5	.1	yes
2%	.9	.23	yes
3%	3.5	.71	yes
>3%	--	--	no

(Mowed established grass)
Parabolic Full Swale Capacity (15' by 6")

FIGURE 4 Design concepts for mild grades (under 3 percent) (not to scale).

The individual properties along the street can provide driveways right across the swale. This is shown in Figure 4, as well. The swale would be vegetated and mowed; it probably would integrate into the landscaping of residential property.

A problem with grassy shoulders is a need to maintain vehicle loads. When wet, grassy areas with clayey soil soften and become rutted. To provide adequate bearing and avoid rutting, patio blocks, such as shown in Figure 5, can be placed next to the pavement at the roadside edge of the swale. Their open structure can be filled with sandy soil and grass planted on top. Such open concrete blocks would have to be placed on select material to avoid differential settlement. Whoever performs the ditch-side maintenance to remove accumulated silt must take care to not dislodge the blocks.

Steeper grades than the 3 percent shown in Figure 4 will cause roadside channels to have erosive velocities if the channels have the same slope as the street grade. Therefore, the channel slopes must be maintained at a 3 percent or lower slope even if the road grade is higher. How? One approach is to break the swale grade at driveways. The driveway can serve as a "check dam" that lets the water drop using a drop inlet and a culvert. Figure 6 shows a schematic of the concept. The swale runs at a slope of 3 percent or less to a drop inlet to a culvert under the driveway. Water exits the culvert on a new invert elevation adjusted to enable the carrying of the swale slope along at less than 3 percent.

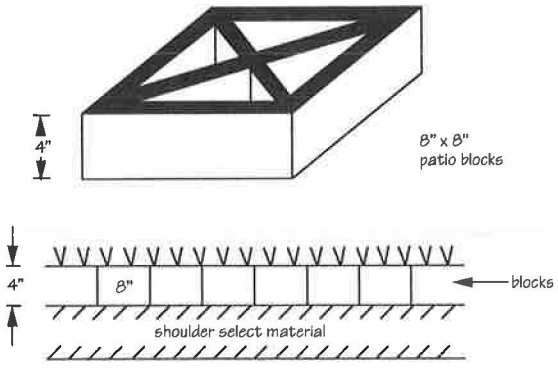

FIGURE 5 Parking support using open concrete blocks: *top*, system to allow turf to grow in swale and to bear load of parked vehicles using open concrete patio blocks; *bottom*, open concrete blocks filled with sandy soil.

The exit end wall could be an obstacle in the traveled way—that is, it might be a safety hazard to errant vehicles. If needed, safety bars can be provided that will protect vehicles and not cause significant hydraulic consequences.

Water in a swale could accumulate to sufficient quantities to overtop the edge of pavement and spread into the traveled way. This situation can be handled by switching from a series of drop inlet and culvert systems to a storm drain beneath and parallel to the swale. Inlets would be provided above driveway entrances as with the culvert scheme and would drop water in excess of what the swale can hold into the storm sewer.

The grassy swale design alternative would provide water quality benefits for highway and street systems: street and adjacent property wash-off would go through grassed swales. Cost savings would accrue because of the deduction of curb-and-gutter costs from projects. Cost increases would be attributed to specialized driveway entrance designs, careful grading, and provision of bearing blocks for shoulder parking. Added costs would be sensitive to topography: steeper grades would necessitate more extensive measures to keep swale grades under 3 percent.

To sum up, the balance of costs is unknown; there would be some savings and there would be some costs. Design of roadside treatments would be more tedious; design costs would increase to accommodate the tedious roadside ditch details and grading plans.

PRELIMINARY REACTIONS

The Lake Barcroft Watershed Improvement District (WID), an agency of Virginia's Soil and Water Conservation De-

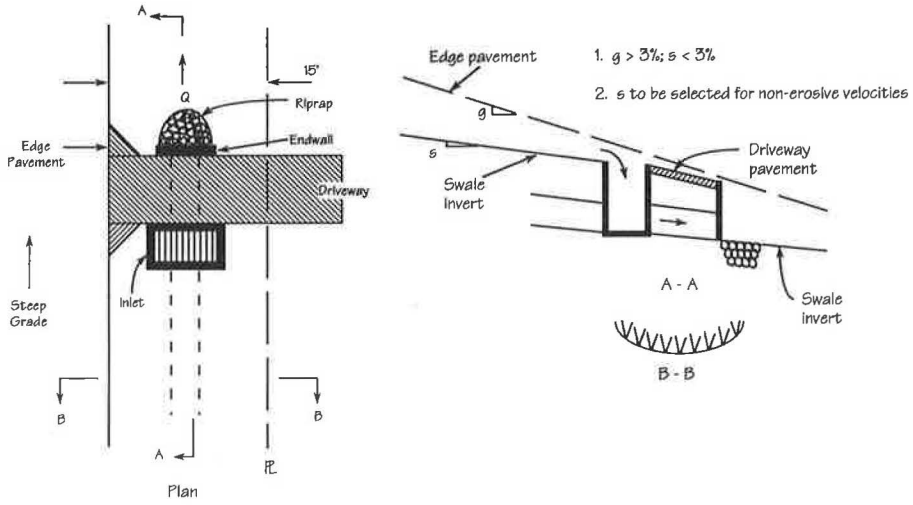

FIGURE 6 Design concepts for steep grades (over 3 percent) (not to scale).

partment, embraces the concept. The WID manages a large real estate lake and receives suburban drainage conveyed through public streets and state highway department and county storm sewers. Its view is that public agencies and state highway departments are expected to carry an inordinate portion of the costs of controlling storm water compared with the revenue from those who yield storm water flows.

The WID sees storm water as the vehicle that carries all the pollution and debris from upstream areas to the lake over which it has oversight. Individual property owners have roofs and pavements that deny infiltration and water retention and instead concentrate the storm waters and rapidly pass them on. The local resident is not required to do anything: retard flow, remove debris, control erosion, or husband lawn chemicals.

With grassy swales, the WID sees many benefits:

1. Debris would be retained in the grassy swales and not make it to the lake.
2. The grassy swales would become integral portions of property owners' front yards; owners would mow and maintain the swales to keep up appearances.
3. The frontage throughout the WID property owners' area would transform from a mixture of ditches, gutters, and swales to a uniform, grassed shoulder appearance if a retrofit program were implemented.

The WID sees the proposed solution as a reversal of the usual practice of shunting everything downstream. Instead of curbs and gutters, the WID desires a more attractive system of grassed swales along the edges of residential streets. Instead of rushing downstream, storm water would linger momentarily near where the raindrops fell. Some would seep into the underground water table. Another portion would temporarily pond and then flow off gradually after the storm. In both cases, at least a portion of the pollution would stay put. To shift costs to their source, the homeowner would have to rake the leaves and other debris and put it in the solid waste disposal system. But this is fair since not only would the owner acquire a large, neat, attractive frontage, but the owner is the one who contributed the debris originally.

The authors presented the grassy swale concept to the Virginia Lake Management Association in April 1992, and the lake manager for Lake Monticello, near Charlottesville, Virginia, composed a poem that expresses local reaction. John Aker, of Palmyra, Virginia, entitled the poem "Swales of Grass"; it is provided in Appendix A.

The authors have met with local government officials and state highway personnel. Preliminary discussions indicate considerable resistance to new standards—bureaucratic inertia being what it is, this reaction is hardly noteworthy. However, there is a clear need for code revisions with respect to zoning. A broad interpretation of state highway department standards indicates that grassy swales are acceptable within a cross section. The institutional difficulty will be in revising the local ordinances to allow such cross sections in ½-acre and higher densities and to develop detailed engineering standards to go with code revisions. This discussion, of course, pertains to Northern Virginia, but it is probably representative of other urban and suburban institutional settings as well.

Another indication of the impacts of BMPs is the localities' concern about maintenance. This parallels the concerns of state highway departments. Once facilities are provided, there will be a long-term need to maintain them. An example of the maintenance concern is a manual prepared by the Rappahannock Area Regional Planning District, Fredericksburg, Virginia, that offers guidance to municipalities on standards for construction of BMPs to minimize maintenance and estimates of what to expect in terms of maintenance needs (*10*). With grassy swales being an integral and prevalent aspect of highway and road cross sections, maintenance would be directed at removing silt and managing vegetation as needed. For large highway facilities, state highway workers or "adopt-a-highway" organizations would perform routine maintenance. For local streets, homeowners could play a role.

ENVIRONMENTAL BENEFITS

On the basis of literature research and measurements compiled by the Washington Metropolitan Council of Governments (*11*), the Chesapeake Bay regulations within the state

of Virginia tabulate (*12*) phosphorus removal efficiencies. The Chesapeake Bay Preservation Act considers phosphorus to be the target nutrient for control of the ecologic response of bay coastal waters. This attitude is typical across the country for drainage to all lakes and coastal waters, and NPS local controls and regulations are likely to be oriented toward phosphorus. The average efficiencies of phosphorus removal are 10 to 20 percent for grassy swales and 40 percent for vegetated buffers (100 ft wide). Phosphorus carried in storm waters is about 50 percent soluble and 50 percent affixed to sediment. Thus, if the sediment can be settled out and removed, up to about 50 percent of the phosphorus in storm flows can be eliminated physically by settling. This physical removal of sediment and affixed phosphorus by deposition in swales and natural buffers is the benefit of using vegetated swales to collect pavement drainage. Field measurements in local settings would quantify water quality benefits and refine values in the literature.

Thus, the conventional wisdom of the benefit of swales and natural buffers is 10 to 40 percent phosphorus removal with 50 percent as an upper limit. This level of BMP effectiveness is clearly desirable to protect downstream receiving waters from being overfertilized with plant nutrients that cause eutrophication. Downstream streams, lakes, and coastal waters would all benefit from phosphorus reduction. And although the primary focus is phosphorus reduction, downstream silt loads would also be reduced. Siltation in downstream rivers, lakes, and estuaries would be decreased, reducing maintenance and possible dredging and preserving riparian property values.

CONCLUSIONS

1. Grassy swales as highway and street side channels convey pavement drainage and function as a best management practice to reduce NPS pollution.
2. Benefits of grassy swales are reduced phosphorus and silt loadings to receiving waters—stream, lakes, coastal zones—and reduced costs associated with the elimination of curb and gutter and paved ditches.
3. Costs of grassy swales include more detailed design of roadside drainage and driveway features to keep swale invert slopes under erosion thresholds.
4. Maintenance of grassy swales includes removing silt and managing vegetation. Silt and debris reductions in swales should save costs associated with reduced maintenance for storm drains, which clog when transporting debris loads. Adjacent property owners can also be expected to provide maintenance to maintain appearances.
5. Technical difficulties of grassy swales are as follows:
   - –Maintaining mild side ditch drainage slopes when street grades are high;
   - –Providing drop structures at driveways to break and restart mild ditch slopes;
   - –Making structures, inlets, and end walls safe for traffic, if warranted; and
   - –Providing sufficient room without excessive right-of-way costs.
6. Technical aids for designing swales, as well as hard drainage features, exist in the HYDRAIN software system and supporting FHWA guidance documents.
7. Leadership at the national level is needed to accelerate the acceptance and implementation of grassy swales. On the basis of the authors' experience, a top-down approach will overcome inertia resistance to change and is preferable to a bottom-up, or grass roots, approach. Model specifications and local ordinances are needed to assist state highway departments and local jurisdictions.
8. The issue cuts across several TRB committees as it pertains to hydrology, hydraulics, water quality, environmental impacts, and highway geometrics. The TRB committees should coordinate needed information gathering and research to provide leadership and provide the needed top-down approach.

ACKNOWLEDGMENTS

The authors wish to thank the anonymous TRB reviewers for valuable suggestions. Robert Winter, Washington State Department of Transportation, provided comments and a view from the perspective of the Puget Sound as well as the design in which a swale with an underdrain functions as a biofilter.

REFERENCES

1. *Public Facilities Manual*. Fairfax County, Va. (updated periodically).
2. *Drainage Manual*. Virginia Department of Transportation, Richmond, 1983.
3. *Road and Bridge Specifications and Standards*. Virginia Department of Transportation, Richmond, 1989.
4. *Chesapeake Bay Preservation Act Regulations*. VR 173-02-01.1. Commonwealth of Virginia, 1988.
5. *Stormwater Management Manual for the Puget Sound Basin*. Puget Sound Regional Planning Commission, Wash., Feb. 1992.
6. Johnson, F. L., and F. M. Chang. *Drainage of Highway Pavements*. Hydraulic Engineering Circular 12; FHWA-TS-84-202. FHWA, U.S. Department of Transportation, 1984.
7. Young, G. K., and J. S. Krolak. *HYDRAIN—Integrated Drainage Design System*. Version 4.0, Vol. 3. HYDRA—Storm Drains. FHWA, U.S. Department of Transportation, 1992.
8. Chen, Y. H., and G. K. Cotton. *Design of Roadside Channels with Flexible Linings*. Hydraulic Engineering Circular 15; FHWA-87-8. FHWA, U.S. Department of Transportation, 1988.
9. Young, G. K., and J. S. Krolak. *HYDRAIN—Integrated Drainage Design System*, Version 4.0, Vol. 7. HYCHL—Roadside Channels. FHWA, U.S. Department of Transportation, 1992.
10. GKY and Associates, Inc. *BMP Facilities Manual*. Rappahannock Area Development Commission, Fredericksburg, Va., 1991.
11. *Controlling Urban Runoff: A Practical Manual for Planning Urban BMPs*. Metropolitan Washington Council of Government, Washington, D.C., 1987.
12. *Local Assistance Manual*. Chesapeake Bay Local Assistance Department, Commonwealth of Virginia, 1989.

APPENDIX A

Swales of Grass

John Aker

In fair Fairfax's upscale 'burbs,
I find no gutters and no curbs;
Its sculpted hills and classy dales
Are drained by keen, green grassy swales.

There facing upstream stands Stu Finley,
And with glee (disguised quite thinly),

"Send me not your trash," he rails;
"Trap it in your grassy swales."

"Too long my lovely lake has been
Your unwilling, huge trash bin.
But now it's o'er at last," he wails,
"Thanks to our neat grassy swales."

And for the record, notes Ken Young,
"Too long, too long, had mankind clung
To a plan that crassly fails;
Now gaze upon my grassy swales."

"For high- and byway sanitation,
There's but one choice for this nation,
Besides which others vastly pale:
Our silt-consuming grassy swale."

And just to prove that they approve
This revolutionary move,
Flashy girls and dashing males
Now play croquet on grassy swales.

Just a dream? Perhaps a vision?
The Board of Supes must reach decision;
While they bide I brashly hail
That gleaning, greening grassy swale.

To handle future highway runoff,
These two a great idea have spun off;
So folks, don't turn a ghastly pale
When one suggests a grassy swale!

Extreme Rainfall Frequency Analysis for Louisiana

BABAK NAGHAVI AND FANG XIN YU

A comparative study of five popular frequency distributions and three parameter estimation methods was conducted on the rainfall data from 92 stations in Louisiana. Computed results showed that the log-Pearson Type 3 (LPEAR3) distribution along with the method of moments was the best choice for the Louisiana rainfall data. Maximum annual 24-hr rainfall maps for return periods of 2, 5, 10, 25, 50, and 100 years were developed by using hourly precipitation data. These new isohyetal maps were compared with the U.S. Weather Bureau Technical Paper 40 maps based on the performance indexes of the standardized mean square error (*MSE*) and the standardized bias (BIAS). On the average, the new maps reduced the *MSE* by 58 percent and the BIAS by 80 percent. A first-order error analysis was performed on the parameters of the LPEAR3 distribution. Computed results showed that the predicted quantiles of the LPEAR3 distribution were most sensitive to the parameter of population mean and least sensitive to the coefficient of skewness.

Many times in hydrologic studies, flood discharges and hydrographs must be estimated for ungauged sites. The accuracy of estimated flood discharges from a rainfall-runoff model depends heavily on the accuracy of the estimated rainfall values. The first extended rainfall frequency study in the United States was made by Yarnell (*1*) and was presented in the form of maps for several combinations of return periods and durations for the continental United States. The only published report with regard to precipitation in Louisiana was found to be *Louisiana Rainfall* (*2*), published by the Louisiana Department of Public Works in 1952.

The U.S. Weather Bureau updated the rainfall maps with additional data and published them as TP-40 (*3*) in 1961. To date, TP-40 is the most widely used source of rainfall information. This rainfall atlas contains 50 maps of the United States with contour lines of rainfall amounts for durations varying from 30 min to 24 hr and return periods from 2 to 100 years. The accuracy and resolution of TP-40 maps are limited because of the small number of rain gauges available at the time of preparation and the short period of records at each gauge station, and the TP-40 maps have wide contour intervals and lack the detail necessary for the accurate design of drainage structures in a particular watershed.

A supplement to TP-40, HYDRO-35 (*4*), was published by the National Oceanic and Atmospheric Administration of the National Weather Service in 1977. HYDRO-35 provides rainfall contour maps for 5- to 60-min durations and 2-, 10-, and 100-year return periods for the eastern and central United States. This set of maps is a useful addition to TP-40 for estimating design rainfalls of short durations or developing intensity-duration-frequency (I-D-F) charts. Other studies have been undertaken along similar lines by Pennsylvania State University for the Pennsylvania Department of Transportation (*5*) and the Arizona Department of Transportation (*6*). However, results of these studies are only applicable to those two states.

One of the major objectives of rainfall frequency analysis is to estimate the magnitude of extreme rainfall or the rainfall intensity for a given duration and return period. The rainfall quantiles, in conjunction with a rainfall-runoff model, are used to compute flood quantiles of a stream. Several studies have been reported in the literature to compare the performance of various distributions with various parameter estimation methods (*7–10*). However, there is no general consensus on either the performance of a specific distribution or a specific parameter estimation method. For example, Arora and Singh (*10*) concluded, on the basis of their Monte Carlo simulation results, that the LPEAR3 with the method of moments (MOM) performed poorly and suggested a revision of the recommendation by the U.S. Water Resources Council (*11*) of using LPEAR3-MOM; others, however, found that LPEAR3-MOM gave consistent and efficient estimates (*11,12*).

In this paper the authors will make a comparative evaluation of five distributions and three parameter estimation methods for the Louisiana rainfall data and discuss the development of maximum annual 24-hr rainfall maps for return periods of 2, 5, 10, 25, 50, and 100 years.

ANALYSIS OF RAINFALL DATA

Hourly precipitation data were obtained from the National Climatic Data Center of the National Weather Service, U.S. Department of Commerce. The raw data contain records of 92 rain gauges in Louisiana. The average record length of the 92 stations is 18 years with minimum and maximum values of 2 and 40 years. However, almost every station had periods of missing records. Records at stations within a 10-mi radius were combined when no single station had a continuous record of sufficient length to provide a complete data set for a reliable statistical analysis. This grouping of rain gauges provided 26 synthesized (representative) stations, which are shown in Figure 1. Mass curves were developed for the entire period of records for all 26 representative stations to check for consistency of the records. These curves showed that no further adjustment to records was needed. The average record length of the 26 synthesized stations is 38 years; minimum and maximum values are 30 and 40 years. The group of stations that composed a synthesized station were designated as primary

Louisiana Transportation Research Center, 4101 Gourrier Avenue, Baton Rouge, La. 70808.

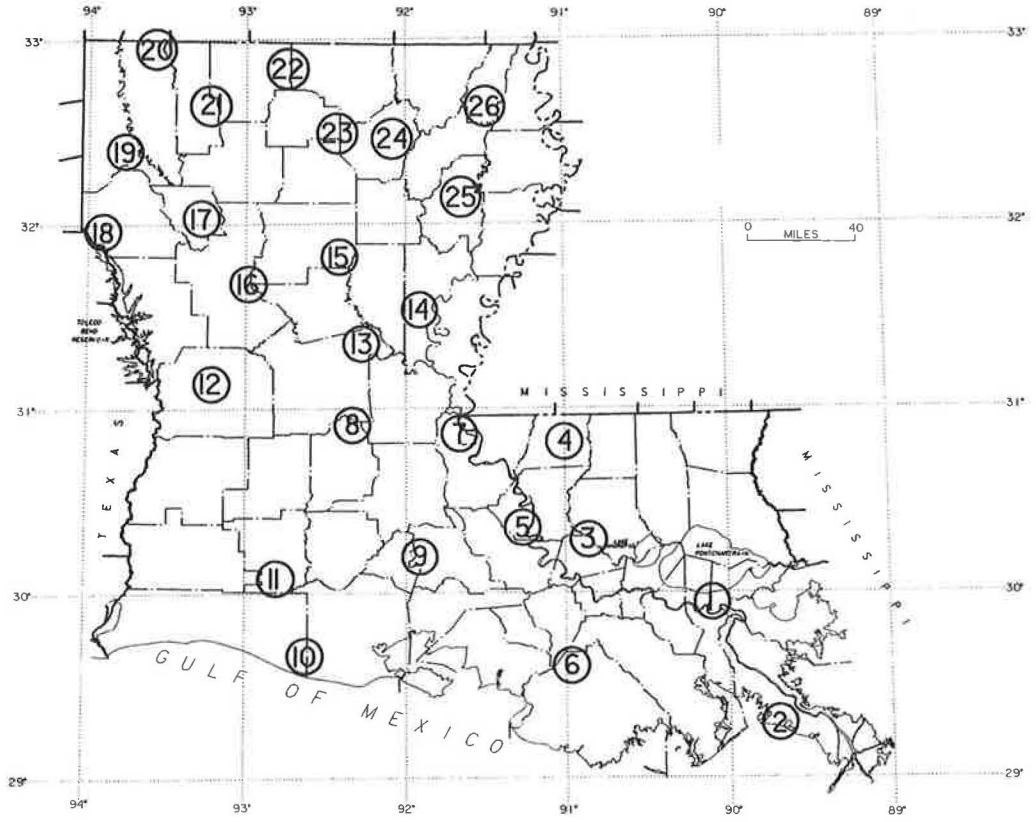

FIGURE 1 Representative rain stations in Louisiana.

stations. The stations outside the group of primary stations were designated as secondary stations. Missing data were directly substituted from the primary stations, and the inverse-distance-squared method was used to fill the data gaps from the nearby secondary stations.

The complete data sets for the synthesized stations were examined for possible errors in the filling of data gaps by checking the annual precipitation between the synthesized and primary stations. When the annual precipitation of the synthesized stations exceeded the annual precipitation of the primary stations by more than 15 percent, the selection of secondary stations was modified. The suitability of the synthesis was further examined using correlation plots of monthly rainfall between primary, secondary, and synthesized stations. Use of these plots ensured that the homogeneity property was not severely violated when filling the data gaps.

With 26 complete data sets representing the 26 synthesized stations, the annual maximum 1-, 3-, 6-, 12-, 24-, 36-, 48-, 60-, 72-, and 96-hr rainfall depth series at each synthesized station was calculated. This was done by making the rainfall data continuous by inserting zero values for non-rainfall hours, then scanning the continuous data and finding the maximum XX-hr annual rainfall depth.

SELECTION OF DISTRIBUTIONS AND PARAMETER ESTIMATION METHODS

A quantitative and practical approach for the selection of an appropriate distribution and a parameter estimation method for the available data is to test some of the most frequently used distributions in applied hydrology along with the most popular parameter estimation methods. By using such statistical criteria as mean square error (*MSE*) and bias, the descriptive performances of different combinations of the distributions and estimation methods were compared and then the best combination was selected (*13*). In this study, five popular distributions and three parameter estimation methods widely used in applied hydrology were considered for a comparative evaluation. The five probability distributions are

- Two-parameter log-normal (LNO2),
- Three-parameter log-normal (LNO3),
- Pearson Type 3 (PEAR3),
- Log-Pearson Type 3 (LPEAR3), and
- Extreme-value Type 1 (GUMBEL).

The three parameter estimation methods are MOM, maximum-likelihood estimate (MLE), and principle of maximum entropy (POME).

These five distributions and three estimation methods have been discussed by various investigators (*7,8,10,13*). Therefore, they are not discussed here.

The descriptive performance indexes for the evaluation of different combinations of distributions and estimation methods, using observed data, are the standardized *MSE* and the standardized bias (BIAS) (*14*). The *MSE* at each station for a selected rainfall duration is defined as

$$MSE = \frac{1}{n}\sum_{i=1}^{n}\left[\frac{x_c(i) - x_o(i)}{\bar{x}}\right]^2 \quad (1)$$

where

$x_c(i)$ = computed rainfall values for ith plotting position, ranked in descending order;
$x_o(i)$ = observed rainfall values for ith plotting position, ranked in descending order; and
$\bar{x}$ = observed sample mean at same station.

Similarly, the standardized bias (BIAS) at a station for a selected rainfall duration is defined as

$$\text{BIAS} = \frac{1}{n}\sum_{i=1}^{n}\left[\frac{x_c(i) - x_o(i)}{\bar{x}}\right] \quad (2)$$

A computer program was developed to estimate the parameters of the five distributions by three estimation methods, using the annual maximum rainfall series at each of the 26 synthesized stations, and to compute the *MSE* and BIAS for all combinations of the selected distributions and estimation methods at each station. The average *MSE* and BIAS were calculated for all combinations of distributions and methods over 26 stations. The average *MSE* and BIAS values for the 26 stations are given in Tables 1 and 2. Table 1 indicates that in terms of the average *MSE* for 26 stations, LPEAR3-MOM is the preferred combination of distribution and estimation method for Louisiana rainfall data. On the other hand, Table 2 indicates that LNO3-MLE gave the least average BIAS for the 26 stations. In practice, however, *MSE* is considered to be a more preferable performance index than BIAS when the corresponding BIAS is not excessively large. Since the LPEAR3-MOM has the smallest average *MSE* with the corresponding BIAS comparable to other methods, LPEAR3-MOM was selected as the most appropriate combination of distribution and estimation method for the Louisiana rainfall data.

DEVELOPMENT OF 24-hr ISOHYETAL MAPS

Quantiles of the 24-hr maximum rainfall for the 26 stations were computed by using LPEAR3 distribution with the MOM estimation method. The computed quantiles often change sharply from one station to another. Therefore, several rules were devised to make the isohyetal drawings meaningful. First, the means of the quantile values were computed from each 1-degree quadrangle of latitude and longitude to filter out possible random errors. The "initial" 24-hr isohyetal curves for various return periods were based on these average values. However, various types of errors exist that render the initial isohyetal curves unacceptable. To improve the initial curves, the following rules were applied:

1. If a station quantile in a 1-degree quadrangle deviates from its mean by three standard deviations, that quantile is eliminated from the computed data set.
2. If only one or two stations exist in a 1-degree quadrangle, adjacent station values are used to compute the mean value.

TABLE 1 Average *MSE* for 26 Stations for 24-hr Annual Maximum Rainfall Series

		LNO2	LNO3	PEAR3	LPEAR3	GUMBEL
MOM	MAX	0.06289	0.05298	0.05722	0.05388	0.06815
	AVG	0.01001	0.00872	0.00843	**0.00780**	0.01055
	MIN	0.00146	0.00124	0.00119	0.00104	0.00144
MLE	MAX	0.07293	0.08230	0.08704	0.06683	0.07452
	AVG	0.01234	0.01721	0.01885	0.01126	0.01434
	MIN	0.00118	0.00171	0.00195	0.00106	0.00088
POME	MAX	0.07293	0.08677	0.08946	0.07058	0.07262
	AVG	0.01234	0.01859	0.01900	0.01095	0.01255
	MIN	0.00118	0.00129	0.00174	0.00112	0.00098

TABLE 2 Average BIAS for 26 Stations for 24-hr Annual Maximum Rainfall Series

		LNO2	LNO3	PEAR3	LPEAR3	GUMBEL
MOM	MAX	-0.00373	0.00071	0.00069	-0.00003	-0.00772
	AVG	-0.00855	-0.00918	-0.00924	-0.01181	-0.01033
	MIN	-0.01481	-0.02654	-0.01821	-0.02674	-0.01316
MLE	MAX	-0.00352	0.00090	0.00415	-0.00307	-0.00230
	AVG	-0.00992	**0.00029**	0.00255	-0.01169	-0.01750
	MIN	-0.01997	-0.00160	0.00151	-0.02310	-0.03728
POME	MAX	-0.00351	0.00413	0.00499	-0.00375	-0.00802
	AVG	-0.00992	0.00232	0.00370	-0.00978	-0.00964
	MIN	-0.01996	-0.00476	0.00206	-0.01841	-0.01157

3. If a station is located between two adjacent 1-degree quadrangles, the quantile at that station is used in computations by both adjacent 1-degree quadrangles.

4. In the corner quadrangles where the trend of the isohyetal lines is not clear, nearby individual station values are given higher importance than average values.

5. When the isohyetal curves change sharply in a small local area, the curve is modified on the basis of the nearby curve pattern, geographical and climatological conditions, or the reliability of the nearby station data. This condition is necessary to provide smooth transitions for the isohyetal curves.

The final 24-hr isohyetal maps for the return periods T = 2, 5, 10, 25, 50, and 100 years were based on these rules. Figure 2 shows an example of the isohyetal map for the 50-year return period. A similar analysis was also conducted for rainfall durations of 1, 3, 6, 12, 36, 48, 60, 72, 84, and 96 hr (*13*).

VERIFICATION OF RESULTS

A comparison was made between the new isohyetal maps ("NewMaps") and the TP-40 maps for the return periods of 2, 5, 10, 25, 50, and 100 years. The standardized *MSE* and standardized bias (BIAS) were used as the performance indexes for the evaluation. *MSE* and BIAS were computed by using values from each map at the corresponding stations. The "observed" values are the predicted quantiles from the observed data by using the log-Pearson Type 3 distribution with MOM. Table 3 gives the average *MSE* and BIAS for six return periods. Table 4 gives the predicted quantiles from the TP-40 maps, the NewMaps, and LPEAR3-MOM at five typical stations for six return periods. On the average, for return periods of less than or equal to 25 years, the NewMaps are superior to the TP-40 maps in terms of both *MSE* and BIAS. For return periods of 50 and 100 years, the NewMaps are superior to the TP-40 maps in terms of *MSE* but have slightly larger values of BIAS. On the average, for all of the 26 synthesized stations corresponding to six return periods, the NewMaps reduced the *MSE* by 58 percent and the BIAS by 80 percent, compared with the TP-40 maps.

SENSITIVITY OF PREDICTED QUANTILES TO ERROR IN MODEL PARAMETERS

An error analysis was performed to evaluate effects of errors in estimated parameters on predicted rainfall quantiles by using the LPEAR3 distribution with MOM for parameter estimation. The procedure of first-order analysis outlined by Singh and Yu was followed (*15*). The parameters of the LP3 distribution for the annual maximum 24-hr rainfall at Station 1 for a return period of 50 years were estimated using MOM. The estimated parameters were $\bar{y}$ = 1.558, S_y = 0.3772, and G_y = 0.5366, and the estimated 50-year quantile was 29.06 cm (11.44 in.). The coefficient of variation of the 50-year quantile was calculated by changing the coefficient of variation of each parameter from −1 to +1. Computed results

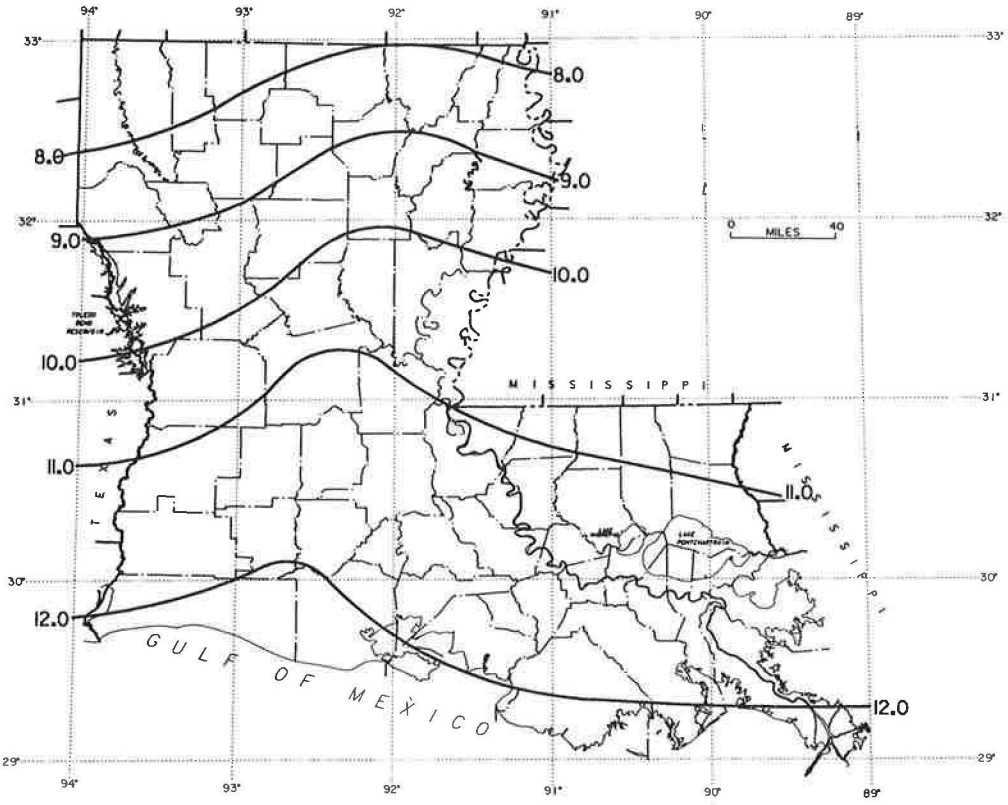

FIGURE 2 24-hr rainfall (inches) for 50-year return period in Louisiana.

TABLE 3 Average *MSE* and BIAS for TP-40 and New Maps

Return Period	TP-40 MAPS		NewMaps	
	MSE	BIAS	MSE	BIAS
2	0.035	0.167	0.004	0.005
5	0.024	0.120	0.004	0.016
10	0.021	0.102	0.004	0.006
25	0.018	0.050	0.010	0.010
50	0.022	0.013	0.016	0.030
100	0.034	-0.008	0.029	0.024

TABLE 4 Predicted Quantiles for Five Typical Stations

Station Number	Method	Return Period (year)					
		2	5	10	25	50	100
	TP-40	13.34	18.03	21.21	24.64	27.18	30.99
5	NewMaps	11.94	16.64	19.3	24.38	28.7	33.15
	LPEAR3	10.97	15.47	18.95	24.03	28.32	33.1
	TP-40	14.48	18.8	22.35	26.42	30.48	33.78
10	NewMaps	12.95	18.29	21.59	26.92	31.12	35.56
	LPEAR3	12.6	18.06	22.17	27.91	32.64	37.72
	TP-40	12.19	15.75	18.29	21.34	23.37	26.42
15	NewMaps	10.92	14.99	17.78	21.59	25.53	28.19
	LPEAR3	11.46	15.37	17.91	21.06	23.37	25.65
	TP-40	11.43	14.73	17.53	20.32	22.35	25.4
20	NewMaps	8.38	11.68	14.22	16.76	19.56	22.61
	LPEAR3	8.36	11.68	14.4	18.44	21.95	25.91
	TP-40	11.94	14.99	17.53	20.32	22.23	25.15
25	NewMaps	10.67	13.97	16.51	20.57	24.13	27.56
	LPEAR3	9.55	13.00	16.18	21.36	26.24	32.13

are plotted and shown in Figure 3. It is clearly demonstrated by this figure that the output error is most sensitive to errors in parameter $\bar{y}$, less sensitive to parameter S_y, and least sensitive to parameter G_y. Fortunately, the ranks of accuracy in estimating these three parameters are in reverse order of the sensitivity analysis. That is why the moment method of parameter estimation, based on the log-transformed data, often yields satisfactory results.

CONCLUSIONS

From this study, the following conclusions are drawn:

1. The log-Pearson Type 3 distribution along with MOM is the best combination of distribution and estimation method for the 26 synthesized Louisiana rainfall data sets.
2. For return periods of less than or equal to 25 years, the newly developed isohyetal maps are superior to the TP-40 maps in terms of both *MSE* and BIAS. For return periods of 50 and 100 years, the newly developed maps are superior to the TP-40 maps in terms of *MSE* but have a slightly larger BIAS. On the average, for all 26 synthesized stations corresponding to six return periods, the new maps reduced the *MSE* by 58 percent and the BIAS by 80 percent, as compared with the TP-40 maps. Thus, the NewMaps greatly improved the accuracy of the TP-40 maps on the basis of the available observed station data.
3. Estimated rainfall quantiles are most sensitive to the error in the estimated parameter $\bar{y}$ and least sensitive to error in the estimated parameter of skewness.
4. Results of this research are expected to enhance the accuracy of the predicted rainfall quantiles in the Louisiana region.

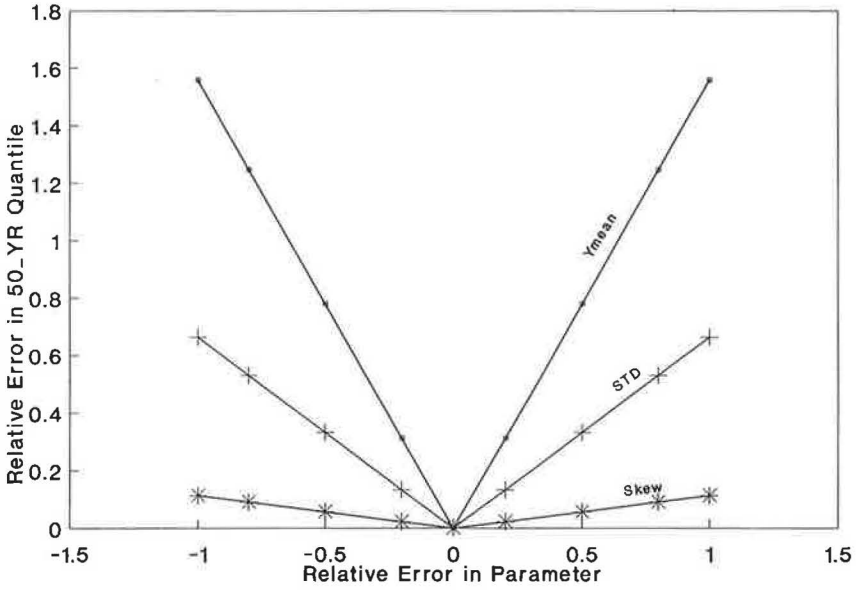

FIGURE 3 First-order analysis.

ACKNOWLEDGMENTS

The authors wish to thank Andrea Populus and Karen Jarreau for their assistance in the editing and the graphics in this paper. This project was funded by FHWA through the Louisiana Transportation Research Center.

REFERENCES

1. Yarnell, D. L. *Rainfall-Intensity-Frequency Data.* Miscellaneous Publication 204. U.S. Department of Agriculture, 1935.
2. *Louisiana Rainfall, Intensity-Duration-Frequency Data and Depth-Area-Duration Data.* Louisiana Department of Public Works, Baton Rouge, 1952.
3. *Rainfall Frequency Atlas of the United States.* Technical Paper 40. U.S. Department of Commerce, 1961.
4. *Five- to 60-Minute Precipitation Frequency for the Eastern and Central United States.* Technical Memorandum NWS HYDRO-35. National Oceanic and Atmospheric Administration, National Weather Service, Silver Spring, Md., 1977.
5. Aron, G., et al. *Pennsylvania Department of Transportation Storm Intensity-Duration-Frequency Charts.* FHWA-PA-85-032. Pennsylvania State University, University Park, 1986.
6. *Storm Rainfall Probability Atlas for Arizona.* FHWA-AZ-88-276. Arizona Department of Transportation, Phoenix, 1988.
7. Kuczera, G. Robust Flood Frequency Models. *Water Resources Research*, Vol. 18, No. 2, 1982, pp. 315–324.
8. Wallis, J. R., and E. F. Wood. Relative Accuracy of Log Pearson III Procedures. *Journal of the Hydraulics Division*, ASCE, Vol. 111, No. HY7, 1985, pp. 1043–1056.
9. Arora, K., and V. P. Singh. On Statistical Intercomparison of EV1 Estimates by Monte Carlo Simulation. *Advances in Water Resources*, Vol. 10, 1987, pp. 87–107.
10. Arora, K., and V. P. Singh. A Comparative Evaluation of the Estimators of the Log Pearson Type 3 Distribution. *Journal of Hydrology*, Vol. 105, 1989, pp. 19–37.
11. *Guidelines for Determining Flood Flow Frequency.* Bulletin 15. Hydrology Subcommittee, U.S. Water Resources Council, Washington, D.C., 1967.
12. Jain, D., and V. P. Singh. Comparison of Some Flood Frequency Distributions Using Empirical Data. In *Hydrologic Frequency Modeling* (V. P. Singh, ed.), D. Reidel Co., Germany, 1987, pp. 467–485.
13. Naghavi, B., V. P. Singh, and F. X. Yu. *LADOTD 24-Hour Rainfall Frequency Maps and I-D-F Curves.* Report 236. Louisiana Transportation Research Center, Baton Rouge, 1991.
14. Naghavi, B., and F. X. Yu. Generalized Skew Coefficients of Annual Floods for Louisiana Streams. *Water Resources Bulletin*, Vol. 27, No. 2, 1991, pp. 209–216.
15. Singh, V. P., and F. X. Yu. Derivation of an Infiltration Equation Using Systems Approach. *Journal of Irrigation and Drainage Engineering*, ASCE, Vol. 116, No. 6, 1990, pp. 837–858.